AWARD NUMBER: W81XWH-18-1-0685

TITLE: **Development of Therapeutic Strategies for NF1-Associated Optic Pathway Glioma**

PRINCIPAL INVESTIGATOR: Yuan Zhu, Ph.D.

CONTRACTING ORGANIZATION: Children's National Research Institute of the Children's National Hospital

REPORT DATE: JANUARY 2023

TYPE OF REPORT: Final Report

PREPARED FOR: U.S. Army Medical Research and Development Command
Fort Detrick, Maryland 21702-5012

REPORT DOCUMENTATION PAGE

Form Approved
OMB No. 0704-0188

1. REPORT DATE	2. REPORT TYPE	3. DATES COVERED
JANUARY 2023	Final	**30SEPT2018 - 29SEPT2022**

4. TITLE AND SUBTITLE

Development of Therapeutic Strategies for NF1-Associated Optic Pathway Glioma

5a. CONTRACT NUMBER

5b. GRANT NUMBER
W81XWH-18-1-0685

5c. PROGRAM ELEMENT NUMBER

6. AUTHOR(S)
Yuan Zhu, Ph.D.

E-Mail: yzhu@childrensnational.org

5d. PROJECT NUMBER

5e. TASK NUMBER

5f. WORK UNIT NUMBER

7. PERFORMING ORGANIZATION NAME(S) AND ADDRESS(ES)
Name: Children's National Research Institute at Children's National Hospital

Address: Room 5340, 5th floor main,
111 Michigan Ave. NW,
Washington, DC 20010

8. PERFORMING ORGANIZATION REPORT NUMBER

9. SPONSORING / MONITORING AGENCY NAME(S) AND ADDRESS(ES)

U.S. Army Medical Research and Development Command
Fort Detrick, Maryland 21702-5012

10. SPONSOR/MONITOR'S ACRONYM(S)

11. SPONSOR/MONITOR'S REPORT NUMBER(S)

12. DISTRIBUTION / AVAILABILITY STATEMENT

Approved for Public Release; Distribution Unlimited

13. SUPPLEMENTARY NOTES

14. ABSTRACT
Approximately 15%-20% of individuals with neurofibromatosis type 1 (NF1) develop low-grade glioma, mainly along the optic pathway (optic pathway glioma or NF1-OPG). Almost all NF1-OPGs arise in children younger than 7 years of age, suggesting that a complete loss of NF1 due to the "second-hit" must occur in developing neural stem and/or progenitor cells during a critical window of optic nerve development. However, the phenotypic consequences of *Nf1* loss on glial cell lineages in the developing optic nerve remain unknown. The overall objective of this proposal is to understand the disease mechanism that transforms NF1-OPGs from a neurodevelopmental defect into a blinding disease and, more importantly, to design preventive or early interventional treatments that can effectively prevent or reverse visual deterioration. Two specific aims are proposed. Aim 1: To determine cellular targets and molecular mechanisms of the developmental defect(s) caused by *Nf1* loss that induces progressive OPGs. Aim 2: To develop preventive and early interventional therapies that improve visual impairment in a preclinical NF1-OPG model. This project will develop a novel concept about the pathogenesis of NF1-OPG – the severity of developmental defects in glial lineages of the developing optic nerve determines the fate of OPGs, and will provide insights on how developmental defects in the optic nerve determine the behavior of OPGs – from asymptomatic to progressive.

15. SUBJECT TERMS
Neurofibromatosis type 1 (NF1), Optic pathway glioma (OPG), astrocyte precursor cells (APCs), Oligodendrocyte precursor cells (OPCs), neurodevelopmental disorder (NDD), retinal ganglion cells (RGCs), visual impairment, RAS, MEK, ERK/MAPK

16. SECURITY CLASSIFICATION OF:			17. LIMITATION OF ABSTRACT	18. NUMBER OF PAGES	19a. NAME OF RESPONSIBLE PERSON
a. REPORT	b. ABSTRACT	c. THIS PAGE			USAMRDC
U	U	U	UU	94	19b. TELEPHONE NUMBER *(include area code)*

TABLE OF CONTENTS

1. INTRODUCTION

Approximately 15%-20% of individuals with neurofibromatosis type 1 (NF1) develop low-grade glioma, mainly along the optic pathway (optic pathway glioma or NF1-OPG). Genetic studies have shown that loss of the remaining wild-type *NF1* alleles in somatic cells, also known as "second-hit" compared to the "first-hit" in the germline, leads to tumor formation. Importantly, NF1-OPGs arise predominantly in children younger than 7 years of age, suggesting that a complete loss of NF1 as a result of the "second-hit" must occur in developing neural stem and/or progenitor cells during a critical window of optic nerve (ON) development. Thus, **we propose the central hypothesis of this proposal that NF1-OPG is a neurodevelopmental disorder (NDD) arising from *NF1* inactivation in a neural stem and/or progenitor population(s) that is only transiently present in the developing ON.** The overall objective of this proposal is to investigate the cellular and molecular mechanisms that transform NF1-OPGs from a NDD into a blinding disease, and more importantly, to design preventive or early interventional treatments that can effectively prevent or reverse visual deterioration. Two specific aims are proposed.

Aim 1: To determine cellular targets and molecular mechanisms of the developmental defect(s) caused by *Nf1* loss that induces progressive OPGs.

Aim 2: To develop preventive and early interventional therapies that improve visual impairment in a preclinical NF1-OPG model.

2. Keywords

Neurofibromatosis type 1 (NF1), Optic pathway glioma (OPG), neurodevelopmental disorder (NDD), astrocyte precursor cells (APCs), oligodendrocyte precursor cells (OPCs), retinal ganglion cells (RGCs), visual impairment, RAS, MEK, ERK/MAPK signaling pathway

3. Accomplishments

- **What were the major goals of the project?**
    - *List the major goals of the project as stated in the approved SOW. If the application listed milestones/target dates for important activities or phases of the project identify these dates and show actual completion dates or the percentage of completion.*

Task 1/Specific Aim 1: To determine cellular targets and molecular mechanisms of the developmental defect(s) caused by *Nf1* loss that induces progressive OPGs.

Task 1.1/Specific Aim 1.1: To determine cellular targets of the developmental defect(s) caused by *Nf1* loss that induces progressive OPGs.

a) We will continue the analysis on the phenotypic alterations in the optic nerve of *Nf1*^{hGFAP}CKO mice at E17.5, P0.5, P8 and P15. We expect to complete these studies by the end of Year 1 (Months 1-12).

b) We will expand and generate cohorts of Pax2-cre;*Nf1*$^{flox/flox}$ and Pax2-cre;*Nf1*$^{flox/KO}$ mice along with their littermate controls for short-term developmental studies (see below) and long-term tumor analysis. All these crosses will carry one Rosa26- td-Tomato-Reporter transgene to facilitate the identification of *Nf1*$^{-/-}$ cells in mutant nerves or brains. Specifically, we will establish timely breeding to collect embryos at E17.5 and newborn pups at P0.5, P8 and P15 (Months 1-12).

c) We will expand and generate cohorts of Olig2-creER;*Nf1*$^{flox/flox}$ and Olig2-creER;*Nf1*$^{flox/KO}$ mice along with their littermate controls for short-term developmental studies (see below) and long-term tumor analysis (Months 7-24). For the inducible experiments with the Olig2-creER, we initially will generate more breeders with right genotypes in order to generate more mutants. In the meantime, we will continue to optimize Tamoxifen (TM) dosing conditions, particularly for TM induction on embryos (Months 7-12).

d) We will collect optic nerve and brain tissues for paraffin and cryostat sections for histological analysis as well as molecular analysis (Months 7-12)

We expect to finish short-term developmental studies by the end of the first year. We will use approximately 6 male and 20 to 30 female breeders for the experiments proposed for each GEM model. Long-term tumor analysis will be extended to Year 2 (Months 13-24).

- **What was accomplished under these goals?**
    - *For this reporting period describe: 1) major activities; 2) specific objectives; 3) significant results or key outcomes, including major findings, developments, or conclusions (both positive and negative); and/or 4) other achievements. Include a discussion of stated goals not met. Description shall include pertinent data and graphs in sufficient detail to explain any significant results achieved. A succinct description of the methodology used shall be provided. As the project progresses to completion, the emphasis in reporting in this section should shift from reporting activities to reporting accomplishments.*

Task 1: 100% of completion

Major activities, Specific objectives and Significant results

Background and Specific objectives: The optic nerve (ON) is a unique structure in the central nervous system (CNS) in which lack neuronal cell bodies, but contain two major macroglial populations, astrocytes and oligodendrocytes, arising from anatomically distinct regions of the developing CNS. Astrocyte lineage cells, also known as Type 1 astrocytes, are derived locally from neuroepithelial cells in the embryonic ON via Pax2-expressing astrocytic precursor cells ($Pax2^+$ APCs) (labelled in green, Figure 1A). However, oligodendrocyte lineage cells are derived from migrating glial progenitors (GPs), which have been previously referred to as Oligodendrocyte-Type 2 Astrocyte (O-2A) progenitors based on their differentiation potential to Type 2 astrocytes under a specific culture condition. Due to a lack of evidence for generating Type 2 astrocytes in vivo, however, O-2A progenitors were subsequently referred to as oligodendrocyte precursor cells (OPCs). A major source of migrating GPs is radial glia (RG) stem cells that reside in the embryonic hypothalamic ventricular zone (hVZ-RG). Of note, RG is primary neural stem cell (NSC) population(s) throughout the developing CNS. Migrating GPs expressing BLBP and Olig2 migrate through the optic chiasm and reach the distal portion of the ON at birth (labelled in red, Figure 1A). Thus, **ON-derived local APCs and brain-derived migrating GPs, which are marked by the expression of Pax2 and BLBP/Olig2, respectively, are the two candidates for NF1-OPG.**

Experimental design

Task 1.1a-d is to determine the cellular target(s) underlying NF1-associated optic pathway glioma (NF1-OPG) by employing three different Cre drivers, human glial fibrillary acidic protein (hGFAP) cre driver (**1.1a**), Pax2-cre (**1.1b**) and Olig2-cre^{ER} (**1.1c**), to specifically to target an *Nf1* mutation into one or both precursor populations in the developing ON. All tissue samples will be analyzed by using histological and molecular approaches (**1.1d**).

Significant results

Specific timing and location of tumor initiation

Task 1.1a (Observation) (100% of completion)

We used the conventional hGFAP-cre driver to target local APCs as well as migrating GPs via indirectly targeting their precursors, hVZ-RG stem cells (Figure 1B, C). In the embryonic ON in which is completely comprised of

local APCs, we unexpectedly observed no abnormality in the number of Pax2^{+} APCs, proliferation rate or Erk activation in the ON of the *Nf1*^{hGFAP}CKO model at embryonic day 17.5 (E17.5) (Figure 1D, E). In contrast, we observed a dramatic increase of BLBP^{+} and Olig2^{+} migrating GPs at birth or postnatal day 0.5 (P0.5) when the migratory front of GPs reached the distal portion, but not proximal portion of the ON (Figure 2A-D). Thus, the timing at the neonatal, not embryonic stages, as well as the location of abnormal glial expansion in the distal ON associated with migrating GPs, collectively support the model wherein migrating GPs, but not local APCs, are susceptible to *Nf1* loss, and thus they are the cell-lineage-of-origin for NF1-OPG.

It is known that both human and mouse pediatric low-grade gliomas, including NF1-OPG, are driven by abnormal activation of MEK/ERK signaling. To further test this model, we investigated the dependency of Erk signaling of migrating GPs versus local APCs. Consistently, a complete loss of Erk/MAPK signaling by inactivating both *Mek1* and *Mek2* (termed M0) almost eliminated the entire migrating BLBP+ or Olig2^{+} populations, while having relatively little effect on local Pax2+ cells (Figure 2A-D). It should be noted that in the control distal ON, we calculated that ~15% of the total Pax2^{+} cells arose from migrating BLBP^{+}/Olig2^{+} GPs that acquired Pax2 expression, which was in agreement with an ~11% of loss of Pax2^{+} cells in the M0 ON at P0.5 (Figure 2C, D). Importantly, abnormal activation of Erk signaling was enriched in Olig2^{+} cell populations of the P0.5 *Nf1*^{hGFAP}CKO ON (Figure 2E, F). This increase was almost exclusively observed in the *Nf1*$^{-/-}$ compartment, evidenced by the td-Tom^{+} reporter expression (Figure 2G, H). Together, the dependency of Erk signaling creates the vulnerability of migrating GPs to hyperactive Erk/MAPK signaling for tumor formation upon *Nf1* loss (Figure 2I).

Task 1.1b (Validation) (100% of completion)

To further rule out Pax2^{+} APCs as a cell-of-origin for NF1-OPG, we used the Pax2-cre that specifically targets an *Nf1* mutation into ON-derived local APCs. Consistent with the conclusion from the *Nf1*^{hGFAP}CKO model in Task 1.1a, we observed little or no defect in the neonatal ON of *Nf1*^{Pax2}CKO mice, including the number of Pax2^{+}, Olig2^{+}, or p-Erk^{+} cells (Figure 3A-F). These results support the conclusion that Nf1 has no role in the development of local astrocytic lineage in the ON. Thus, we demonstrate that local astrocytes are unlikely a cell-of-origin for astrocytic tumors in the ON (NF1-OPG).

Task 1.1c (Validation) (100% of completion)

Olig2 is specifically expressed in migrating GPs in the brain, but not the ON, during embryonic stages. To more directly target migrating GPs with an Nf1 mutation, we therefore used an inducible Olig2-cre^{ER} driver to target Olig2-expressing cells, many of which also expressed BLBP, in the brain at E15.5, a timepoint when no cell expressed Olig2 in the ON. This targeting strategy therefore allowed us to trace the fate of control and *Nf1*$^{-/-}$ BLBP/Olig2-expressing cells after they migrate into the ON postnatally. As shown in the Figure 4, we applied the Tamoxifen (TM) at E15.5, then collected samples and analysis at 1 day(s) post induction (1 dpi), 6 dpi and 4 months (4M or 120 dpi) later (Figure 4A, E, I). At 1 dpi, the TM-induced cells (td-Tomato^{+}) in the hypothalamic (Hyp) region were quantified and analyzed in the control and *Nf1*^{Olig2creER}CKO mutant mice (Figure 4B, C). The vast majority (>80%) of these induced cells expressed Olig2 and BLBP, which validated the specificity of this inducible Cre driver targeting Olig2^{+} progenitors in the embryonic brain (many of which also expressed BLBP at

this stage). Due to one-pulse induction of TM on the inducible Olig2-creER driver, the number of targeted cells was small in the hypothalamic region and no difference between the control and *Nf1*^{Olig2creER}CKO hypothalamic region 24 hours after induction (Figure 4C). Importantly, none of the targeted cells was found in the distal ON 24 hours after induction, validating the specificity of this inducible strategy into brain-derived, but not locally derived progenitors from the ON (Figure 4D). By contrast, at 6 dpi, the targeted cells were observed along the migratory pathway at the distal portion of ON, though not reached the proximal portion (Figure 4F). Migrating GPs derived from Olig2^{+} progenitors in the E16.5 brain exhibited a similar phenotype to what was observed in the *Nf1*^{hGFAP}CKO model, including a subset of migrating GPs acquired the local APC marker, Pax2, a majority of which co-expressed OPC markers, Olig2 and PDGFRα (Figure 4H). Of note, we did not observe a significant difference in the cell number of the targeted migrating GPs between the control and mutant groups, which could be at least partially attributed to the variations among the TM-induced mice from the current protocol (Figure 4G). However, 4 months after the TM-induction, 2 out of 3 *Nf1*^{Olig2creER}CKO mutant ON analyzed showed OPG-like phenotypes in the distal ON, exhibiting enlarged ON in the distal region (Figure 4J, K), abnormal glial expansion (Figure 4L, M), and increased infiltration and accumulation of Iba1^{+} microglia (Figure 4N, O). Thus, this inducible model provides a strategy to directly target and trace the migrating GPs and their progeny from the embryonic hypothalamic region to the postnatal ON, revealing a previously unrecognized phenotype – migrating GPs acquire local APC marker, Pax2, with the potential to differentiate into astrocytes in vivo. More importantly, despite having a small sample size, we observed OPG-like lesions in 2 of 3 inducible *Nf1*^{Olig2creER}CKO mice, providing direct evidence for the model: brain-derived migrating GPs as the source of NF1-OPG. Together, this type of the temporally controlled Cre driver models provides an important system to further dissect the outcome(s) of *Nf1* loss in different developmental stages from hVZ-RG stem cells, to hypothalamic mantle zone radial glia (hMZ-RG), to migrating GPs, in the context of NF1-OPG with distinct prognoses.

Task 1.1d (100% of completion)

All the experimental materials have been collected, analyzed and published in Developmental Cell (see the attached manuscript).

In summary, we made an unexpected observation that NF1-OPG, despite exhibiting robust astrocytic differentiation as a pilocytic astrocytoma, appears not to arise from the local astrocytic lineage, but instead from the migrating GPs from the brain. Migrating GPs mainly give rise to oligodendrocytes in the postnatal ON. Thus, we propose a new concept regarding the developmental origin of NF1-OPG (also see the attached Preview for our Developmental Cell paper). Together, NF1-OPG, despite being characterized as an astrocytic tumor in the ON, arises from a brain-derived glial lineage(s) that migrates into the ON after birth and mainly differentiate into oligodendrocytes to myelinate the ON. Given that we have completed all the tasks by Year 3, no major activity was performed during this one-year non-cost extension period.

- **What were the major goals of the project?**
    - *List the major goals of the project as stated in the approved SOW. If the application listed milestones/target dates for important activities or phases of the project identify these dates and show actual completion dates or the percentage of completion.*

Task 1.2/Specific Aim 1.2: To determine molecular mechanisms of the developmental defect(s) caused by *Nf1* loss that induces progressive OPGs.

a) We will generate and expand the MADM-*Nf1*^{hGFAP}CKO colony to generate a sufficient number of MADM-*Nf1*^{hGFAP}CKO mice for long-term tumor analysis (Months 1-24).

b) We will establish timely breeding of MADM-*Nf1*^{hGFAP}CKO mice to collect embryos at E17.5 and newborn pups at P0.5, P8 and P15 and collect optic nerve and brain tissues for paraffin and cryostat sections for histological analysis as well as molecular analysis (Months 7-12).

c) We will continue to optimize the dissection of optic nerves from neonatal MADM-*Nf1*^{hGFAP}CKO mice, particularly for those younger than P5 (prior to myelination) and determine the amount of cells and RNAs that can be isolated from each nerve. We will determine the number of optic nerves required to produce a sufficient amount of mRNAs for sequencing analysis (Months 7-12).

d). We will work with Dr. Hongjun Song's laboratory to develop protocols to isolate mRNAs and construct library from sibling *Nf1*$^{-/-}$ and *Nf1*$^{+/+}$ cells, which purified by FACS techniques (Months 13-24).

e) We will work with Novogene Corporation Inc. to perform RNA-sequencing analysis of isolated sibling *Nf1*$^{-/-}$ and *Nf1*$^{+/+}$ cells of the optic nerve at different neonatal stages (Months 13-24).

f) We will work with Novegene and laboratories of Drs. Hongjun Song and Wei Li to perform bioinformatics analysis to identify potential targets that are differentially expressed during a critical window of neonatal period of development when *Nf1*$^{-/-}$ glial cells undergo the most dramatic expansion compared to their sibling cells (Months 13-24).

g) We will validate these targets using our GEM models (Months 25-36).

We expect to finish most of the experiments proposed Aim 1 by the end of the second year except for the experiments that will validate the potential targets for driving abnormal expansion of *Nf1*$^{-/-}$ glial cells in the developing optic nerve. We will use approximately 6 male and 20 to 30 female breeders for these experiments. All the experiments proposed in Aim 1 will be conducted in the laboratory of Dr. Yuan Zhu. Targets identified using the RNA-sequencing approach described in Aim 1.2 will be validated using RT-PCR and Western blot

analysis on optic nerves from control and mutant mice at different developmental stages. In vivo validation of these novel targets is outside the scope of this grant, but will be addressed in future studies.

- **What was accomplished under these goals?**
    - *For this reporting period describe: 1) major activities; 2) specific objectives; 3) significant results or key outcomes, including major findings, developments, or conclusions (both positive and negative); and/or 4) other achievements. Include a discussion of stated goals not met. Description shall include pertinent data and graphs in sufficient detail to explain any significant results achieved. A succinct description of the methodology used shall be provided. As the project progresses to completion, the emphasis in reporting in this section should shift from reporting activities to reporting accomplishments.*

Major activities, Specific objectives and Significant results:

Background and Specific objectives:

The major focus of this subaim is to employ a mouse model system termed **the Mosaic Analysis with Double Markers (MADM) system** to develop a new-generation of NF1-OPG models. The MADM system targets a small number of *Nf1*$^{+/-}$ mitotic progenitors to produce sibling *Nf1*$^{-/-}$ and *Nf1*$^{+/+}$ cells tagged by red and green fluorescent protein (RFP and GFP) with a 1:1 ratio, respectively. Thus, the MADM system provides an in vivo system to better model tumor initiation from *NF1*$^{-/-}$ cells on the *NF1*$^{+/-}$ heterozygous background seen in human patients. Furthermore, RFP-labeled *Nf1*$^{-/-}$ and GFP-labeled *Nf1*$^{+/+}$ cells allowed us to investigate growth advantage conferred by *Nf1* loss among sibling cells in the same tissues.

Significant results:

Task 1.2a-c (100% of completion).

We first used a MADM-wild type (MADM-WT) model in which both red and green sibling cells were WT for *Nf1* In the MADM-WT model, due to the random assortment of symmetric and asymmetric divisions of stem cells, we observed some variations in the R/G ratio between individual brain sections (Figure 5A). However, this individual variation balanced to a net 1:1 R/G ratio (0.988) when we combined multiple sections from each of the 6 MADM-WT brains. Having validated the MADM-WT system, we next investigated their littermates, the MADM-Nf1 mice. In the hypothalamic region, *Nf1*$^{-/-}$ cells only exhibited a minor growth advantage over sibling *Nf1*$^{+/+}$ cells with a R/G ratio of 1.159. Strikingly, when we compared the R/G ratio inside the III-VZ with that in the surrounding MZ, we consistently observed a reverse patten of the R/G ratio inside the III-VZ with more green *Nf1*$^{+/+}$ cells versus in the surrounding MZ with more red *Nf1*$^{-/-}$ cells, 0.4 versus 1.8, respectively. These results provide more direct evidence that *Nf1* loss disrupts the balance between stem-cell maintenance and differentiation, driving hVZ-RG cells out of the hypothalamic ventricle to become hMZ-RG cells in the MZ.

While the R/G ratio inside the III-VZ was maintained between 0.4 and 0.45 from E17.5 to P0.5, red *Nf1*$^{-/-}$ cells continued to expand with a R/G ratio increasing to 3.12 in the MZ of the MADM-Nf1 brain at P0.5. This continuous

expansion could at least partially be caused by the higher proliferative rate of *Nf1*$^{-/-}$ BLBP^{-}Olig2^{+} cells in the MZ. Importantly, the sibling green *Nf1*$^{+/+}$ cells and red *Nf1*$^{-/-}$ cells were also distinct in the differentiation status. The percentage of the green *Nf1*$^{+/+}$ cells expressing BLBP was dramatically reduced from 70% inside the III-VZ to 16% in the MZ, while the percentage of green *Nf1*$^{+/+}$ cells expressing Olig2 was inversely increased from only 9% in the III-VZ to 69% in the MZ. This pattern is consistent with normal glial differentiation from hVZ-RG stem cells to more differentiated OPCs (BLBP^{+}Olig2^{-} → BLBP^{+}Olig2^{+}→ BLBP^{-}Olig2^{+}). In contrast, the majority of the abnormally expanded red *Nf1*$^{-/-}$ cells in the MZ expressed both BLBP and Olig2 at 78% and 65%, respectively. When a pair of sibling green and red cells was captured during mitotic division on the border of the III-VZ niche, the red *Nf1*$^{-/-}$ cell with Olig2 expression was always observed on the border of the niche, while the sibling green *Nf1*$^{+/+}$ cells lacking Olig2 expression remained inside the niche. These results suggest premature, but impaired, glial differentiation as a mechanism for the disruption of the balance between stem-cell maintenance and gliogenesis of hVZ-RG cells. Despite not directly causing increased proliferation, *Nf1* loss increases BLBP^{+} hMZ-RG cells in the hypothalamic region via two mechanisms: (1) overproducing BLBP^{+}Olig2^{-} and BLBP^{+}Olig2^{+} cells in the MZ by dislocating hVZ-RG stem cells out of the III ventricle; and (2) impairing differentiation of BLBP^{+} cells in the MZ, which serve as the source of migrating GPs for the ON.

We used the MADM-Nf1 system to further validate the model wherein BLBP^{+} migrating GPs, but not Pax2^{+} local APCs, contribute to initial expansion in the *Nf1*-deficient ON. At birth, almost the entire population of red and green cells (>99%) were observed within local Pax2^{+} populations, but not migrating BLBP^{+} populations in the distal ON of the MADM-Nf1 model, which was due to infrequent Cre-mediated interchromosomal recombination. No difference in the R/G ratio was observed in the P0.5 MADM-Nf1 ON, further validating the model that *Nf1* loss has no effect on local APCs. We next used the fluorescence-activated cell sorting (FACS) method to investigate RFP- and GFP-positive cells from the same ON of both MADM-WT and MADM-Nf1 mice at different postnatal stages (P15, P21 and P30) (Figure 5B, C). Both green and red *Nf1*$^{+/+}$ cells in the MADM-WT ON, or green *Nf1*$^{+/+}$ cells in the MADM-Nf1 ON, were similarly low and comprised 2% to 4% of the total cells (Figure 5B, C). While a 1:1 R/G ratio was constantly observed in the MADM-WT ON, a dramatic increase in the R/G ratio was observed in the MADM-Nf1 ON (Figure 5B, C). Importantly, the increase of *Nf1*$^{-/-}$ cells over their sibling *Nf1*$^{+/+}$ cells reached a plateau with about a 9-fold increase (~20% of the total cells) in the MADM-Nf1 ON during the first three postnatal weeks (Figure 5C). Despite only a small number of cells being targeted with *Nf1* deletion, some MADM-Nf1 mice did develop OPGs with robust GFAP expression similar to those observed in the conventional *Nf1*^{hGFAP}CKO model (Figure 5D). The R/G ratio in the OPGs remains consistent at 7-8 from P30 to P60, indicating this cell population no longer significantly undergoes expansion in the mature ON (Figure 5D, E). More importantly, red *Nf1*$^{-/-}$ cells with expression of BLBP and Olig2 greatly contributed to the tumor masses in the MADM-Nf1 model (Figure 5D, E). The MADM-Nf1 system not only validates the model wherein *Nf1* loss in brain-derived migrating progenitors leads to NF1-OPG formation, but also shows that abnormal expansion of migrating GPs mainly occurs during a specific developmental time window in the ON.

Task 1.2d-g (100% of completion*).

Due to the COVID-19, each institution involved in this project adopted different policies regarding how many researchers could work at a given time. It became increasingly difficult to engage collaborative work outside our institution, particularly for those that are not supported by this grant, including Dr. Hongjun Sun (now relocated to the University of Pennsylvania) and Dr. Wei Li at the National Eye Institute of the National Institutes of Health (NIH/NEI). To this date, Dr. Wei Li's lab at the NIH/NEI has not still fully gone back to the normal schedule. Given a paradigm shift of the discovery, we changed the strategy to expand the scope of the experiments proposed in Task 1.1 and Task1.2a-c. In addition, we developed a BLBP-driven enhanced green fluorescent protein (eGFP) transgenic reporter to isolate $BLBP^{+}$ stem/progenitor cells from the embryonic hypothalamic region of control and *Nf1*^{hGFAP}CKO mice. RNA-sequencing (RNA-seq) analysis showed that in the *Nf1*^{hGFAP}CKO brain, $BLBP^{+}$/$eGFP^{+}$ populations accumulated developmentally stalled stem/progenitor-like cells, while $BLBP^{-}$/$eGFP^{-}$ populations exhibited impaired both glial and neuronal differentiation, and subsequently, showed abnormal immune responses. Finally, we used a simple candidate approach, demonstrating that abnormal Mek-Erk/MAPK signaling is the driving force for NF1-OPG formation (see Task 2). These results provide molecular insights on how hyperactive Erk signaling upon *Nf1* loss blocks normal differentiation of migrating GPs and persistence of these abnormal stem/progenitor cells induces OPG formation.

***Notes**: We made unexpected observation regarding the cell lineage-of-origin for NF1-OPG using a variety of GEM models, including a newly developed MADM-NF1 model. Despite the interruption by the COVID-19, we have successfully redirected some of our efforts to strengthen this novel finding at the cellular mechanism for NF1-OPG pathogenesis. During this one-year non-cost extension period, we spent some efforts in generating and analyzing RNA-seq data. However, we realized that the molecular mechanism underlying NF1-OPG initiation turns out be simple – abnormal activation of the Ras-Raf-Mek-Erk/MAPK signaling pathway. This conclusion is based on both genetic inactivation of *Mek1*/*Mek2* and pharmacological MEK inhibition (also see the attached Preview for our Developmental Cell paper). Instead of using genomic approaches to further dissect molecular mechanisms, we decided to explore a different direction to target tumor-associated inflammatory responses as a novel therapeutic approach based on our work. Consequently, I teamed two investigators at the National Institutes of Health/National Eye Institute (NIH/NEI) to apply for a DOD grant under the Synergistic Idea Award mechanism. This grant started on July 1, 2022 (see below for details). In this regard, we conclude that we have fully completed this subaim.

- **What were the major goals of the project?**
    - *List the major goals of the project as stated in the approved SOW. If the application listed milestones/target dates for important activities or phases of the project identify these dates and show actual completion dates or the percentage of completion.*

Task 2/Specific Aim 2: To develop preventive and early interventional therapies that improve visual impairment in a preclinical NF1-OPG model.

2.1: To determine the time course of visual impairment during OPG progression

a) Drs. Zhu and Stasheff's laboratories will continue to expand the mouse colony for the *Nf1*^{hGFAP}CKO model with a particular focus to remove the retinal degeneration 1 (rd1) allele. This will ensure the retinal integrity of the *Nf1*^{hGFAP}CKO model that was recently transferred to the National Eye Institute/National Institutes of Health (NEI/NIH) (Months 1-12).

b) Dr. Stasheff will continue to train Emma Jecrois and Austin Friend from Dr. Zhu's laboratory on basic techniques of behavioral assays, anatomical and electrophysiologic assays of RGCs (Months 1-12).

Behavioral assays: The collaborative team will establish differences in late-stage mutant vs. control littermates (Months 1-12).

Anatomic assays: The collaborative team will determine the anatomic differences using OCT in parallel with behavioral assays (Months 1-12) and histology in parallel with in vitro electrophysiologic experiments (Months 1-12).

Electrophysiologic experiments: The collaborative team will determine most different measures on late-stage mutant vs. control littermates (Months 1-12), developmental time course (Months 13-36) and compare MEKi effects (Months 13-36).

We will use 8 to 10 mice of each genotype as described in Aim 1. In total, we will need 50 to 60 mice for the experiments. The milestone of the subaim is to train Dr. Zhu's laboratory personnel who will assist Dr. Stasheff to establish the phenotypic abnormalities of individual *Nf1*^{hGFAP}CKO mice measured by behavioral, anatomical and electrophysiologic assays, which will be correlated with histopathological assessment at the completion of each experiment. The behavioral assays from Aim 2.1 were specifically developed by Dr. Tudor Badea of the NIH to measure optomotor and optokinetic responses. These are established experimental assays designed explicitly to demonstrate the retention of visual acuity and contrast sensitivity.

- **What was accomplished under these goals?**
    - *For this reporting period describe: 1) major activities; 2) specific objectives; 3) significant results or key outcomes, including major findings, developments, or conclusions (both positive and negative); and/or 4) other achievements. Include a discussion of stated goals not met. Description shall include pertinent data and graphs in sufficient detail to explain any significant results achieved. A succinct description of the methodology used shall be provided. As the project progresses to completion, the emphasis in reporting in this section should shift from reporting activities to reporting accomplishments.*
    -

Major activities, Specific objectives and Significant results:

Background and Specific objects: The major activities of this sub-Task are to establish a mouse colony for the *Nf1*^{hGFAP}CKO model at the NIH/NEI), and train our lab personnel for the specific technologies, including behavioral, anatomic and electrophysiological assays. We encountered some unexpected events during the study of this Task: (1) the NIH did not allow us to directly transfer the mice from our institution (due to different health requirements) and (2) the presence of the retinal degeneration 1 (rd1) allele in our colony (which leads to degeneration of photoreceptors and thus compromises the analysis of retinal degeneration caused by tumors in the ON). In collaboration with Dr. Steven Stasheff (the Optional Qualified Collaborator), we have successfully rederived the *Nf1*^{hGFAP}CKO model, transferred to and built the breeding colony at the NEI/NIH campus. Importantly, we have entirely removed the *rd1* alleles from the *Nf1*^{hGFAP}CKO model and are in the process of characterizing tumor and retinal phenotypes the *Nf1*^{hGFAP}CKO model in the NIH/NEI campus. Moreover, we have trained and continued to train our lab members, including Drs. Wang Zheng, Emma Jecrois and a newly hired technician, Matt Krause, to work with the researchers.

Significant results:

Task 2.1a (100% of completion).

We have successfully (1) rederived the *Nf1*^{hGFAP}CKO model into the clean facility at the NIH/NEI, (2) removed the *rd1* alleles from the colony, and (3) established the *Nf1*^{hGFAP}CKO model on multiple genetic backgrounds to validate the robustness of tumor phenotypes in this model. However, the training process was largely halted by the COVID-19 during which our lab members were not allowed to work in the NIH campus. Indeed, Dr. Wei Li's lab was only allowed to work at 25% to 50% of the personnel capacity for the majority of 2020 and 2021. The NIH labs are gradually recovering from the previous levels during 2022.

Task 2.1b (100% of completion).

With the support of our lab for genotyping mice, Dr. Francisco Nadal-Nicolas was able to perform visual/behavioral (optomotor response, OMR), anatomical/imaging (optical tomography coherence, OCT), and histological analysis of OPGs and retinas (Figure 6A). We demonstrated that the *Nf1*^{hGFAP}CKO mice consistently exhibited visual impairments by the OMR assay, despite having a wide range of phenotypic variations from

Group 1 (relatively normal), Group 2 (mildly defective) and Group 3 (severely defective) (Figure 6B). Similarly, loss of axons by histological analysis was consistent with a significant decrease of retinal thickness by the OCT assay (Figure 6C) and dramatic loss of retinal ganglion cells (RGCs) (Figure 6D).

In summary, we will finish up the data analysis to correlate histological presence of tumors, axonal degeneration and RGC loss with the defects detected by non-invasive assays, behavioral and imaging assays in Year 3, establishing a two-step model of OPG-induced retinal degeneration (Figure 6E). The ultimate goal is to establish the behavioral and imaging biomarkers to measure therapeutic efficacy of the treatment strategies proposed in Task 2.2. During this one-year non-cost extension period, we submitted a proposal to continue this area of the research and received funding from the Visual Restoration Initiative sponsored by the Gilbert Family Foundation (see below for details).

- **What were the major goals of the project?**
    - *List the major goals of the project as stated in the approved SOW. If the application listed milestones/target dates for important activities or phases of the project identify these dates and show actual completion dates or the percentage of completion.*

Task 2.2: To develop MEKi-based preventive and early interventional therapies in NF1-OPG models

a) We will continue to optimize the doses and delivery of the "MEKi-in-Milk" protocol that will treat both control and *Nf1*^{hGFAP}CKO mice during neonatal stages from P0.5 to P21 and develop a protocol to treat young adult mice from P30 to P51. Phenotypic analyses of control and *Nf1*^{hGFAP}CKO mice with these two different treatment protocols will be performed in Dr. Zhu's laboratory (Months 1-12).

b). Emma Jecrois and Austin Friend from Dr. Zhu's laboratory will start to work with Dr. Stasheff to generate multiple cohorts of control and *Nf1*^{hGFAP}CKO mice treated with the two treatment protocols determined above in year 1. The vehicle- and MEKi-treated control and *Nf1*^{hGFAP}CKO mice will be subjected to the behavioral, anatomical and electrophysiologic assays described in Aim 2.1. After the completion of these experiments, histological analyses will be performed to determine the treatment effects on optic nerves, retinas and brains of control and *Nf1*^{hGFAP}CKO mice. Dr. Enrico Radaelli will provide his expertise on the histopathological evaluation of tissue samples from the vehicle- and MEKi-treated mice (Months 13-36).

The most of the experiments proposed in Task 2 will be performed in Year 2 and Year 3. In total, we will need 8 to 10 mice of control and *Nf1*^{hGFAP}CKO mice for each cohort of vehicle- or MEKi-treated experiments. In total, we need about 80 to 100 mice for the three assays proposed in the application. The milestone of the subaim is to establish a preclinical platform to test novel therapies for NF1-OPG using the MEKi as a starting point.

- **What was accomplished under these goals?**
    - *For this reporting period describe: 1) major activities; 2) specific objectives; 3) significant results or key outcomes, including major findings, developments, or conclusions (both positive and negative); and/or 4) other achievements. Include a discussion of stated goals not met. Description shall include pertinent data and graphs in sufficient detail to explain any significant results achieved. A succinct description of the methodology used shall be provided. As the project progresses to completion, the emphasis in reporting in this section should shift from reporting activities to reporting accomplishments.*

Major activities, Specific objectives and Significant results:

Task 2.2a (100% of completion).

We have completed the experiments proposed in Task 2.2. We compared three clinically relevant MEK inhibitors (MEKi), GSK1120212 (Trametinib), AZD6244 (Selumetinib) and PD0325901 (MEKi/PD901, Mirdametinib), at half of the maximal tolerance dose (MTD). Brain tissue penetration of three different MEKis, GSK1120212

(Trametinib), AZD6244 (Selumetinib) and PD0325901 (MEKi/PD901, Mirdametinib), when given either via oral gavage or through IP injection, was determined using the doses previously used for preclinical models. In P30 mice, MEKi/PD901 exhibited equally efficient Erk inhibition in both spleen and brain tissues when given through oral gavage, and was therefore chosen for all subsequent studies (Figure 7A-F). Of note, MEKi/PD901 was specific for inhibiting Erk/MAPK, but not PI3K/Akt or mTORC1 signaling pathway (marked by p-Akt or p-S6) (Figure 7I-L).

Task 2.2b (90% of completion).

In order to develop a clinically applicable protocol, we treated *Nf1*^{hGFAP}CKO mice with a MEKi/PD901 from P0.5-P21, using a "MEKi-in-Milk" protocol that we previously developed to treat developmental defects of the brain (Figure 8A, B). Using the "MEKi-in-milk" protocol, pups received about 1-5% of the mother's MEKi/PD901 dose, a number that was estimated based on the evidence that 10mg/kg MEKi/PD901 given to the lactating mother showed similar brain tissue inhibition in pups (about 50%) as a 0.125mg/kg dose of MEKi/PD901 given IP directly (Figure 7G-J). Similar to the dose-dependent inhibitory effects by the genetic approaches, a dose-dependent effect of MEKi was also observed – 5mg/kg MEKi/PD901 (PD5) caused a varying degree of Erk/MAPK inhibition, while the 20mg/kg dose (PD20) exerted the most consistent inhibition of both Erk/MAPK signaling and rescue of developmental defects. Unfortunately, most of the PD20-treated mice did not achieve long-term survival into P60. Thus, our study focused on short- (P21) and long-term (P60) effects of 10mg/kg PD901 (PD10) from P0.5-P21. At P21, the PD10 protocol almost completely inhibited Erk activation and rescued the increased cellularity and enlarged ON that were consistently observed in the untreated or vehicle-treated *Nf1*^{hGFAP}CKO mice. At P60, sustained inhibition of Erk signaling and elimination of abnormally expanded GFAP^{+}Olig2^{+} and BLBP^{+} cells with subsequent improvement in the ON size and cellularity were observed in 8 of the 9 MEKi-treated *Nf1*^{hGFAP}CKO mice (Figure 8C-I). The one exception was correlated with insufficient inhibition of Erk signaling within the ON (Figure 8F). Importantly, this transient treatment protocol led to sustained Erk inhibition with normalized glial progenitor cell populations within the ON analyzed at P60, over a month after the completion of the treatment (Figure 8E-I). Consequently, abnormal accumulation of reactive microglia, axonal degeneration and loss of RGCs were all prevented by this protocol (Figure 8J-M). Together, these results demonstrate that transient neonatal treatment with a low-dose MEKi is sufficient to rescue developmental defects, preventing NF1-OPG formation and tumor-associated neuronal degeneration with long-lasting benefits (Figure 8N).

In summary, we have completed the preventive study and published in our Developmental Cell paper (Jecrois et al., 2021 and see the attachment). During the non-cost extension period, we analyzed the data when a cohort of control and mutant mice were treated with MEKi from P30 to P51. Unfortunately, the rescue was not as convincingly demonstrated as the data when we treated them earlier from P0.5 to P21. Although we will need to increase the number of mice for the study, these preliminary data suggest that therapeutic effects of MEKi treatment will be significantly reduced if tumors have already caused irreversible damages to the optic nerve and consequently, retinal ganglion cells and vision loss. This observation further underscores the importance of designing preventive and early interventional treatment before tumors cause irreversible neurological damages.

- **What opportunities for training and professional development has the project provided?**
    - *If the project was not intended to provide training and professional development opportunities or there is nothing significant to report during this reporting period, state "Nothing to Report."*
    - *Describe opportunities for training and professional development provided to anyone who worked on the project or anyone who was involved in the activities supported by the project. "Training" activities are those in which individuals with advanced professional skills and experience assist others in attaining greater proficiency. Training activities may include, for example, courses or one-on-one work with a mentor. "Professional development" activities result in increased knowledge or skill in one's area of expertise and may include workshops, conferences, seminars, study groups, and individual study. Include participation in conferences, workshops, and seminars not listed under major activities.*

Although this project was not designed to focus on training and professional developmental opportunities for the researchers, we have tried to explore the unique opportunity to work with the intramural program at the NIH. Consequently, Dr. Wang Zheng, a postdoctoral fellow and Dr. Emma Jecrois, recently graduated from the University of Michigan in 2018, are having the research opportunity of exposing the state-of-art equipment and facilities at the NIH, including computerized behavioral testing and ultrastructural imaging. We have trained Dr. Emma Jecrois, an African American, to perform independent research, preparing and writing a scientific article for publication, which was published in Developmental Cell, October 2021 (see the attached manuscript).

- **How were the results disseminated to communities of interest?**
    - *If there is nothing significant to report during this reporting period, state "Nothing to Report."*
    - *Describe how the results were disseminated to communities of interest. Include any outreach activities that were undertaken to reach members of communities who are not usually aware of these project activities, for the purpose of enhancing public understanding and increasing interest* ***in learning and careers in science, technology, and the humanities.***

Due to the COVID-19 pandemic, we were not able to attend the conferences, which we normally would present our results such as the Annual conference sponsored by the American Association for Cancer Research (AACR) and the Children's Tumor Foundation (which attracts researchers and clinicians in the NF field all over the world). Of note, we were able to present at 2022 Children's Tumor Foundation Annual Conference at Philadelphia.

Seminar presentation:

International:

1. "Mouse Models of Neurofibromatosis type 1 (NF1)-associated Low-Grade Glioma, The Pediatric Low Grade Glioma Coalition Meeting, Ladenburg, Germany, January 13-14, 2020.
2. "Mouse Models of NF1-associated Tumors in the Nervous System, Translational Cancer Research Seminar, Department of Neurology, University Hospital Hamburg-Eppendorf, Hamburg, Germany, January 15, 2020.

National:

1. "Mouse Models of NF1-associated Malignant Peripheral Nerve Sheath Tumor (NF1-MPNST)", Histopathology Workshop on NF Animal Models, the Children's Tumor Foundation, Palms Spring, California, October 3-5, 2018.
2. "Stem and Progenitor Cell Division and the Development of Brain Tumors, Cancer Biology and Genetics Seminar, National Cancer Institute, National Institutes of Health, October 11, 2018.
3. "Modeling Neurofibromatosis type 1 (NF1)-associated Low- and High-Grade Glioma", NF1-Low Grade Glioma/Anaplastic Piloid Astrocytoma Conference, Bethesda, Maryland, February 19-20, 2019.
4. "Mouse Models of Neurofibromatosis type 1 (NF1)-associated Low- and High-Grade Glioma", Session 10: Animal Models, 2019 Children's Tumor Foundation International Neurofibromatosis (NF) Conference, San Francisco, CA, September 20-24, 2019.
5. "Investigate Mouse Models of Pediatric Brain Tumors as a Neurodevelopmental Disorder", Department of Biochemistry and Molecular Genetics, University of Virginia, Charlottesville, Virginia, March 25, 2021.
6. "Investigating and Exploring Developmental Vulnerability of Tumors in the Nervous System", Department of Pediatrics, University of Texas Southwestern Medical Center, Dallas, Texas, April 21, 2022.

7. “Develop preventative therapy for NF1-associated optic pathway glioma by targeting developmental vulnerability in a murine model”, Children’s Tumor Foundation Annual Conference, Philadelphia, PI, June 20, 2022.

Publications:

1. Jecrois, E.S., Zheng, W., Bornhorst, M., Li, Y., Treisman, D.T., Mugayo, D., Huynh, S., Andrew, S.F., Wang, Y., Jiang, J., Pierce, B.P., Mao, H., Krause, M.K., Friend, A., Stasheff, S.F., Nadal-Nicolas, F., Li, W., Zong, H., Packer, R.J. and **Zhu, Y.** (2021). Treatment during a developmental window prevents NF1-associated optic pathway glioma formation by targeting Erk-dependent migrating glial progenitors. *Developmental Cell*. 2021 Aug 20:S1534-5807(21)00634-1. doi: 10.1016/j.devcel.2021.08.004. Online ahead of print. PMID: 34428430.
2. **Zhu, Y**, Zheng, W, Jecrois, E.S., Pierce, B.P. and Treisman, D.T. (2021). A therapeutic window for preventive therapy in NF1-associated optic pathway glioma, *Molecular & Cellular Oncology* (Mini review). 30 Nov. 2021.

News outlets:

Our Dev Cell paper was published online ahead of time and reported by multiple news outlets, including the following:

Innovation District: https://innovationdistrict.childrensnational.org/using-targeted-signaling-pathway-therapy-to-prevent-pediatric-glioma-formation/

News Release: https://childrensnational.org/news-and-events/childrens-newsroom/2021/a-tumor-hijacked-signaling-pathway-can-be-treated-to-prevent-pediatric-low-grade-gliomas

EurekAlert!: https://www.eurekalert.org/news-releases/926152.

Twitter: https://twitter.com/ChildrensNatl/status/1429853667419623427

LinkedIn: https://www.linkedin.com/posts/children%27s-national-medical-center_using-targeted-signaling-pathway-therapy-activity-6835619832990326784-IQU6

-

- **What do you plan to do during the next reporting period to accomplish the goals?**
    - *If this is the final report, state "Nothing to Report."*
    - *Describe briefly what you plan to do during the next reporting period to accomplish the goals and objectives.*
- *“Nothing to Report”.*

4. IMPACT: *Describe distinctive contributions, major accomplishments, innovations, successes, or any change in practice or behavior that has come about as a result of the project relative to:*

- **What was the impact on the development of the principal discipline(s) of the project?**
    - *If there is nothing significant to report during this reporting period, state "Nothing to Report."*
    - *Describe how findings, results, techniques that were developed or extended, or other products from the project made an impact or are likely to make an impact on the base of knowledge, theory, and research in the principal disciplinary field(s) of the project. Summarize using language that an intelligent lay audience can understand (Scientific American style).*

Nearly 20% of children with NF1 develop low-grade gliomas with the majority arising along optic pathway, also known as optic pathway glioma (NF1-OPG), which predominantly occur in children younger than 7 years of age. Similarly, sporadic pediatric low-grade gliomas (pLGG), the most common brain tumor in children, infrequently occur in adults. The rarity of pLGGs in adults, including NF1-OPG, suggest that these childhood tumors arise from neural stem/progenitors that are only transiently present in the developing CNS. Over the past 8 years, David Gutmann and his colleagues provided the evidence and proposed the model wherein NSCs in the III-VZ give rise to NF1-OPG in GEM models. However, the ON and III-VZ arise from distinct segments of the developing neural tube and thus the progeny of neuroepithelial cells/NSCs in these two regions have distinct lineage relationships. Furthermore, NSCs in the developing III-VZ do not migrate into the ON and thus cannot be a direct cell-of-origin for NF1-OPG. Neuroepithelial cells in the embryonic ON are one of the few exceptions, giving rise to only astrocytes (also known as Type 1 astrocytes), via astrocyte precursor cells (APCs), specified by a transcriptional factor, Pax2. The oligodendrocyte lineage in the mature ON arises from migrating $BLBP^{+}$ GPs, the progeny of NSCs in the III-VZ via their differentiated progeny that migrate into the ON after birth. Using multiple GEM models, including the MADM-Nf1 model, we identified a cell lineage-of-origin, but more precisely, a cell lineage-of-origin for NF1-OPG. This conclusion is based on (1) the developmental timing (neonatal), (2) the location of initial cellular expansion in the distal ON, and (3) the dependency on Erk/MAPK signaling in this developing cell lineage. Finally, in contrast to the NF1-OPG models developed by Dr. Gutmann, which develop tumors in adulthood, our NF1-OPG models have a developmental origin, thus mimicking the pediatric nature of these tumors in humans. The availability of two independent NF1-OPG models with different disease onset mechanism and visual outcomes will greatly help the researchers perform translational studies to benefit different patient populations with NF1-OPGs.

- **What was the impact on other disciplines?**
    - *If there is nothing significant to report during this reporting period, state "Nothing to Report."*
    - *Describe how the findings, results, or techniques that were developed or improved, or other products from the project made an impact or are likely to make an impact on other disciplines.*

NF1-associated tumors, including OPG, are driven by inactivating *NF1* via two genetic events, of which the "first-hits" are the hereditary (H) germline mutations and the "second-hits" are somatic mutations by replication errors (R) during stem/progenitor cell divisions. Despite the fact that neither of the two tumor-driver events are preventable, we demonstrate a chemopreventative strategy that can neutralize abnormal differentiation and eliminate the tumorigenic potential of *Nf1*$^{-/-}$ progenitors – a preventative strategy for tumors whose driver mutations are unpreventable (Figure 7N).

By using a very low dose of MEKi during the neonatal stages via the "MEKi-in-Milk" protocol, we show that this treatment protocol, despite its temporary nature, achieved long-term prevention of NF1-OPG formation and tumor-associated RGC loss. Thus, we provide proof-of-principle needed to inform chemoprevention therapeutic trials for children with NF1-OPG. The ongoing clinical trials using MEKi at 10-20 times higher doses than the one used in this study on infants with NF1 (as young as 1 month of age) will provide the necessary safety information for the feasibility of this chemopreventive strategy. The low-dose and transient nature of the "MEKi-in-Milk" protocol also avoids long-lasting MEKi treatment and its potential adverse effects on the vulnerable developing CNS. This principle may be applicable to children with the developmental disorders with high risks of developing pediatric tumors, such as other RASopathies (i.e. Costello syndrome) that exhibits much more severe neurodevelopmental defects.

- **What was the impact on technology transfer?**
    - *If there is nothing significant to report during this reporting period, state "Nothing to Report."*
    - *Describe ways in which the project made an impact, or is likely to make an impact, on commercial technology or public use, including:*
        - *transfer of results to entities in government or industry;*
        - *instances where the research has led to the initiation of a start-up company; or*
        - *adoption of new practices.*

"Nothing to Report".

- **What was the impact on society beyond science and technology?**
    - *If there is nothing significant to report during this reporting period, state "Nothing to Report."*
    - *Describe how results from the project made an impact, or are likely to make an impact, beyond the bounds of science, engineering, and the academic world on areas such as:*
        - *improving public knowledge, attitudes, skills, and abilities;*

- *changing behavior, practices, decision making, policies (including regulatory policies), or social actions; or*
- *improving social, economic, civic, or environmental conditions.*

The major clinical challenge for a disease like NF1-OPG is delayed diagnosis when children with tumors have already experienced visual impairment caused by loss of retinal ganglion cells (RGCs), the only neurons connecting the eye with the brain. The current chemotherapy is designed to inhibit tumor growth, but with no ability to restore neuronal loss and thus unlikely improve visual functions. Therefore, prevention, early diagnosis and intervention will be critical to eliminate the negative impacts caused by tumors in the brain. Our study will provide a mechanistic basis and the proof-of-principle evidence for researchers and clinicians to develop preventive therapy for these brain tumors by treating this pediatric tumor as a neurodevelopmental disorder, a disease term that is often associated with neuropsychiatric diseases such as Autistic Spectrum Disorder (ASD), Attention-Deficit and Hyperactivity Disorder (ADHD), and learning disabilities. Recent clinical trials using MEKi have further provided the support for the notion of treating patients before tumors cause irreversible neurological damages.

5. CHANGES/PROBLEMS: *The Project Director/Principal Investigator (PD/PI) is reminded that the recipient organization is required to obtain prior written approval from the awarding agency Grants Officer whenever there are significant changes in the project or its direction. If not previously reported in writing, provide the following additional information or state, "Nothing to Report," if applicable:*

- **Changes in approach and reasons for change**
    - *Describe any changes in approach during the reporting period and reasons for these changes. Remember that significant changes in objectives and scope require prior approval of the agency.*

"Nothing to Report"

- **Actual or anticipated problems or delays and actions or plans to resolve them**
    - *Describe problems or delays encountered during the reporting period and actions or plans to resolve them.*

Due to the COVID-19 pandemic, our collaborative work with researchers at the NIH/NEI and University of Pennsylvania was significantly delayed or halted, particularly for those proposed in Task 1.2 and Task 2.1. More importantly, we realized that the molecular mechanism underlying NF1-OPG resulted from a single-pathway alteration – abnormal activation of Ras-Raf-Mek-Erk/MAPK signaling. Therefore, there is no urgent need to perform genome-wide studies (e.g. RNA-seq) to identify additional molecular targets for this tumor. Instead, we took a simple candidate approach, demonstrating that abnormal Mek-Erk/MAPK signaling is the driving force for NF1-OPG formation (see Figure 6 and Figure 7 in the attached manuscript). Based on your work, we proposed a new direction to target tumor-associated inflammation (see below for details).

- **Changes that had a significant impact on expenditures**
    - *Describe changes during the reporting period that may have had a significant impact on expenditures, for example, delays in hiring staff or favorable developments that enable meeting objectives at less cost than anticipated.*

"Nothing to Report".

- **Significant changes in use or care of human subjects, vertebrate animals, biohazards, and/or select agents**

- *Describe significant deviations, unexpected outcomes, or changes in approved protocols for the use or care of human subjects, vertebrate animals, biohazards, and/or select agents during the reporting period. If required, were these changes approved by the applicable institution committee (or equivalent) and reported to the agency? Also specify the applicable Institutional Review Board/Institutional Animal Care and Use Committee approval dates.*

- **Significant changes in use or care of human subjects**
- **Significant changes in use or care of vertebrate animals.**
- **Significant changes in use of biohazards and/or select agents**

“Nothing to Report”.

6. PRODUCTS: *List any products resulting from the project during the reporting period. If there is nothing to report under a particular item, state "Nothing to Report."*

- **Publications, conference papers, and presentations**

  Report only the major publication(s) resulting from the work under this award.

  - **Journal publications.** *List peer-reviewed articles or papers appearing in scientific, technical, or professional journals. Identify for each publication: Author(s); title; journal; volume: year; page numbers; status of publication (published; accepted, awaiting publication; submitted, under review; other); acknowledgement of federal support (yes/no).* Yes

Publications:

1. Jecrois, E.S., Zheng, W., Bornhorst, M., Li, Y., Treisman, D.T., Mugayo, D., Huynh, S., Andrew, S.F., Wang, Y., Jiang, J., Pierce, B.P., Mao, H., Krause, M.K., Friend, A., Stasheff, S.F., Nadal-Nicolas, F., Li, W., Zong, H., Packer, R.J. and **Zhu, Y.** (2021). Treatment during a developmental window prevents NF1-associated optic pathway glioma formation by targeting Erk-dependent migrating glial progenitors. *Developmental Cell*. 2021 Aug 20:S1534-5807(21)00634-1. doi: 10.1016/j.devcel.2021.08.004. Online ahead of print. PMID: 34428430.
2. **Zhu, Y,** Zheng, W, Jecrois, E.S., Pierce, B.P. and Treisman, D.T. (2021). A therapeutic window for preventive therapy in NF1-associated optic pathway glioma, *Molecular & Cellular Oncology* (Mini review). 30 Nov. 2021.

  - **Books or other non-periodical, one-time publications.** *Report any book, monograph, dissertation, abstract, or the like published as or in a separate publication, rather than a periodical or series. Include any significant publication in the proceedings of a one-time conference or in the report of a one-time study, commission, or the like. Identify for each one-time publication: Author(s); title; editor; title of collection, if applicable; bibliographic information; year; type of publication (e.g., book, thesis or dissertation); status of publication (published; accepted, awaiting publication; submitted, under review; other); acknowledgement of federal support (yes/no).*

  “Nothing to Report”

- **Other publications, conference papers, and presentations.** *Identify any other publications, conference papers and/or presentations not reported above. Specify the status of the publication as noted above. List presentations made during the last year (international, national, local societies, military meetings, etc.). Use an asterisk (*) if presentation produced a manuscript.*

Meeting presentations by Yuan Zhu:

International:

1. "Mouse Models of Neurofibromatosis type 1 (NF1)-associated Low-Grade Glioma, The Pediatric Low Grade Glioma Coalition Meeting, Ladenburg, Germany, January 13-14, 2020.
2. "Mouse Models of NF1-associated Tumors in the Nervous System, Translational Cancer Research Seminar, Department of Neurology, University Hospital Hamburg-Eppendorf, Hamburg, Germany, January 15, 2020.

National:

1. "Mouse Models of NF1-associated Malignant Peripheral Nerve Sheath Tumor (NF1-MPNST)", Histopathology Workshop on NF Animal Models, the Children's Tumor Foundation, Palms Spring, California, October 3-5, 2018.
2. "Stem and Progenitor Cell Division and the Development of Brain Tumors, Cancer Biology and Genetics Seminar, National Cancer Institute, National Institutes of Health, October 11, 2018.
3. "Modeling Neurofibromatosis type 1 (NF1)-associated Low- and High-Grade Glioma", NF1-Low Grade Glioma/Anaplastic Piloid Astrocytoma Conference, Bethesda, Maryland, February 19-20, 2019.
4. "Mouse Models of Neurofibromatosis type 1 (NF1)-associated Low- and High-Grade Glioma", Session 10: Animal Models, 2019 Children's Tumor Foundation International Neurofibromatosis (NF) Conference, San Francisco, CA, September 20-24, 2019.
5. "Investigate Mouse Models of Pediatric Brain Tumors as a Neurodevelopmental Disorder", Department of Biochemistry and Molecular Genetics, University of Virginia, Charlottesville, Virginia, March 25, 2021.
6. "Investigating and Exploring Developmental Vulnerability of Tumors in the Nervous System", Department of Pediatrics, University of Texas Southwestern Medical Center, Dallas, Texas, April 21, 2022.

7. "Develop preventative therapy for NF1-associated optic pathway glioma by targeting developmental vulnerability in a murine model", Children's Tumor Foundation Annual Conference, Philadelphia, PI, June 20, 2022 (Poster Presentation and attached Abstract).

- **Website(s) or other Internet site(s)**

  List the URL for any Internet site(s) that disseminates the results of the research activities. A short description of each site should be provided. It is not necessary to include the publications already specified above in this section.

"Nothing to Report".

- **Technologies or techniques**

  Identify technologies or techniques that resulted from the research activities. In addition to a description of the technologies or techniques, describe how they will be shared.

  "Nothing to Report".

- **Inventions, patent applications, and/or licenses**

  Identify inventions, patent applications with date, and/or licenses that have resulted from the research. State whether an application is provisional or non-provisional and indicate the application number. Submission of this information as part of an interim research performance progress report is not a substitute for any other invention reporting required under the terms and conditions of an award.

"Nothing to Report".

- **Other Products**

  Identify any other reportable outcomes that were developed under this project. Reportable outcomes are defined as a research result that is or relates to a product, scientific advance, or research tool that makes a meaningful contribution toward the understanding, prevention, diagnosis, prognosis, treatment, and/or rehabilitation of a disease, injury or condition, or to improve the quality of life. Examples include:

  - *data or databases;*

- *biospecimen collections;*
- *audio or video products;*
- *software;*
- *models;*
- *educational aids or curricula;*
- *instruments or equipment;*
- *research material (e.g., Germplasm; cell lines, DNA probes, animal models);*
- *clinical interventions;*
- *new business creation; and*
- *other.*
-

1. We have developed a series of genetically engineered mouse (GEM) models for NF1-OPG and deposited the Jackson Lab for the research community.
2. Biospecimen from different stages of NF1-OPG have been collected for future research.
3. We have established behavioral, anatomical and histological assays to measure OPG-induced axonal degeneration, RGC loss, and visual impairments.

7. PARTICIPANTS & OTHER COLLABORATING ORGANIZATIONS

- **What individuals have worked on the project?**
    - *Provide the following information for: (1) PDs/PIs; and (2) each person who has worked at least one person month per year on the project during the reporting period, regardless of the source of compensation (a person month equals approximately 160 hours of effort). If information is unchanged from a previous submission, provide the name only and indicate "no change."*

1. Yuan Zhu (PD/PI), no change
2. Steven Stasheff (OQC), no change
3. Wang Zheng (researcher), left the lab on August 26, 2022.
4. Emma Jecrois (researcher), left the lab on October 14, 2021.
5. Heather Gordish -Dressman (collaborator, statistician), no change.

- **Has there been a change in the active other support of the PD/PI(s) or senior/key personnel since the last reporting period?**
    - *If there is nothing significant to report during this reporting period, state "Nothing to Report."*
    - *If the active support has changed for the PD/PI(s) or senior/key personnel, then describe what the change has been. Changes may occur, for example, if a previously active grant has closed and/or if a previously pending grant is now active. Annotate this information so it is clear what has changed from the previous submission. Submission of other support information is not necessary for pending changes or for changes in the level of effort for active support reported previously. The awarding agency may require prior written approval if a change in active other support significantly impacts the effort on the project that is the subject of the project report.*

PI/PD, Dr. Yuan Zhu has received grant funding from the NIH and Gilbert Family Foundation in 2021, DOD and Gilbert Family Foundation 2022.

R01NS116421 (PI: Zhu) 4/1/2021 – 3/31/2026
Level of Effort: 20%
Source: NIH/NINDS
Annual Direct Costs:
Title of Project: Developmental Origin, Injury and Epigenomic Regulation of NF1-associated Peripheral Nerve Sheath Tumors
Project Goal: The goals of this project are to investigate the development $Nf1^{-/-}$ Remak pocket defect and its associated axonal degeneration (nerve injury) drive $Nf1^{-/-}$ SCs to form PNFs and nerve injury

response induces an epigenomic switch, rendering reprogrammed PNFs or SCs susceptible to malignant transformation by sequential loss of CDKN2A and PRC2.

The Gilbert Family Foundation Award 2021 (PI: Packer). 4/1/2021 – 3/31/2026
Role: Project Leader for Project 2 (Zhu)
Level of Effort: 10%
Source: The Gilbert Family Foundation
Annual Direct Costs: (Zhu Lab)
Title of Project: Development of Clinical Trials for Transformed Low-Grade Gliomas in NF1 patients
Project Goal: The main objective of this proposal is to investigate and develop novel therapeutic strategies for transformed low-grade gliomas in NF1 patients.

W81XWH2210577 (Overall PI: Zhu) 4/1/2021 – 3/31/2026
Co-PIs: Wei Li and Han-Yu Shih
Level of Effort: 15%
Source: Department of Defense (DOD)
Annual Direct Costs: (Zhu Lab)
Title of Project: Investigate and target inflammatory components during NF1-OPG formation
Project Goal: We propose to investigate and treat NF1-OPG as an optic nerve injury causing neuronal degeneration. We will identify specific subsets of OPG-associated microglia and develop therapeutic strategies to prevent vision loss by immunometabolically modulating microglia, preventing and alleviating OPG-associated nerve injury and RGC death. Finally, we will develop novel NF1-OPG models based on the MADM technology with the resolution of distinguishing *Nf1*$^{-/-}$ cells from sibling *Nf1*$^{+/+}$ cells, identifying the mechanism underlying OPG-induced an inflammatory response. If successful, this project will provide a strategy to treat patients with NF1-OPGs before visual impairment becomes irreversible.

The Gilbert Family Foundation Award 2023 (PI: Zhu). 2/1/2023 – 1/31/2026
Level of Effort: 10%
Source: The Gilbert Family Foundation
Annual Direct Costs:
Title of Project: Development and characterization of genetically engineered mouse models for NF1-associated OPG
Project Goal: The main objective of this proposal is to develop and characterize genetically engineered mouse models for NF1-associated optic pathway glioma and provide research support for the Gilbert Family Foundation-sponsored Visual Restoration Initiative.

- **What other organizations were involved as partners?**
    - *If there is nothing significant to report during this reporting period, state "Nothing to Report."*
    - *Describe partner organizations - academic institutions, other nonprofits, industrial or commercial firms, state or local governments, schools or school systems, or other organizations (foreign or domestic) - that were involved with the project. Partner organizations may have provided financial or in-kind support, supplied facilities or equipment, collaborated in the research, exchanged personnel, or otherwise contributed.*

      Provide the following information for each partnership:
        - **Organization Name: National Institutes of Health**
        - **Location of Organization:** (Bethesda, Maryland)
        - **Partner's contribution to the project** *(identify one or more)*
            - **Financial support (No);**
            - **In-kind support** *(e.g., partner makes software, computers, equipment, etc., available to project staff)*; **(Yes)**
            - **Facilities** *(e.g., project staff use the partner's facilities for project activities)*; **(Yes)**
            - **Collaboration** *(e.g., partner's staff work with project staff on the project)*; **(Yes)**
            - **Personnel exchanges** *(e.g., project staff and/or partner's staff use each other's facilities, work at each other's site)*; and **(Yes)**
            - **Other.**
- **Notes:** The collaborative details with the NEI/NIH are provided by Drs. Steven Stasheff and Wei Li in their support letters.

8. SPECIAL REPORTING REQUIREMENTS

- **COLLABORATIVE AWARDS**: *For collaborative awards, independent reports are required from BOTH the Initiating PI and the Collaborating/Partnering PI. A duplicative report is acceptable; however, tasks shall be clearly marked with the responsible PI and research site. A report shall be submitted to https://ebrap.org for each unique award.*
- **QUAD CHARTS:** *If applicable, the Quad Chart (available on https://www.usamraa.army.mil) should be updated and submitted with attachments.*

Not applicable

10. APPENDICES: *Attach all appendices that contain information that supplements, clarifies or supports the text. Examples include original copies of journal articles, reprints of manuscripts and abstracts, a curriculum vitae, patent applications, study questionnaires, and surveys, etc. Reminder: Pages shall be consecutively numbered throughout the report.* ***DO NOT RENUMBER PAGES IN THE APPENDICES.***

1. Eight figures described in the text.

2. Figure legends.

3. A recently published manuscript entitled: "Treatment during a developmental window prevents NF1-associated optic pathway glioma formation by targeting Erk-dependent migrating glial progenitors**".**

4. Preview for the above manuscript for reference.

5. Abstract for poster presentation at 2022 Children's Tumor Foundation Annual Conference.

Figure 1

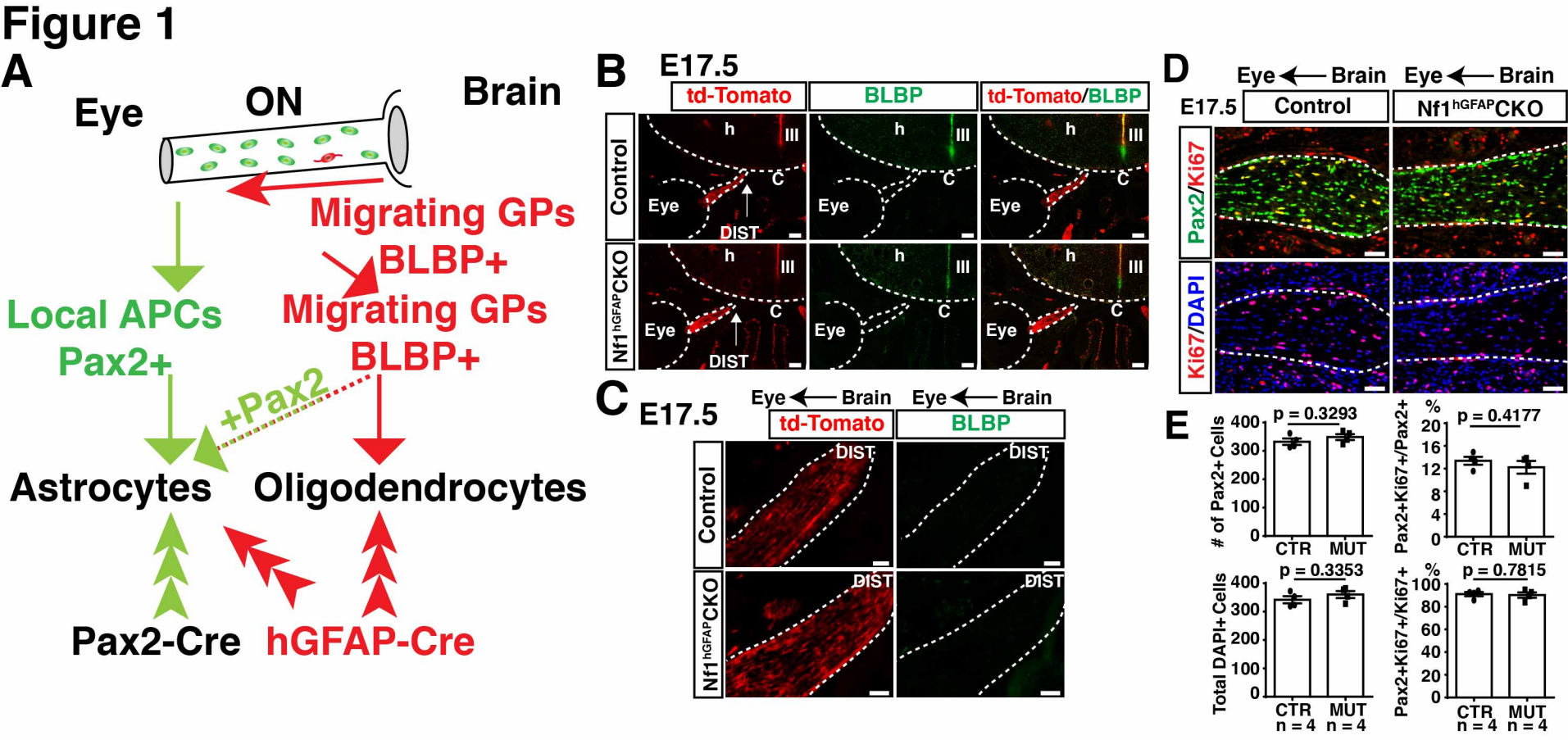
A
Eye
ON
Brain
Migrating GPs
BLBP+
Local APCs
Pax2+
Migrating GPs
BLBP+
+Pax2
Astrocytes
Oligodendrocytes
Pax2-Cre
hGFAP-Cre
B
E17.5
td-Tomato
BLBP
td-Tomato/BLBP
Control
Nf1hGFAPCKO
h
III
C
Eye
DIST
C
E17.5
Eye ← Brain
td-Tomato
BLBP
Control
Nf1hGFAPCKO
DIST
D
Eye ← Brain
E17.5
Control
Nf1hGFAPCKO
Pax2/Ki67
Ki67/DAPI
E
# of Pax2+ Cells
p = 0.3293
CTR
MUT
Pax2+Ki67+/Pax2+
%
p = 0.4177
Total DAPI+ Cells
p = 0.3353
Pax2+Ki67+/Ki67+
%
p = 0.7815
n = 4

FIGURE LEGENDS

Figure 1. Locally derived APCs are not affected by *Nf1* loss.

(A) Schematic of cellular origins of two major glial populations in the developing optic nerve. APC cells (labeled in green) arise locally, while OPCs (labeled in red) migrate from the ventral brain via the optic chiasm at birth. The highlighted arrowheads show the developing precursor populations targeted by hGFAP-cre or Pax2-cre driver.

(B and C) Immunofluorescent co-labeling shows td-Tomato and BLBP expression in the hypothalamic/chiasm/ON (h/c/ON) region (B) and the distal ON (C).

(D and E) Immunofluorescent co-labeling of Pax2 and Ki67 expression in the distal ON (D). The number of $Pax2^+$ APCs, total ON cells ($DAPI^+$), proliferative index of APCs ($Pax2^+Ki67^+/Pax2^+$), and the percentage of proliferating APCs in total proliferating ON cells ($Pax2^+Ki67^+/Ki67^+$) were quantified (E). Dashed lines delineate the ON.

(Q) Schematic summary of the impact of different levels of Mek-Erk signaling on migrating GPs.

All the quantification data are presented as mean ± SEM. Unpaired, two-tailed Student's t-test was used for statistical analysis. ns: not significant. VB: Ventral Brain; III: Third Ventricle; ON: optic nerve; APC: Astrocyte Precursor Cell; GP: Glial Progenitor; CTR: control group; MUT: $Nf1^{hGFAP}$CKO mutant group. Scale bar: 50 μm.

Figure 2

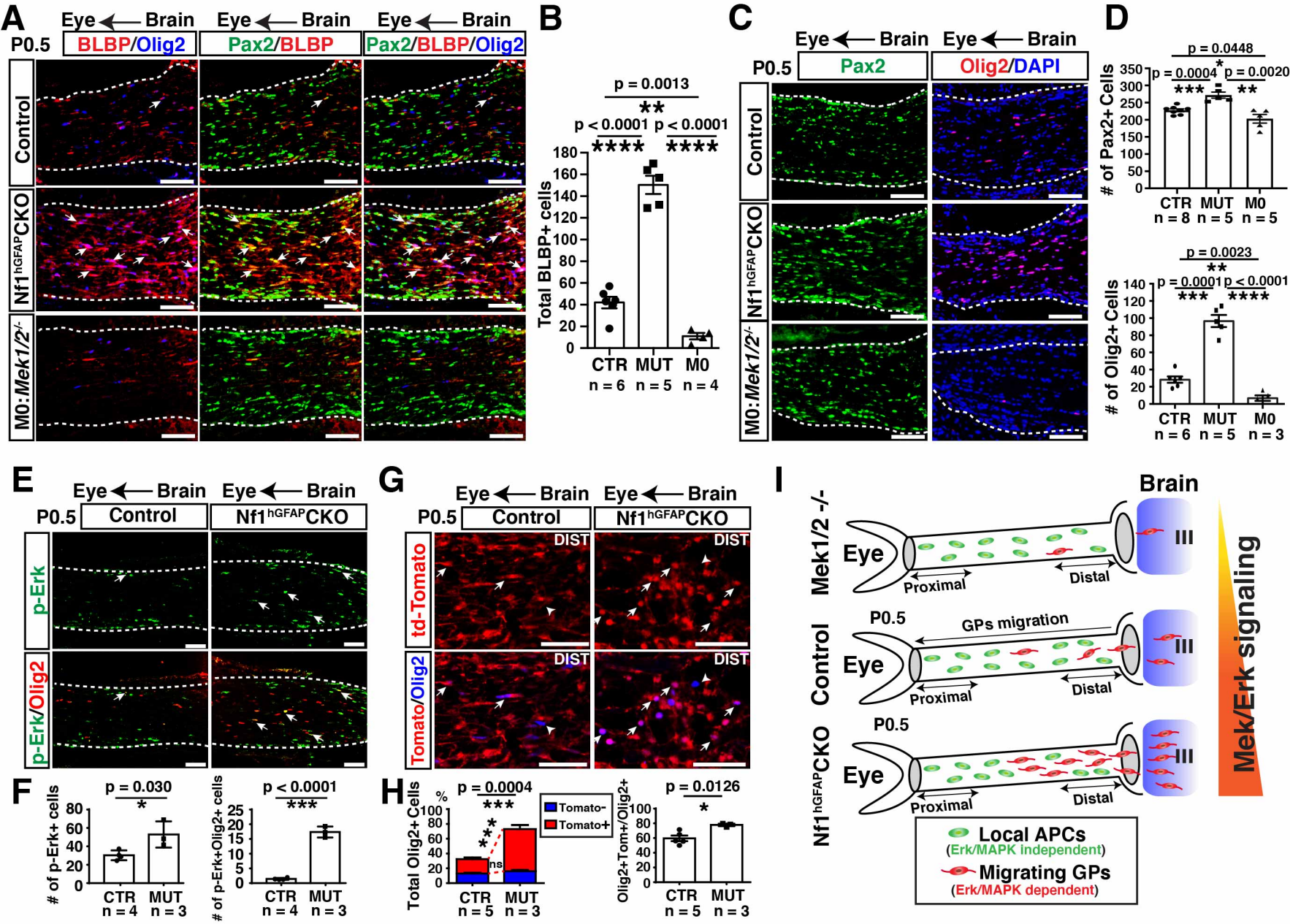
A
Eye ← Brain
P0.5
BLBP/Olig2
Pax2/BLBP
Pax2/BLBP/Olig2
Control
Nf1hGFAPCKO
M0:Mek1/2-/-
B
p = 0.0013
**
p < 0.0001
p < 0.0001
****
****
Total BLBP+ cells
CTR n = 6
MUT n = 5
M0 n = 4
C
Pax2
Olig2/DAPI
D
p = 0.0448
p = 0.0004
p = 0.0020
# of Pax2+ Cells
CTR n = 8
MUT n = 5
M0 n = 5
p = 0.0023
p = 0.0001
p < 0.0001
# of Olig2+ Cells
CTR n = 6
MUT n = 5
M0 n = 3
E
Control
Nf1hGFAPCKO
p-Erk
p-Erk/Olig2
F
p = 0.030
# of p-Erk+ cells
CTR n = 4
MUT n = 3
p < 0.0001
# of p-Erk+Olig2+ cells
CTR n = 4
MUT n = 3
G
td-Tomato
Tomato/Olig2
DIST
H
p = 0.0004
Tomato-
Tomato+
ns
Total Olig2+ Cells
CTR n = 5
MUT n = 3
p = 0.0126
Olig2+Tom+/Olig2+
CTR n = 5
MUT n = 3
I
Brain
Mek1/2 -/-
Eye
Proximal
Distal
III
Control
P0.5
GPs migration
Nf1hGFAPCKO
Mek/Erk signaling
Local APCs
(Erk/MAPK Independent)
Migrating GPs
(Erk/MAPK dependent)

Figure 2. Migrating *Nf1*$^{-/-}$ BLBP^{+} cells cause initial expansion in the distal ON.

(A) Immunofluorescent co-labeling of BLBP, Olig2 and Pax2 expression in the P0.5 distal ON. Arrows mark the BLBP^{+}Pax2^{+}Olig2^{+} triple-positive cells.

(B) The number of BLBP^{+} cells in the P0.5 distal ON was quantified.

(C and D) Expression and quantification of Pax2 or Olig2 in the P0.5 distal ON.

(E and F) Expression and quantification of p-Erk and Olig2 in the P0.5 distal ON. Arrows mark p-Erk^{+} and p-Erk^{+}Olig2^{+} double-positive cells.

(G and H) Expression and quantification of td-Tomato and Olig2 in the P0.5 distal ON. Arrows and arrowheads mark td-Tomato^{+}Olig2^{+}and td-Tomato^{-}Olig2^{+} cells, respectively.

(I) Schematic summary of the impact of different levels of Mek-Erk signaling on migrating GPs.

All the quantification data are presented as mean ± SEM. Unpaired, two-tailed Student's t-test was used for statistical analysis. ns: not significant. VB: Ventral Brain; III: Third Ventricle; ON: optic nerve; APC: Astrocyte Precursor Cell; GP: Glial Progenitor; CTR: control group; MUT: *Nf1*^{hGFAP}CKO mutant group; M0: *Mek*1/2 double-knockout group. Scale bar: 50 μm.

Figure 3

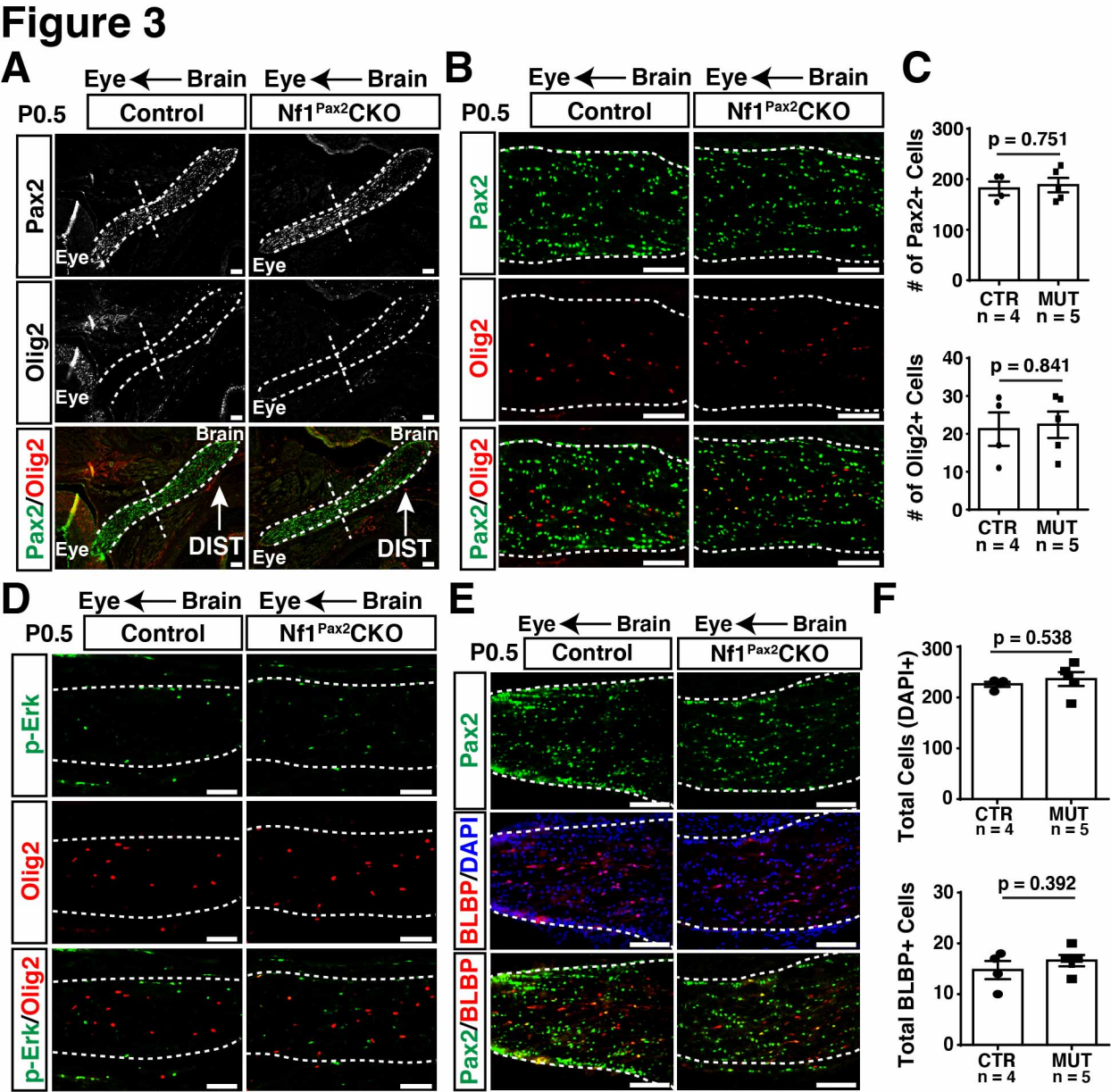
A
Eye ← Brain
Eye ← Brain
P0.5
Control
Nf1Pax2CKO
Pax2
Olig2
Pax2/Olig2
Eye
Brain
DIST
B
Eye ← Brain
Eye ← Brain
P0.5
Control
Nf1Pax2CKO
Pax2
Olig2
Pax2/Olig2
C
# of Pax2+ Cells
p = 0.751
300
200
100
0
CTR
n = 4
MUT
n = 5
# of Olig2+ Cells
p = 0.841
40
30
20
10
0
CTR
n = 4
MUT
n = 5
D
Eye ← Brain
Eye ← Brain
P0.5
Control
Nf1Pax2CKO
p-Erk
Olig2
p-Erk/Olig2
E
Eye ← Brain
Eye ← Brain
P0.5
Control
Nf1Pax2CKO
Pax2
BLBP/DAPI
Pax2/BLBP
F
Total Cells (DAPI+)
p = 0.538
300
200
100
0
CTR
n = 4
MUT
n = 5
Total BLBP+ Cells
p = 0.392
30
20
10
0
CTR
n = 4
MUT
n = 5

Figure 3. No abnormality in the ON of the *Nf1*^{Pax2}CKO model at P0.5.

(A-C) Representative colabeling of Pax2 and Olig2 in the entire (A) and distal (B) ON of control and *Nf1*^{Pax2}CKO mice at P0.5. Quantification of Pax2^{+} and Olig2^{+} cells is shown (C). Dashed lines indicate the forefront of migrating Olig2^{+} cells and the boundary of the ON. DIST indicates the distal portion of the ON.

(D) Immunofluorescent colabeling of p-Erk^{+} and Olig2^{+} in the distal ON of control and *Nf1*^{Pax2}CKO mice at P0.5.

(E and F) The distal ON of P0.5 control and Nf1^{Pax2}CKO mice were co-labeled with Pax2 and BLBP (E). The total cell number and BLBP^{+} number was quantified (F).

All the quantification data are presented as mean ± SEM. Unpaired, two-tailed Student's t test was used for statistical analysis. ns: not significant. CTR: control group; MUT: mutant group. Scale bar: 50 μm.

Figure 4

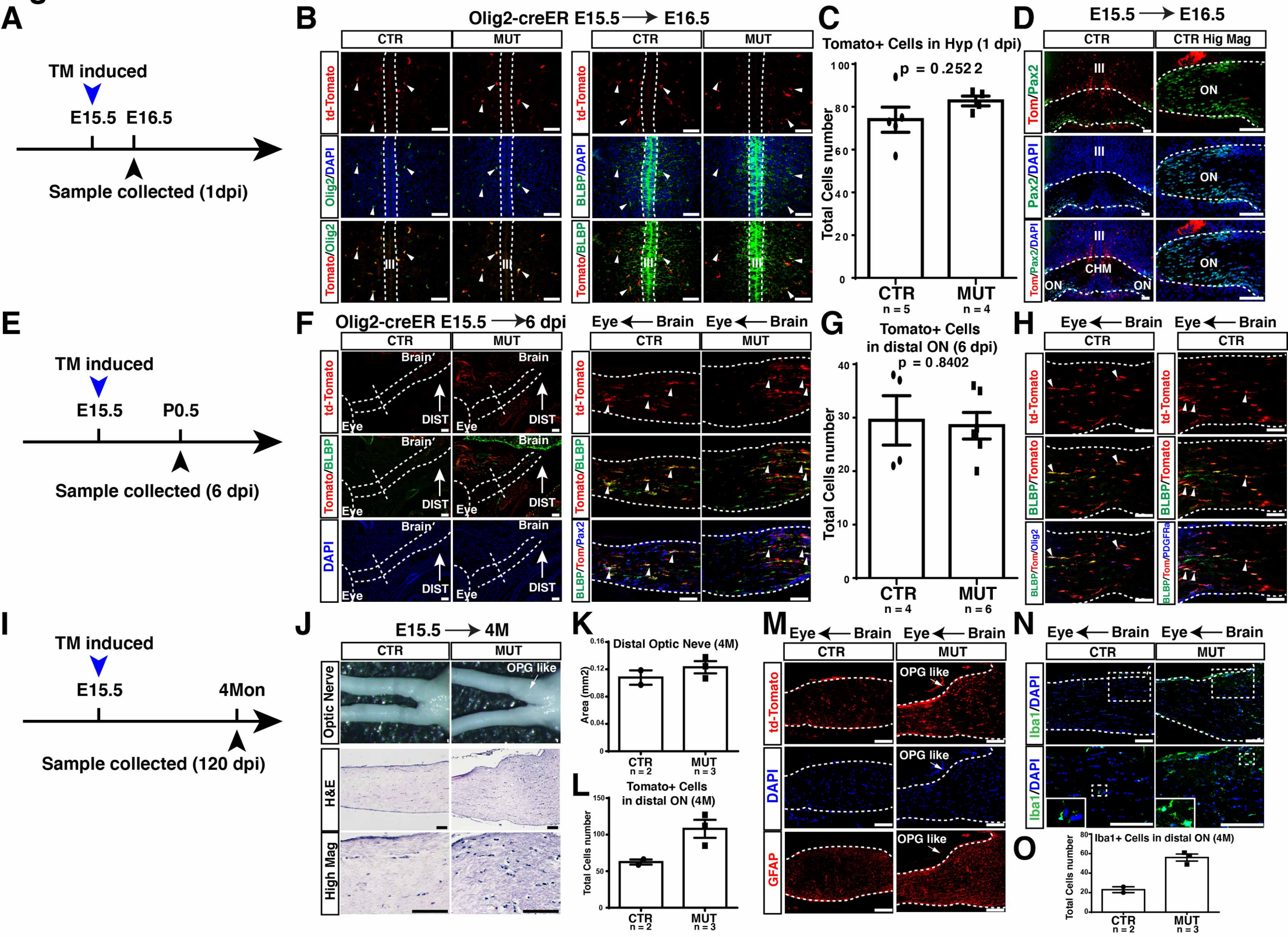
A
TM induced
E15.5 E16.5
Sample collected (1dpi)
B
Olig2-creER E15.5 → E16.5
CTR
MUT
td-Tomato
Olig2/DAPI
Tomato/Olig2
BLBP/DAPI
Tomato/BLBP
III
C
Tomato+ Cells in Hyp (1 dpi)
p = 0.2522
Total Cells number
CTR
MUT
n = 5
n = 4
D
E15.5 → E16.5
CTR
CTR Hig Mag
Tom/Pax2
Pax2/DAPI
Tom/Pax2/DAPI
III
ON
CHM
E
TM induced
E15.5 P0.5
Sample collected (6 dpi)
F
Olig2-creER E15.5 → 6 dpi
Eye ← Brain
CTR
MUT
td-Tomato
Tomato/BLBP
DAPI
BLBP/Tom/Pax2
Brain
Eye
DIST
G
Tomato+ Cells
in distal ON (6 dpi)
p = 0.8402
Total Cells number
CTR
MUT
n = 4
n = 6
H
Eye ← Brain
CTR
td-Tomato
BLBP/Tomato
BLBP/Tom/Olig2
BLBP/Tom/PDGFRa
I
TM induced
E15.5 4Mon
Sample collected (120 dpi)
J
E15.5 → 4M
CTR
MUT
Optic Nerve
H&E
High Mag
OPG like
K
Distal Optic Neve (4M)
Area (mm2)
CTR
MUT
n = 2
n = 3
L
Tomato+ Cells
in distal ON (4M)
Total Cells number
M
Eye ← Brain
td-Tomato
DAPI
GFAP
OPG like
N
Iba1/DAPI
O
Iba1+ Cells in distal ON (4M)
Total Cells number

Figure 4. Targeting Nf1 in migrating glial progenitors by using inducible Olig2-creER driver.

(A, E, I) Schematic drawing of the tamoxifen (TM) inducible schedules by days post injection (dpi), one-day (A), 6-day (E) and long-term (4 months) (I), respectively.

(B and C) Control and mutant heads 1dpi were collected, sectioned and subjected to immunofluorescent staining by td-Tomato and Olig2 or td-Tomato and BLBP (B). The targeted cells labeled by Tomato+ cells in the hypothalamic regions were quantified (C). Arrowheads label double-positive cells (B).

(D) Sections from the optic chiasm and optic nerve (ON) were stained by td-Tomato and Pax2. No targeted Tomato+ cells were observed in the E16.5 ON 1 dpi.

(F-H) Sections of the ONs from control and mutant heads 6 dpi were subjected to immunofluorescent staining by td-Tomato, BLBP and Pax2. The targeted cells in the ON were quantified (G). White dashed lines highlight the boundary of the eye, ON and migratory front of BLBP+ cells in the distal ON (arrows, DIST). Arrowheads point to the double- or triple-positive targeted cells.

(J-N) Whole-mount images of control and mutant ONs were shown 4 months after TM induction, which were stained by H&E (J). The distal ON areas (K) and cellular density (L) were quantified. Sections from control and mutant distal ONs were subjected to immunofluorescent staining by td-Tomato and GFAP (M), and Iba1 (N), which was quantified in (O).

All the quantification data are presented as mean ± SEM. Unpaired, two-tailed Student's t test was used for statistical analysis. ns: not significant. CTR: control group; MUT: mutant group. Scale bar: 50 μm.

Figure 5

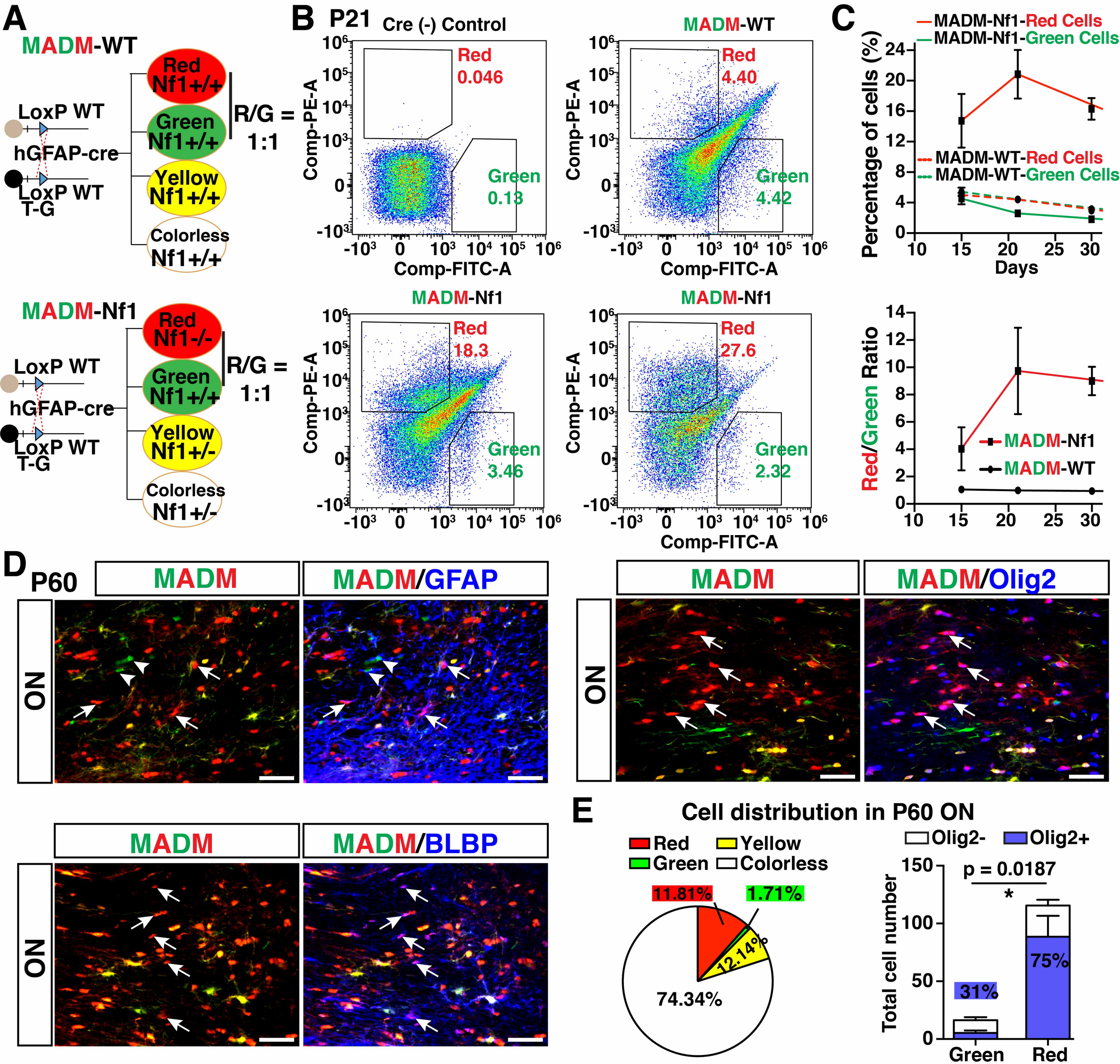
A
MADM-WT
Red Nf1+/+
Green Nf1+/+
Yellow Nf1+/+
Colorless Nf1+/+
R/G = 1:1
LoxP WT
hGFAP-cre
LoxP WT
T-G
MADM-Nf1
Red Nf1-/-
Green Nf1+/+
Yellow Nf1+/-
Colorless Nf1+/-
R/G = 1:1
LoxP WT
hGFAP-cre
LoxP WT
T-G
B P21
Cre (-) Control
Red 0.046
Green 0.13
MADM-WT
Red 4.40
Green 4.42
MADM-Nf1
Red 18.3
Green 3.46
MADM-Nf1
Red 27.6
Green 2.32
Comp-PE-A
Comp-FITC-A
C
MADM-Nf1-Red Cells
MADM-Nf1-Green Cells
MADM-WT-Red Cells
MADM-WT-Green Cells
Percentage of cells (%)
Days
Red/Green Ratio
MADM-Nf1
MADM-WT
D P60
MADM
MADM/GFAP
MADM/Olig2
MADM/BLBP
ON
E
Cell distribution in P60 ON
Red
Yellow
Green
Colorless
11.81%
1.71%
12.14%
74.34%
Olig2-
Olig2+
p = 0.0187
*
Total cell number
31%
75%
Green
Red

Figure 5. MADM-based model validates the role of *Nf1* in inducing abnormal microglial infiltration and forming the Nf1-OPG.

(A) Schematic of the MADM-WT and MADM-Nf1 model under the hGFAP-cre driver.

(B and C) FACS analysis of GFP- and RFP-positive cells in the ON from P15, P21 and P30 mice. Representative FACS images show the distribution of red and green cells from the ON of P21 one control, one MADM-WT, and two MADM-Nf1 mice (B). The percentage of red or green among total cells were quantified and the R/G ratio is shown (C).

(D) Representative images with co-labeling of GFP/RFP (left panels) with additional GFAP, BLBP or Olig2 staining (right panels) from the distal ON of P60 MADM-Nf1 mice. Green cells were marked by arrowheads, which often expressed GFAP, but not Olig2 or BLBP. In contrast, greatly expanded red cells were marked by arrows, which frequently expressed Olig2 and BLBP.

(E) The distribution of the red, green, yellow and colorless (DAPI only) cells in the ON of P60 MADM-Nf1 mice (n = 4) is shown. The percentage of Olig2+ cells within the red and green cell compartments was quantified. Scale bars: 50 μm.

Figure 6

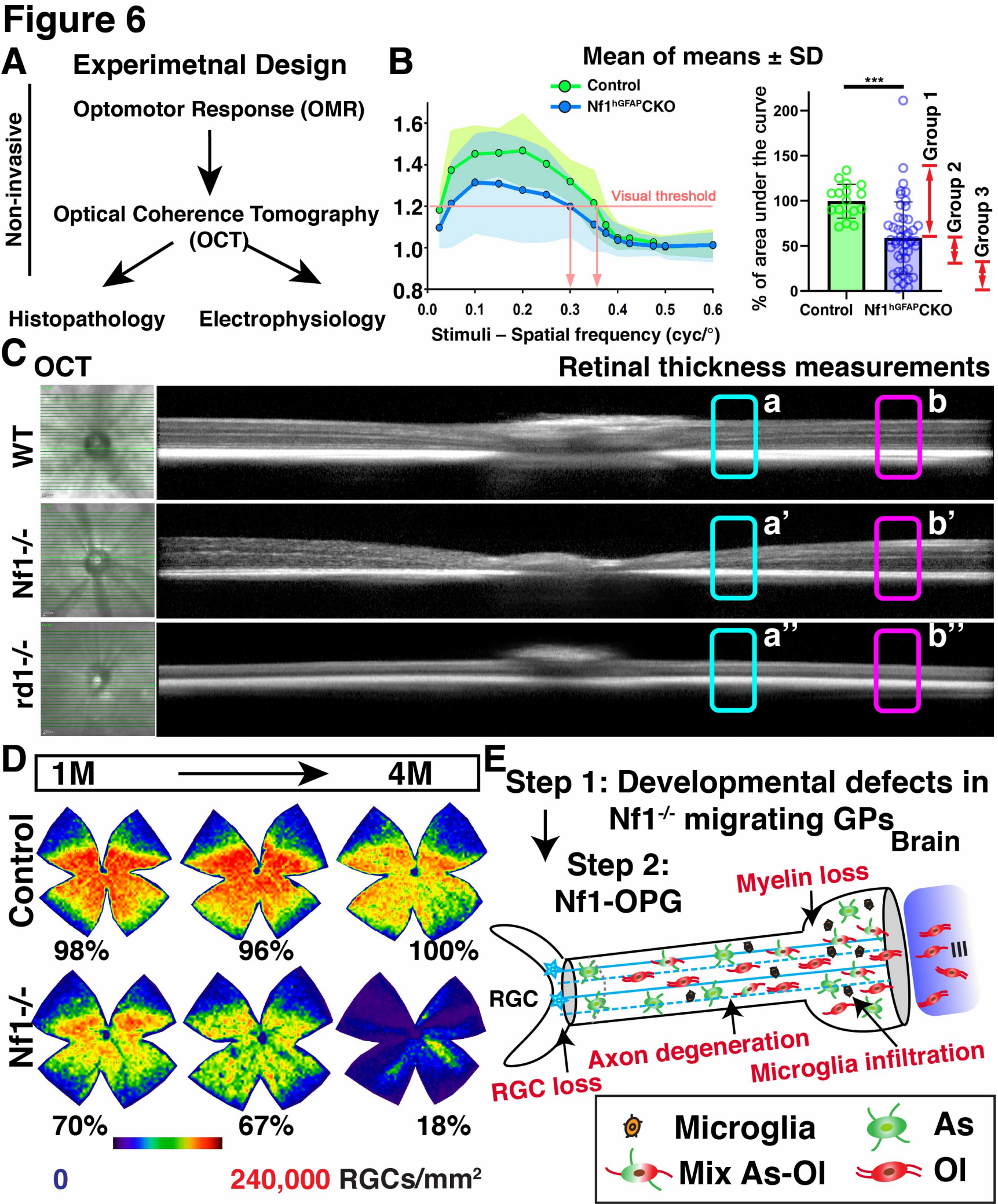
A
Experimetnal Design
Non-invasive
Optomotor Response (OMR)
Optical Coherence Tomography (OCT)
Histopathology
Electrophysiology
B
Mean of means ± SD
Control
Nf1hGFAPCKO
Visual threshold
Stimuli – Spatial frequency (cyc/°)
% of area under the curve
***
Group 1
Group 2
Group 3
Control
Nf1hGFAPCKO
C
OCT
Retinal thickness measurements
WT
Nf1-/-
rd1-/-
a
b
a'
b'
a''
b''
D
1M
4M
Control
Nf1-/-
98%
96%
100%
70%
67%
18%
0
240,000 RGCs/mm²
E
Step 1: Developmental defects in Nf1-/- migrating GPs
Brain
Step 2: Nf1-OPG
Myelin loss
RGC
Axon degeneration
Microglia infiltration
RGC loss
Microglia
As
Mix As-Ol
Ol

Figure 6. Visual/behavioral, anatomical/imaging and histological analysis of control OPG-bearing ONs and retinas in the *Nf1*^{hGFAP}CKO model.

(A) Experimental design of using both non-invasive and invasive assays.

(B) Ratio of the correct versus the incorrect head movement plotted over stimulus spatial frequency in wildtype (WT, left upper panel) and *Nf1*^{hGFAP}CKO mice (Nf1-/-, left lower panel). An average of the ratio of the correct vs the incorrect head movement in WT (left upper panel) and Nf1-/- mice (right panel) is quantified (right). Phenotypic variations among *Nf1*^{hGFAP}CKO mice were observed and classified into three groups.

(C) OCT images of from a wildtype, an Nf1-/-, and a retinal degeneration 1 (rd1-/-, as a control for loss of RGCs) mouse showing changes of retinal thickness in parapapillary and peripheral regions.

(D) Whole-mount preparation of retinas from age-matched littermate control and *Nf1*^{hGFAP}CKO mice reveals different patterns of retinal ganglion cell (RGC) loss caused by OPGs in different *Nf1*^{hGFAP}CKO mice**.**

(E) A model summarizes the pathogenic sequence of NF1-OPG formation: (1) developmental defects in migrating progenitors and (2) subsequent immune responses of increased microglial infiltration and activation, axonal/myelin degeneration and RGC loss.

Figure 7

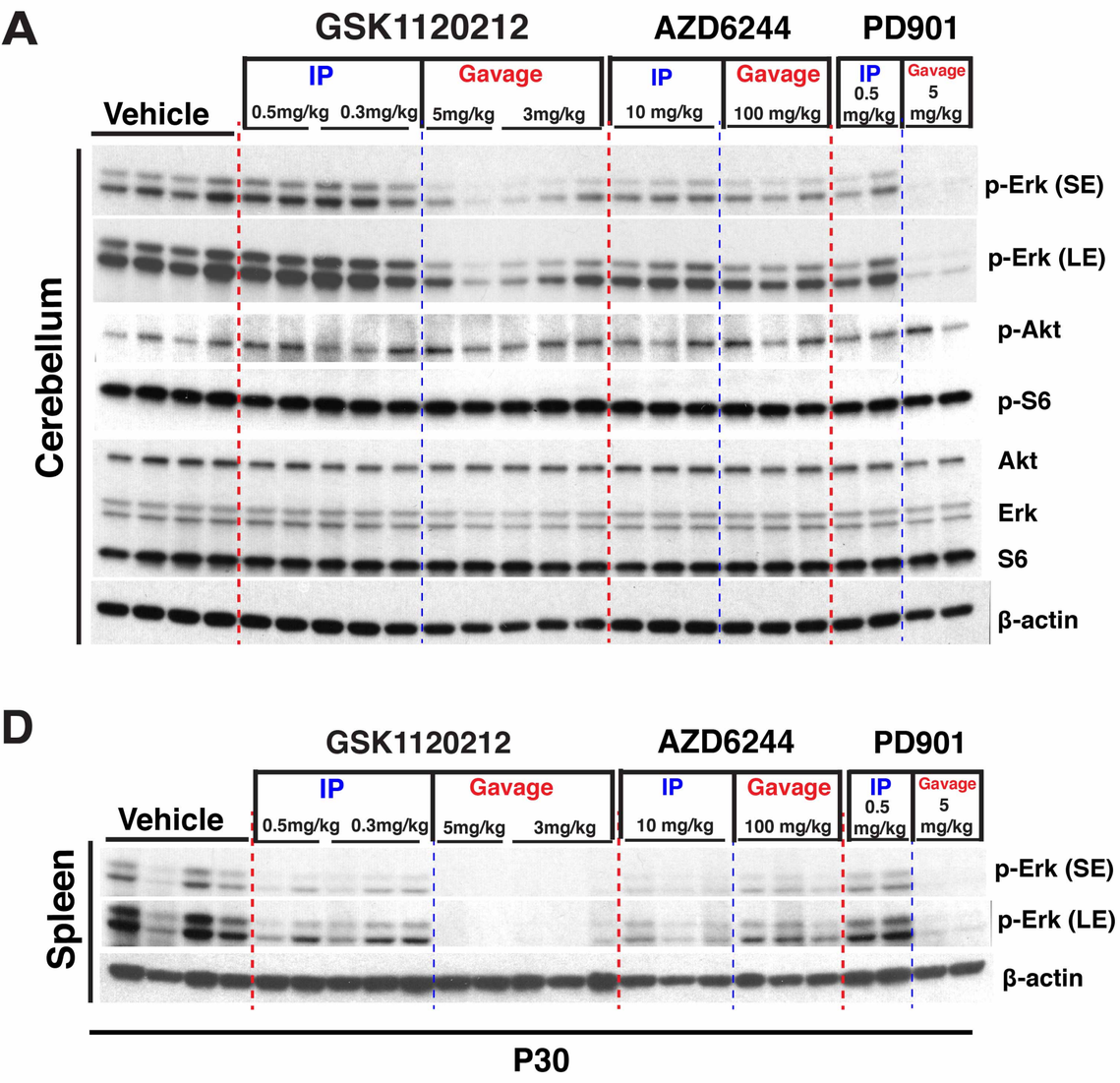
A
GSK1120212
AZD6244
PD901
IP
Gavage
Vehicle
0.5mg/kg
0.3mg/kg
5mg/kg
3mg/kg
10 mg/kg
100 mg/kg
0.5 mg/kg
5 mg/kg
Cerebellum
p-Erk (SE)
p-Erk (LE)
p-Akt
p-S6
Akt
Erk
S6
β-actin
D
Spleen
P30

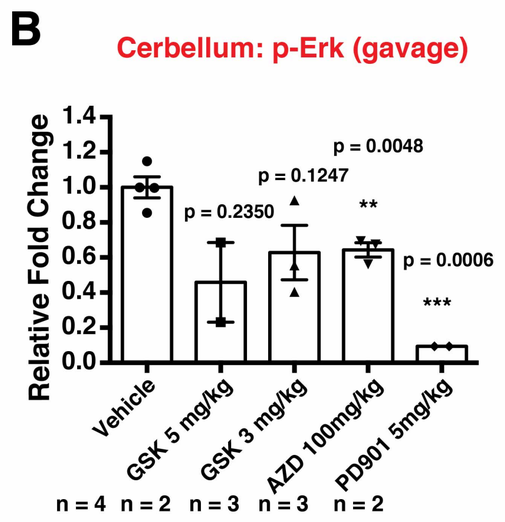
B
Cerebellum: p-Erk (gavage)
Relative Fold Change
p = 0.2350
p = 0.1247
p = 0.0048
p = 0.0006
**
***
Vehicle
GSK 5 mg/kg
GSK 3 mg/kg
AZD 100mg/kg
PD901 5mg/kg
n = 4 n = 2 n = 3 n = 3 n = 2

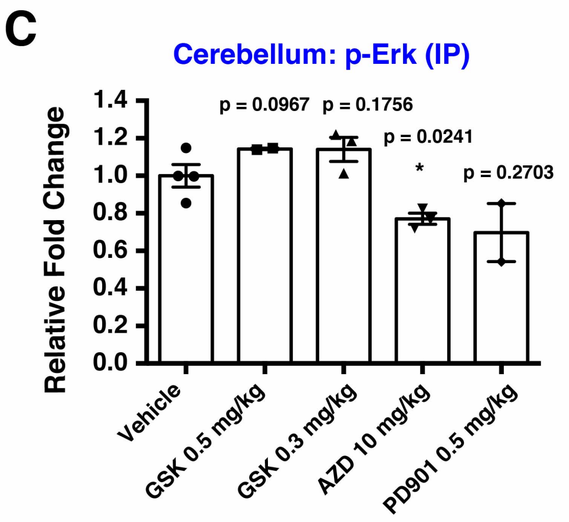
C
Cerebellum: p-Erk (IP)
Relative Fold Change
p = 0.0967
p = 0.1756
p = 0.0241
p = 0.2703
Vehicle
GSK 0.5 mg/kg
GSK 0.3 mg/kg
AZD 10 mg/kg
PD901 0.5 mg/kg

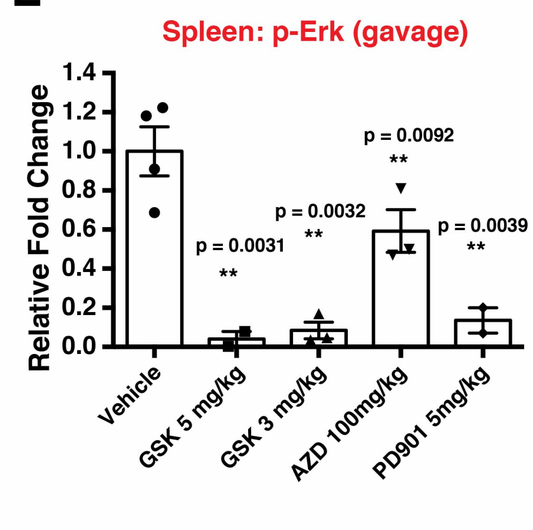
E
Spleen: p-Erk (gavage)
Relative Fold Change
p = 0.0031
p = 0.0032
p = 0.0092
p = 0.0039
Vehicle
GSK 5 mg/kg
GSK 3 mg/kg
AZD 100mg/kg
PD901 5mg/kg

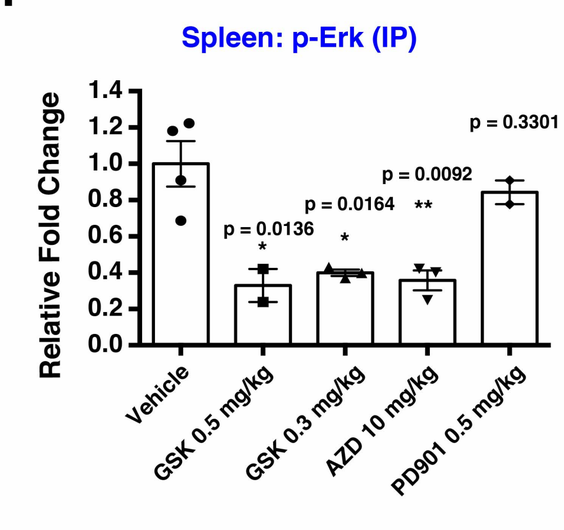
F
Spleen: p-Erk (IP)
Relative Fold Change
p = 0.0136
p = 0.0164
p = 0.0092
p = 0.3301
Vehicle
GSK 0.5 mg/kg
GSK 0.3 mg/kg
AZD 10 mg/kg
PD901 0.5 mg/kg

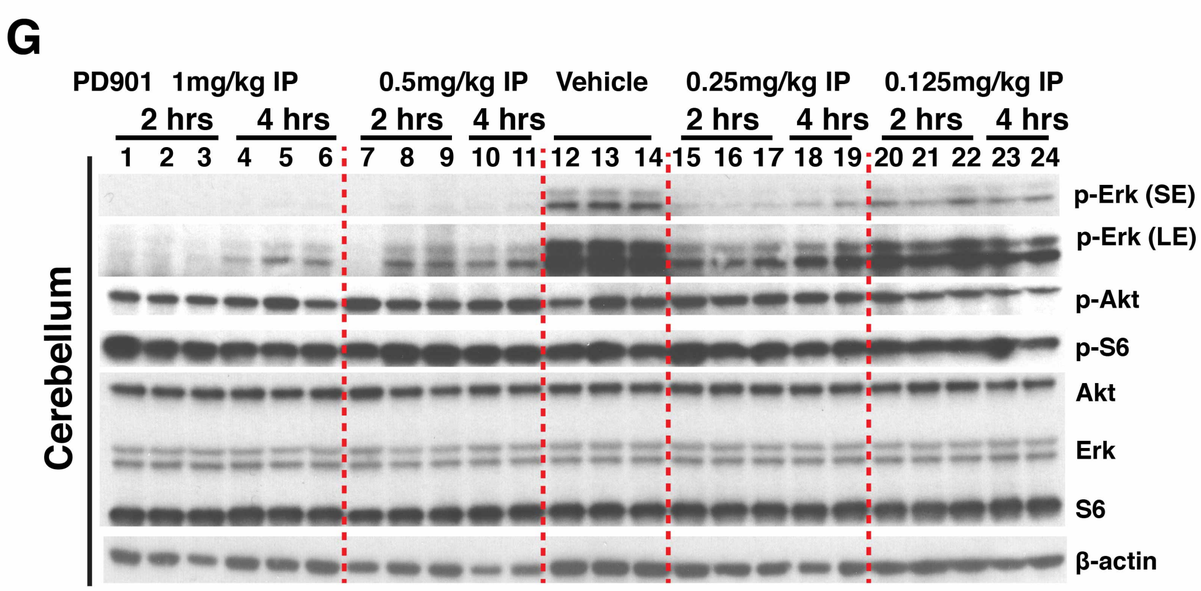
G
PD901 1mg/kg IP
0.5mg/kg IP
Vehicle
0.25mg/kg IP
0.125mg/kg IP
2 hrs
4 hrs
1 2 3 4 5 6 7 8 9 10 11 12 13 14 15 16 17 18 19 20 21 22 23 24
Cerebellum
p-Erk (SE)
p-Erk (LE)
p-Akt
p-S6
Akt
Erk
S6
β-actin

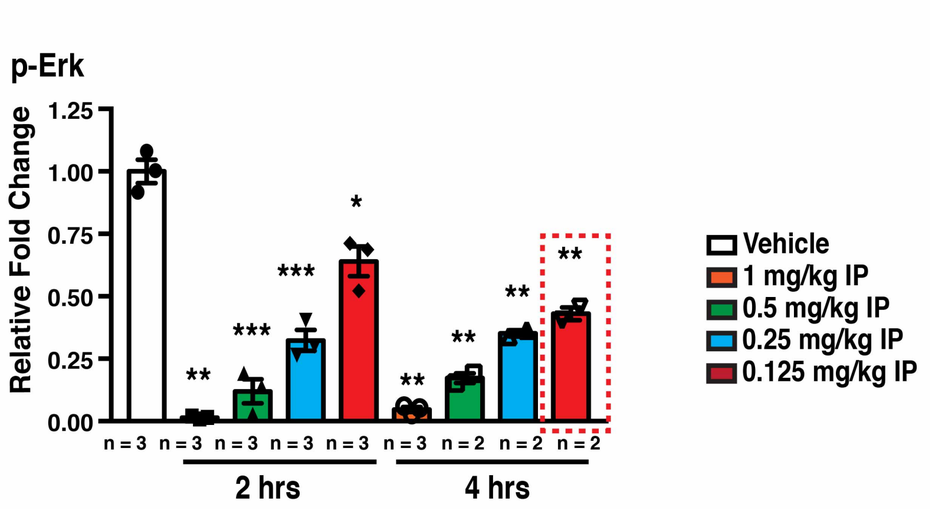
H
p-Erk
Relative Fold Change
n = 3 n = 3 n = 3 n = 3 n = 3 n = 3 n = 2 n = 2 n = 2
2 hrs
4 hrs
Vehicle
1 mg/kg IP
0.5 mg/kg IP
0.25 mg/kg IP
0.125 mg/kg IP

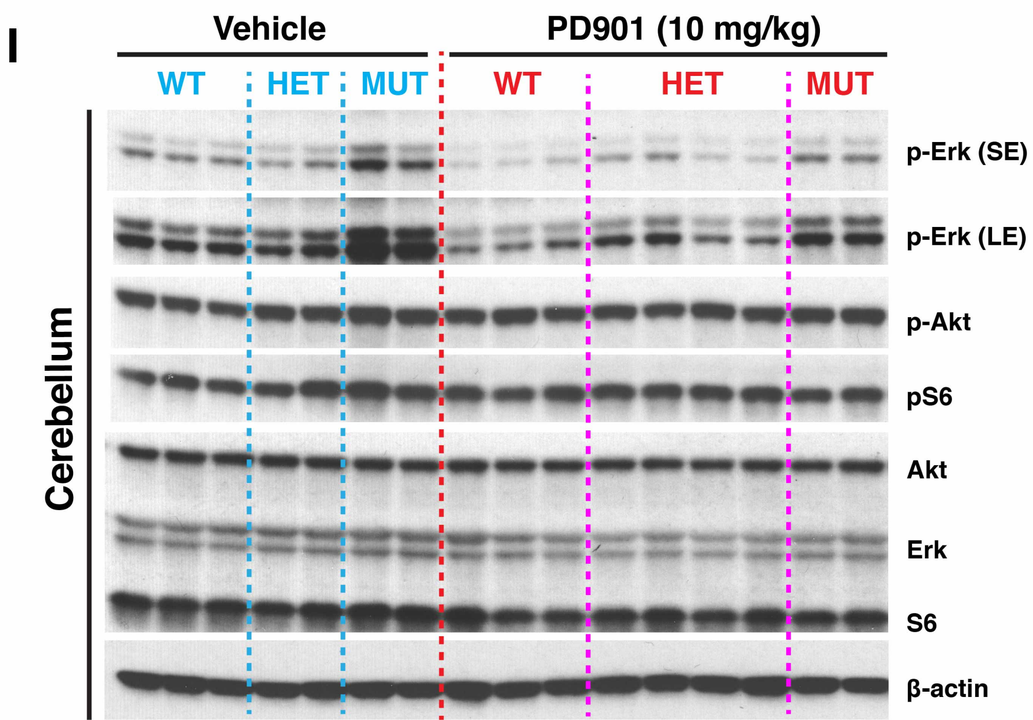
I
Vehicle
PD901 (10 mg/kg)
WT
HET
MUT
Cerebellum
p-Erk (SE)
p-Erk (LE)
p-Akt
pS6
Akt
Erk
S6
β-actin

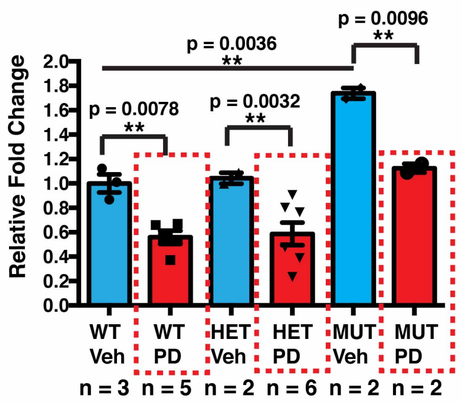
J
p-Erk
Relative Fold Change
p = 0.0078
p = 0.0032
p = 0.0036
p = 0.0096
WT Veh
WT PD
HET Veh
HET PD
MUT Veh
MUT PD
n = 3 n = 5 n = 2 n = 6 n = 2 n = 2

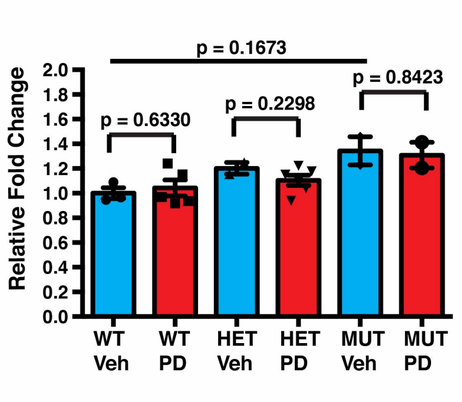
K
p-Akt
Relative Fold Change
p = 0.6330
p = 0.2298
p = 0.1673
p = 0.8423
WT Veh
WT PD
HET Veh
HET PD
MUT Veh
MUT PD

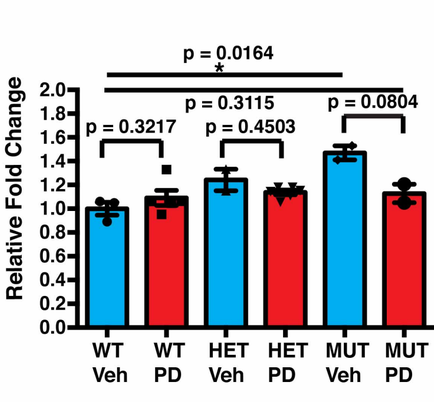
L
p-S6
Relative Fold Change
p = 0.3217
p = 0.4503
p = 0.3115
p = 0.0804
p = 0.0164
WT Veh
WT PD
HET Veh
HET PD
MUT Veh
MUT PD

Figure 7. MEK inhibition studies in the brain.

(A-F) P30 wild-type mice were treated by oral gavage or IP injection with a single dose of different MEKis. Oral gavage was used to administer GSK (5 or 3 mg/kg of body weight (BW)), AZD (100 mg/kg BW) and PD901 (5 mg/kg BW). IP injection was used to administer GSK (0.5 or 0.3 mg/kg BW), AZD (10 mg/kg BW) and PD901 (0.5 mg/kg BW). Mice were sacrificed 4-6 hours (hrs) after treatment. Western blot (WB) analysis was performed on whole cerebellar lysates (A) and spleen lysates (D) from treated mice to investigate Nf1-associated Erk activation, as well as other RTK-associated pathways, Akt and S6. Quantification of the relative fold change in p-Erk level for each MEKi in the cerebellum (B and C) and the spleen (E and F) was performed. Results were normalized against vehicle-treated wild-type. Each lane represents a sample from an individual animal.

(G and H) Western blot analysis was performed on cerebella of P8 wild-type pups treated with PD901 at different doses via IP injection and collected at 2hrs and 4hrs after treatment (G). Quantification of the relative fold change in p-Erk level in the cerebellum of treated pups compared to untreated littermate controls after treatment (H). Each lane represents a sample from an individual animal.

(I-L) Western blot analysis of cerebella of P8 pups from different genotypes (WT, HET, MUT) treated with either vehicle (blue) or 10 mg/kg PD901 (red) via “MEKi in the milk” protocol (I). Quantification of the relative fold change in p-Erk (J), p-Akt (K) p-S6 (L) in vehicle and PD treated cerebella.

All the quantifications are presented as mean ± SEM. Unpaired, two-tailed Student’s t test was used for statistical analysis. Asterisks denote statistically significant differences (** $p < 0.01$, *** $p < 0.001$). SE: short exposure, LE: long exposure, IP: intraperitoneal injection, WT: wild-type, HET: Nf1 heterozygous, MUT: Nf1 mutant.

Figure 8

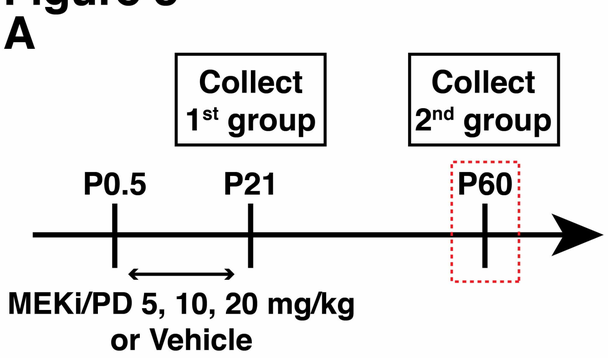
A
Collect 1st group
Collect 2nd group
P0.5
P21
P60
MEKi/PD 5, 10, 20 mg/kg or Vehicle

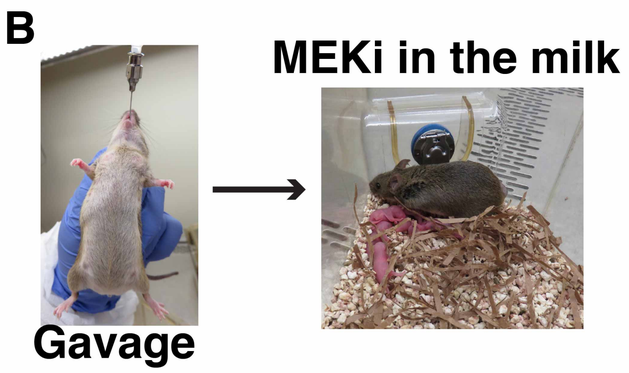
B
Gavage
MEKi in the milk

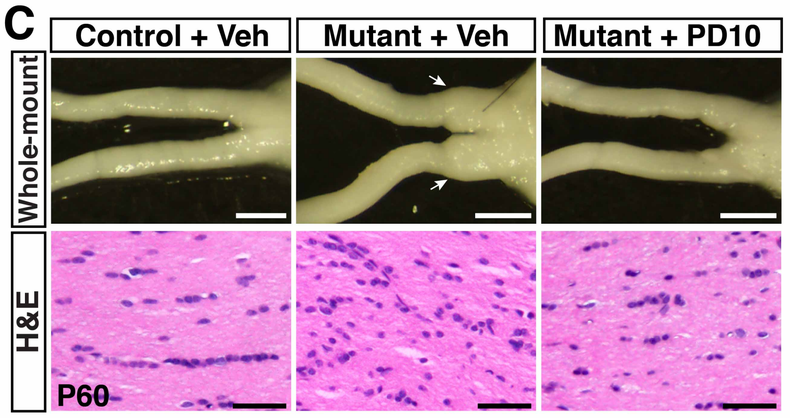
C
Control + Veh
Mutant + Veh
Mutant + PD10
Whole-mount
H&E
P60

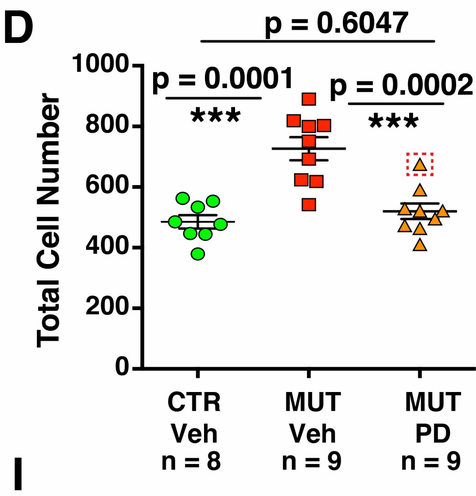
D
p = 0.6047
p = 0.0001
***
p = 0.0002
***
Total Cell Number
1000
800
600
400
200
0
CTR Veh n = 8
MUT Veh n = 9
MUT PD n = 9

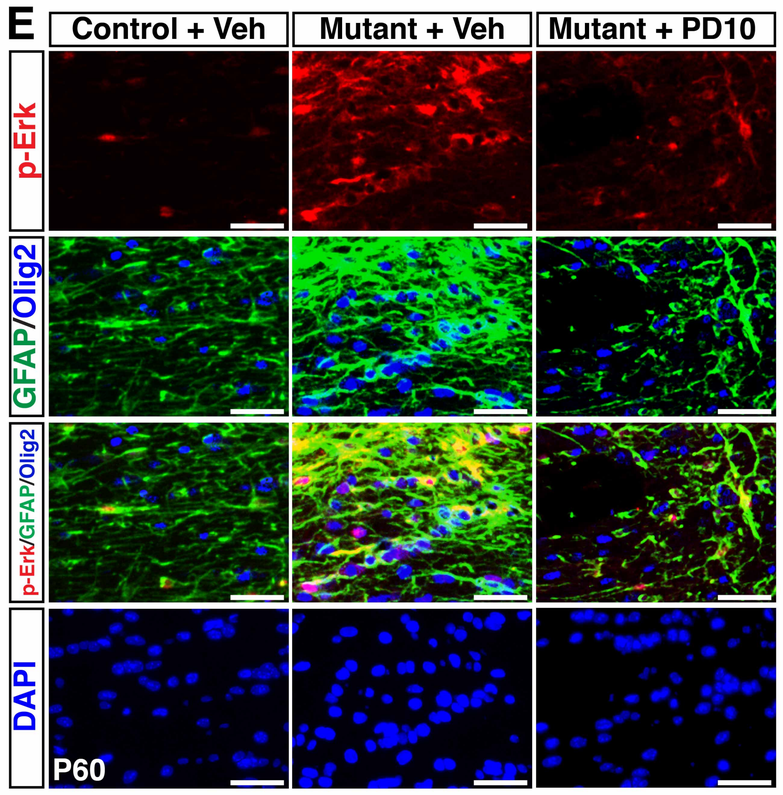
E
Control + Veh
Mutant + Veh
Mutant + PD10
p-Erk
GFAP/Olig2
p-Erk/GFAP/Olig2
DAPI
P60

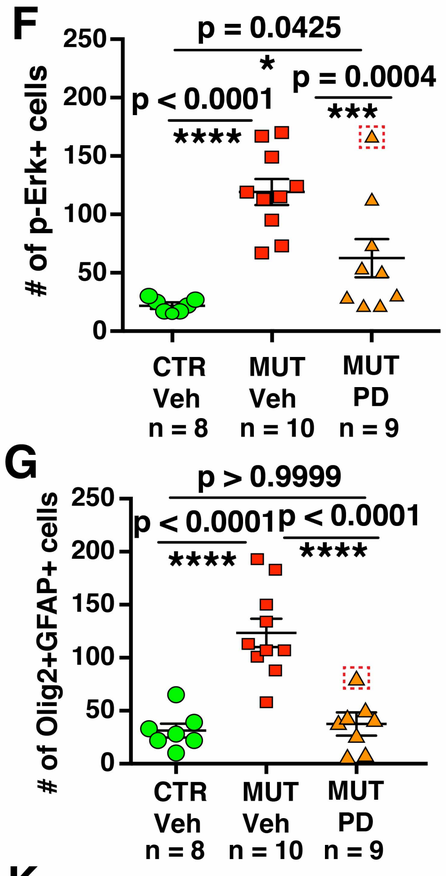
F
p = 0.0425
*
p < 0.0001
****
p = 0.0004
***
# of p-Erk+ cells
250
200
150
100
50
0
CTR Veh n = 8
MUT Veh n = 10
MUT PD n = 9

G
p > 0.9999
p < 0.0001
****
p < 0.0001
****
# of Olig2+GFAP+ cells
250
200
150
100
50
0
CTR Veh n = 8
MUT Veh n = 10
MUT PD n = 9

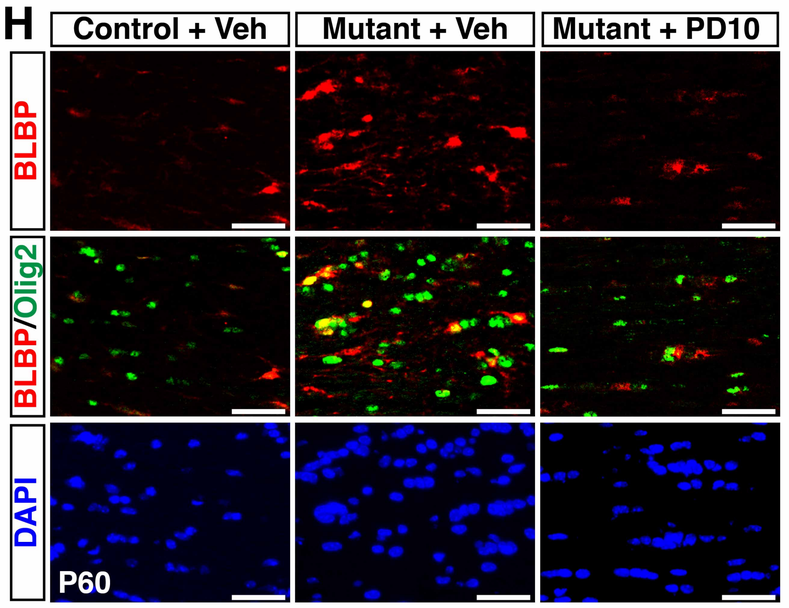
H
Control + Veh
Mutant + Veh
Mutant + PD10
BLBP
BLBP/Olig2
DAPI
P60

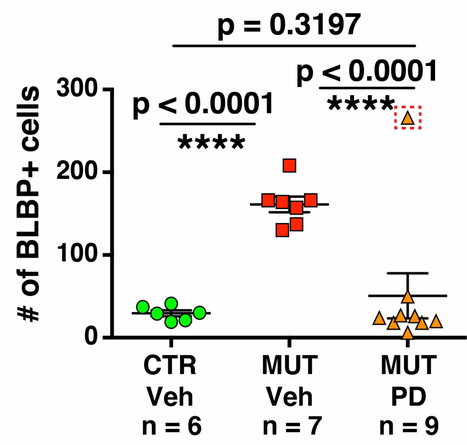
I
p = 0.3197
p < 0.0001
****
p < 0.0001
****
# of BLBP+ cells
300
200
100
0
CTR Veh n = 6
MUT Veh n = 7
MUT PD n = 9

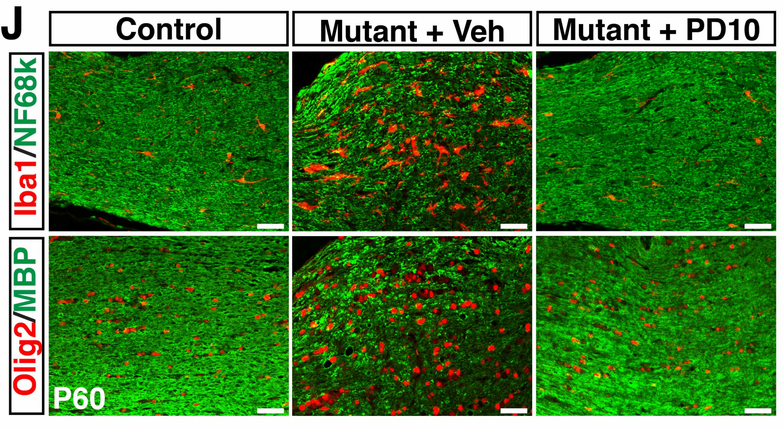
J
Control
Mutant + Veh
Mutant + PD10
Iba1/NF68k
Olig2/MBP
P60

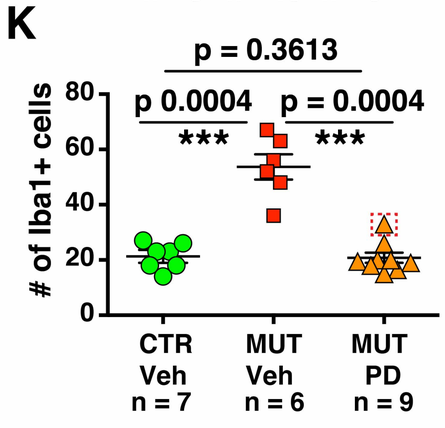
K
p = 0.3613
p 0.0004
***
p = 0.0004
***
# of Iba1+ cells
80
60
40
20
0
CTR Veh n = 7
MUT Veh n = 6
MUT PD n = 9

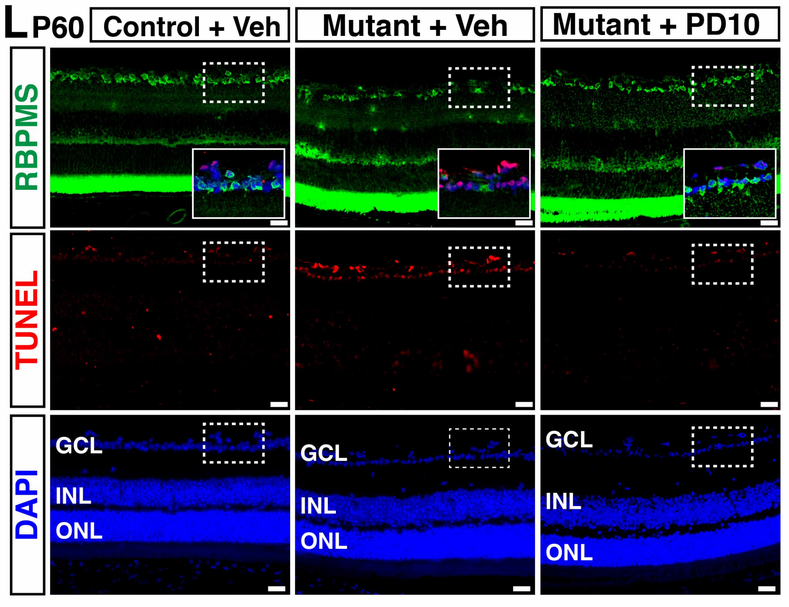
L
P60
Control + Veh
Mutant + Veh
Mutant + PD10
RBPMS
TUNEL
DAPI
GCL
INL
ONL

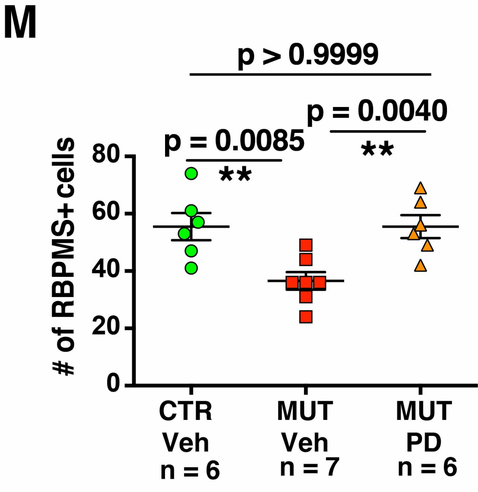
M
p > 0.9999
p = 0.0085
**
p = 0.0040
**
# of RBPMS+ cells
80
60
40
20
0
CTR Veh n = 6
MUT Veh n = 7
MUT PD n = 6

N
Hypothalamus
~E15.5
P0.5
P15
P21
P60
Aged (> 4m)
Disrupt the balance between stem-cell maintenance and gliogenesis, decrease hVZ-RGs and increase hMZ-RGs
Optic Nerve (Nf1-OPG)
Increase number of BLBP+ Migrating GPs, migratory GPs acquire Pax2+ in the distal ON
Increase gliogenesis, persistence of BLBP+ GPs, mixed OPC-APC characteristics
Microglia (WT) infiltration and activation
Myelin loss, axon degeneration and RGC (WT) loss
MEKi-in-milk
PD (~0.125 mg/kg)
Efficacy
Vision
Visual loss
Reversible
Irreversible

Figure 8. The transient MEKi treatment prevents OPG formation.

(A) Experimental design of the P0.5-P21 “MEKi-in-milk” treatment protocol with different doses. Cohorts of vehicle or MEKi-treated mice were collected at either P21 (4hrs after last treatment) or P60 (around 40 days after last treatment) for short- and long-term analysis, respectively.

(B) The “MEKi-in-milk” strategy delivers MEKi into newborn pups via lactating females.

(C and D) Whole-mount images and H&E-stained sections of the distal ON from P60 vehicle (VEH) and MEKi (10 mg/kg PD0325901, PD10) treated control and *Nf1*^{hGFAP}CKO mice (C). The total cell number in the distal ON was quantified (D).

(E-G) Co-labeling and quantification of p-Erk, Olig2 and GFAP in the distal ON of P60 vehicle- and MEKi-treated control and *Nf1*^{hGFAP}CKO mice.

(H and I) Co-labeling and quantification of BLBP and Olig2 in the distal ON of P60 vehicle- and MEKi-treated control and *Nf1*^{hGFAP}CKO mice.

(J and K) Representative images with co-labeling of Iba1/NF68k or Olig2/MBP in the distal ON of P60 vehicle- and MEKi-treated control and *Nf1*^{hGFAP}CKO mice (J). The number of Iba1^{+} microglia was quantified (K).

(L and M) Representative images with co-labeling of RBPMS and TUNEL in the retinas of P60 vehicle- and MEKi-treated control and *Nf1*^{hGFAP}CKO mice (L). The number of RBPMS^{+} RGCs was quantified (M). High magnification images of the boxed areas (L) are presented as insets.

(N) A model for the pathogenic sequence of NF1-OPG formation and the potential efficacy of therapeutic strategies delivered at different disease stages.

The data point highlighted in the boxed area in panels (D, F, G, I, K and M) indicate the only non-rescued MEKi-treated *Nf1*^{hGFAP}CKO mouse. All the quantifications are presented as mean ± SEM. Unpaired, two-tailed Student’s t-test was used for statistical analysis. MEKi: MEK inhibitor; GCL: ganglion cell layer; INL: inner nuclear layer; ONL: outer nuclear layer; hVZ-RG: hypothalamic ventricular zone radial glia; GP: Glial Progenitor; APC: Astrocyte Precursor Cell; OPC: Oligodendrocyte Precursor Cell; III-VZ: third ventricular zone; MZ: mantle zone. Scale bar: 50 μm.

Article

Developmental Cell

Treatment during a developmental window prevents NF1-associated optic pathway gliomas by targeting Erk-dependent migrating glial progenitors

Graphical abstract

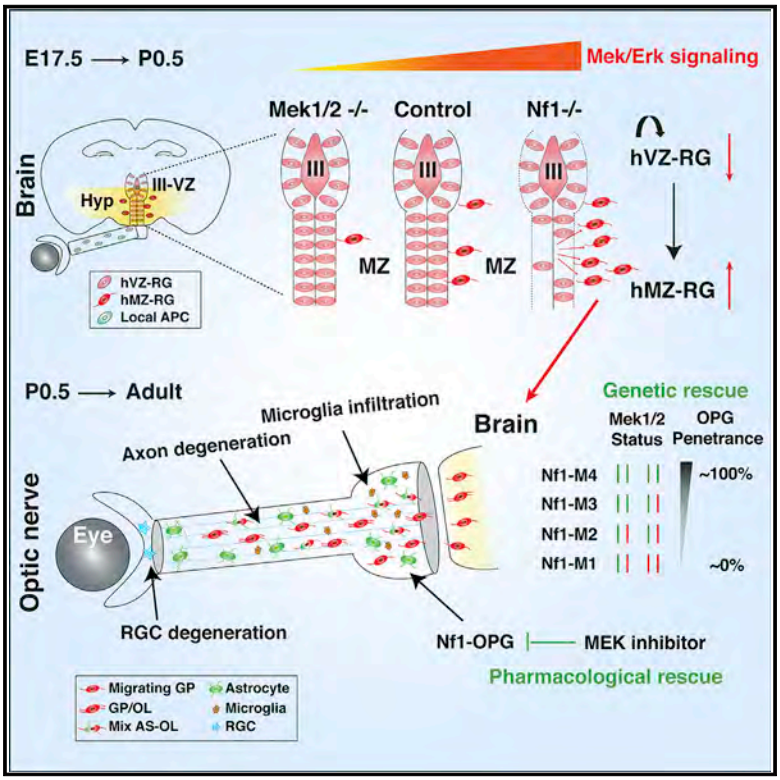

Highlights

- Migrating GPs, not local APCs, are Mek/Erk dependent and thus susceptible to Nf1 loss
- Nf1 is required to maintain the balance between stem-cell maintenance and gliogenesis
- Partial *Mek* loss normalizes differentiation of Nf1$^{-/-}$ migrating GPs and prevents NF1-OPG
- Transient neonatal low-dose MEKi treatment prevents NF1-OPG and neuronal degeneration

Authors

Emmanuelle S. Jecrois, Wang Zheng, Miriam Bornhorst, ..., Hui Zong, Roger J. Packer, Yuan Zhu

Correspondence

yzhu@childrensnational.org

In brief

The mechanism of vulnerability to pediatric low-grade gliomas during development remains unknown. Jecrois et al. demonstrate that NF1-OPG arise from the dependency of Mek-Erk/MAPK signaling during gliogenesis of developmentally transient migrating progenitors in the optic nerve. Transient post-natal treatment with a MEK inhibitor prevents NF1-OPG formation and retinal neuronal degeneration.

Jecrois et al., 2021, Developmental Cell *56*, 2871–2885
October 25, 2021
https://doi.org/10.1016/j.devcel.2021.08.004

CellPress

Developmental Cell

CellPress

Article

Treatment during a developmental window prevents NF1-associated optic pathway gliomas by targeting Erk-dependent migrating glial progenitors

Emmanuelle S. Jecrois,[1,2,3,4,9] Wang Zheng,[1,2,3,9] Miriam Bornhorst,[1,2,3,5,9] Yinghua Li,[1,2,3] Daniel M. Treisman,[1,2,3] Daphine Muguyo,[1,2,3] Sharon Huynh,[1,2,3] Shayne F. Andrew,[1,2,3] Yuan Wang,[1,2,3] Jingwen Jiang,[1,2,3] Brianna R. Pierce,[1,2,3] Hongmei Mao,[1,2,3] Matthew K. Krause,[1,2,3] Austin Friend,[1,2,3] Francisco Nadal-Nicolas,[6] Steven F. Stasheff,[1,6] Wei Li,[6] Hui Zong,[7] Roger J. Packer,[1] and Yuan Zhu[1,2,3,4,8,10,*]

[1]Gilbert Family Neurofibromatosis Institute, Children's National Hospital, Washington, DC 20010, USA
[2]Center for Cancer and Immunology Research, Children's National Hospital, Washington, DC 20010, USA
[3]Center for Neuroscience Research, Children's National Hospital, Washington, DC 20010, USA
[4]Neuroscience Graduate Program, University of Michigan Medical School, Ann Arbor, MI 48109, USA
[5]Center for Genetic Medicine Research, Children's National Hospital, Washington, DC 20010, USA
[6]Retinal Neurophysiology Section, National Eye Institute, National Institutes of Health, Bethesda, MD 20892, USA
[7]Department of Microbiology, Immunology, and Cancer Biology, University of Virginia, Charlottesville, VA 22908, USA
[8]GW Cancer Center, George Washington University, Washington, DC 20052
[9]These authors contributed equally
[10]Lead contact
*Correspondence: yzhu@childrensnational.org
https://doi.org/10.1016/j.devcel.2021.08.004

SUMMARY

The mechanism of vulnerability to pediatric low-grade gliomas (pLGGs)—the most common brain tumor in children—during development remains largely unknown. Using mouse models of neurofibromatosis type 1 (NF1)-associated pLGGs in the optic pathway (NF1-OPG), we demonstrate that NF1-OPG arose from the vulnerability to the dependency of Mek-Erk/MAPK signaling during gliogenesis of one of the two developmentally transient precursor populations in the optic nerve, brain-derived migrating glial progenitors (GPs), but not local progenitors. Hyperactive Erk/MAPK signaling by *Nf1* loss overproduced GPs by disrupting the balance between stem-cell maintenance and gliogenesis of hypothalamic ventricular zone radial glia (RG). Persistence of RG-like GPs initiated NF1-OPG, causing Bax-dependent apoptosis in retinal ganglion cells. Removal of three *Mek1/Mek2* alleles or transient post-natal treatment with a low-dose MEK inhibitor normalized differentiation of $Nf1^{-/-}$ RG-like GPs, preventing NF1-OPG formation and neuronal degeneration. We provide the proof-of-concept evidence for preventing pLGGs before tumor-associated neurological damage enters an irreversible phase.

INTRODUCTION

In addition to hereditary (H) and environmental (E) factors, replication (R) errors during stem/progenitor cell divisions lead to gradual accumulation of oncogenic driver events over time (Song et al., 2018; Tomasetti et al., 2017). This EHR model provides the mechanistic basis for the observation that the incidence of most cancers dramatically increases with age, as driver mutations occur by chance and accumulate. Pediatric tumors, or tumors that occur almost exclusively in children, are therefore a noteworthy deviation from this pattern (Song et al., 2018; Tomasetti et al., 2017). Brain tumors are the most common solid tumors in children, the most frequent of which are pediatric low-grade gliomas (pLGGs) (Jones et al., 2018; Packer et al., 2020). Most pLGGs are sporadic and driven by gain-of-function mutations in *BRAF*, an oncogene in the RAS-ERK/MAPK signaling pathway, predominantly caused by *KIAA1549-BRAF* fusions or, less frequently, by $BRAF^{V600E}$ point mutations (Ryall et al., 2020). The requirement of only one driver event—termed the one-hit model of tumorigenesis—to develop pLGGs is consistent with the high incidence in children. However, the rarity of pLGGs in adults implies the existence of a vulnerable developmental window during which transient stem/progenitor cell divisions in the central nervous system (CNS) randomly lead to replication errors, but only sufficiently accumulate one driver event in the RAS-ERK/MAPK pathway to form pLGGs in children (Ryall et al., 2020).

Approximately 10%–14% of pLGGs are associated with neurofibromatosis type 1 (NF1), a familial cancer predisposition syndrome caused by germline heterozygous loss-of-function alterations in the *NF1* tumor suppressor gene (Ryall et al., 2020). *NF1* encodes a RAS GTPase-activating protein (RAS-GAP),

which negatively regulates RAS-mediated signaling pathways by accelerating the conversion of active RAS-GTP to inactive RAS-GDP (Gutmann et al., 2017). NF1-associated tumorigenesis arises from loss of the remaining *NF1* wild-type alleles in somatic cells (also known as a "second hit"), activating the RAS-ERK/MAPK signaling to form *BRAF*-wild-type pLGGs (D'Angelo et al., 2019; Gutmann et al., 2017; Ryall et al., 2020). The majority of NF1-associated pLGGs develop along the optic pathway (NF1-OPG), also known as optic pathway gliomas, which occur in nearly 20% of children with NF1 (Fisher et al., 2012; Sellmer et al., 2018). Of note, NF1-OPGs are predominantly diagnosed in children younger than 7 years of age with few, if any, adult cases (Sellmer et al., 2018). Similar to sporadic pLGGs, the fact that NF1-OPG is almost exclusively restricted to early developmental periods implies two critical cellular and molecular mechanisms: (1) the existence of transient neural stem and progenitor populations in the developing CNS and (2) their susceptibility to hyperactive ERK/MAPK signaling for neoplastic transformation (Figure S1A).

The identity of the ERK-dependent neural stem/progenitor populations vulnerable to pLGG formation in the developing cerebellum and the hypothalamic/chiasmatic/optic nerve regions—the two most frequent sites for pLGGs—remains largely unknown (Ryall et al., 2020; Tchoghandjian et al., 2009). However, the optic nerve (ON) provides a unique system to study the stem/progenitor-of-origin of NF1-OPG because it is comprised cells from two known macroglial lineages but lacks neuronal cell bodies (Figure 1A). The astrocyte population in the ON arises locally from the neuroepithelial cells in the embryonic ON, which give rise to only astrocytes (type 1 astrocytes), via astrocyte precursor cells (APCs), specified by the Pax2 transcription factor (Miller et al., 1989; Tao and Zhang, 2014). By contrast, the oligodendrocyte lineage in the ON is not locally derived, but the descendants of brain-derived migrating progenitors that reach the distal ON at birth (Figure 1A). Since these migrating progenitors can differentiate into type 2 astrocytes and were previously named as oligodendrocyte and type 2 astrocyte (O-2A) progenitors, we refer to these migrating progenitors as glial progenitors (GPs) (Miller et al., 1989). Migrating GPs are known to arise from radial glia (RG) neural stem cells in the ventricular zone of the third ventricle (III-VZ) during late embryonic stages, and then migrates via the optic chiasm into the distal ON (prechiasmatic region) at birth (Marsters et al., 2016; Ono et al., 2018). Using genetically engineered mouse (GEM) models, previous studies have shown abnormal growth properties of neural stem cells in the developing III-VZ upon *Nf1* loss, suggesting that these might be a cell-of-origin for NF1-OPG (Lee et al., 2012). Given that RG stem cells in the developing III-VZ do not migrate into the ON (Marsters et al., 2016; Miller et al., 1989; Ono et al., 2018; Tao and Zhang, 2014), which of the two developmentally transient precursor populations—local progenitors/APCs, brain-derived migrating GPs, or both—form NF1-OPG, remains uncertain.

RESULTS

Pax2$^+$ local progenitors are not affected upon *Nf1* loss

We first investigated the role of local progenitors in NF1-OPG formation by using a Pax2-cre driver to conditionally knockout *Nf1* (*Nf1*^{Pax2}CKO) in Pax2$^+$ APCs (Ohyama and Groves, 2004; Zhu et al., 2001) (Figure S1B). No significant abnormality in Pax2$^+$ cells, Olig2$^+$ cells, or p-Erk levels was observed at post-natal day 0.5 (P0.5), when migrating GPs, marked by Olig2 expression, just arrived the distal ON from the brain of control and *Nf1*^{Pax2}CKO mice (Figures S1C–S1F). To validate that the local Pax2$^+$ lineage was not affected by *Nf1* loss, we used a second Cre transgenic line driven by the human GFAP promoter (hGFAP-cre), which induced OPG with complete penetrance (Zhu et al., 2005). While the onset of hGFAP-cre expression occurred during the neurogenic phase of RG stem cells in the VZ of the dorsal forebrain between embryonic day 12.5 (E12.5) and E13.5, its expression was relatively late in gliogenic RG stem cells in the hypothalamic region between E14.5 and E15.5 (Li et al., 2020; Ma et al., 2021; Marsters et al., 2016; Zhou et al., 2020). As illustrated by β-galactosidase expression and loss of Pten expression in a Rosa26-driven LacZ reporter and a *Pten* CKO model, respectively (Akgül et al., 2018; Li et al., 2020), hGFAP-cre specifically targeted glial lineages in the hypothalamic region of the ventral forebrain, despite exhibiting robust neuronal targeting in the dorsal forebrain (Figure S1G). Thus, the hGFAP-cre-mediated targeting strategy better models human NF1 conditions by avoiding the introduction of homozygous *Nf1* deletion into multiple neuronal populations in the hypothalamic region, which are derived from multipotent RG stem cells in the III-VZ during earlier embryonic stages (Ma et al., 2021; Zhou et al., 2020).

Similarly, hGFAP-cre-mediated expression of a Rosa26-driven td-Tomato reporter (td-Tom$^+$) in the ON was not detected until E15.5 (Figure S1H). By E17.5, the td-Tom$^+$ reporter was extensively expressed in the ON, which was exclusively comprised Pax2$^+$ APCs, but not migrating GPs that expressed brain lipid binding protein (BLBP) and/or Olig2 (Figures 1B, 1C, and S1I). Similar to the P0.5 *Nf1*^{Pax2}CKO ON, we observed no significant alteration in the number, proliferation rate, or Erk activation (p-Erk levels) in *Nf1*-deficient (Nf1$^{-/-}$) Pax2$^+$ APCs in the E17.5 *Nf1*^{hGFAP}CKO ON (Figures 1D, 1E, and S1I–S1K). Of note, BLBP, a marker initially identified for RG stem cells throughout the developing CNS, was highly expressed in RG stem cells in the III-VZ, which were hereafter referred to as hypothalamic ventricular zone radial glia (hVZ-RG) (Figures 1B and 1C). These results show that local progenitor/APCs are not affected by *Nf1* loss and thus are unlikely to be a cell-of-origin for astrocytic tumors in the NF1-OPG model.

BLBP$^+$ migrating GPs are susceptible to *Nf1* loss and depend on Erk signaling

The number of BLBP$^+$ migrating GPs was dramatically increased (>3-fold) in the P0.5 *Nf1*^{hGFAP}CKO ON compared with the control (Figures 1F and 1G). Conversely, BLBP$^+$ migrating GPs were nearly absent in the P0.5 ON of a hGFAP-cre-mediated conditional knockout *Mek1*$^{flox/flox}$/*Mek2*$^{-/-}$ model (M0) lacking Erk signaling (Li et al., 2012) (Figures 1F and 1G). The vast majority (~80%) of migrating GPs expressed BLBP, but less than half of BLBP$^+$ cells also expressed Olig2 (Figures 1H and 1I). Due to low numbers, more differentiated BLBP$^-$Olig2$^+$ cells were not significantly different between the control and *Nf1*^{hGFAP}CKO ON (Figures 1H and 1I). Thus, BLBP$^+$ cells represent the major migrating population(s) from the optic chiasm to the distal ON at birth, undergoing abnormal expansion in the absence of *Nf1*. Conversely, the near-absence of BLBP$^+$ cells in the M0 ON

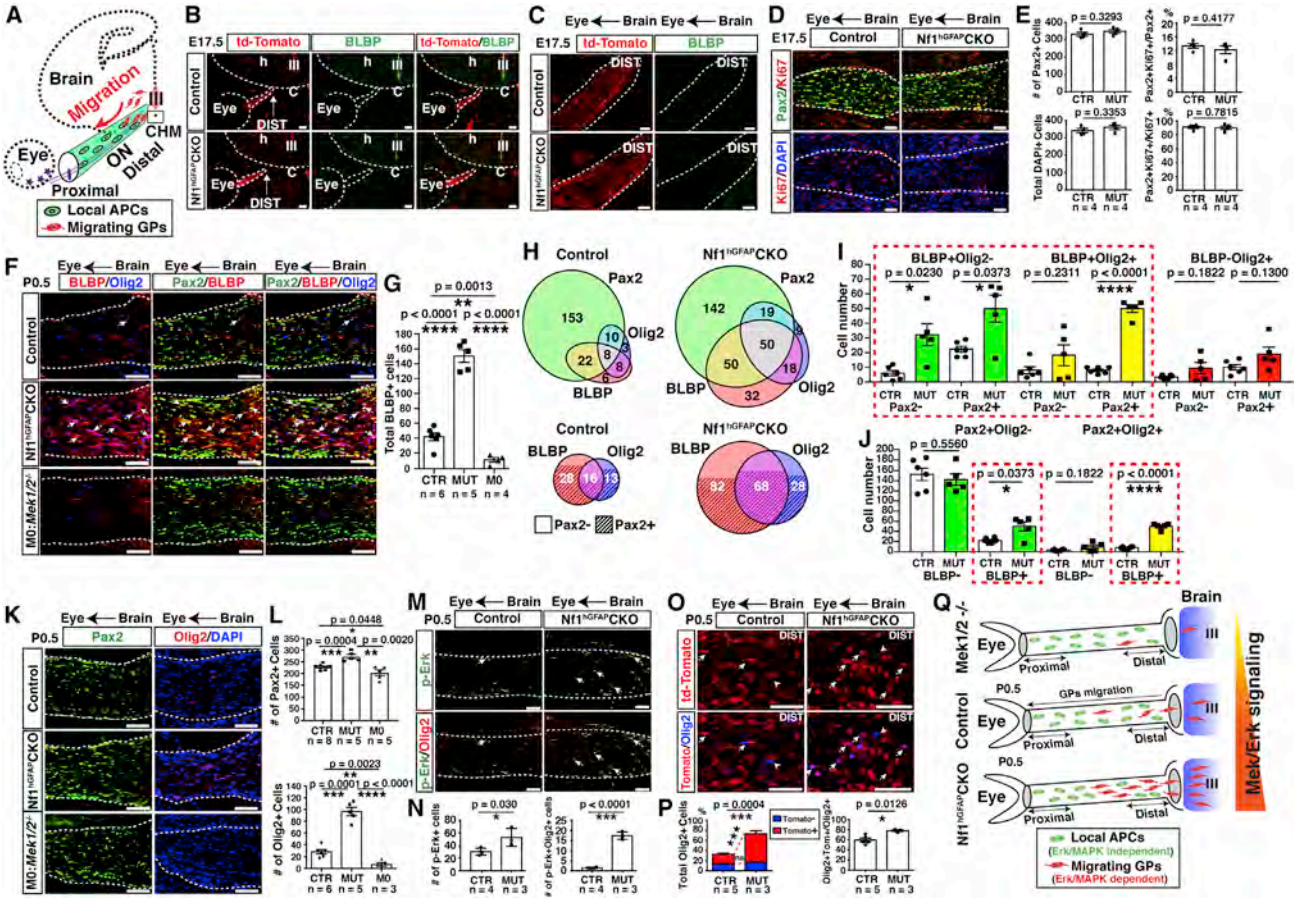

Figure 1. Migrating GPs, not locally derived APCs, are susceptible to *Nf1* loss

(A) Schematic of cellular origins of two macroglial populations in the developing ON. APCs (green) arise locally, while migrating GPs (red) migrate from the ventral brain via the optic chiasm.

(B and C) BLBP and td-Tomato expression in the hypothalamic/chiasm/ON (h/c/ON) region (B) and the distal ON (C).

(D and E) Co-labeling and quantification of Pax2 and Ki67 expression in the distal ON. Dashed lines delineate the ON.

(F–J) Co-labeling of BLBP, Olig2, and Pax2 (F) and quantification of BLBP (G) in the P0.5 distal ON. Arrows mark BLBP$^+$Pax2$^+$Olig2$^+$ cells. Venn diagrams show overlapping expression of Pax2, BLBP, and Olig2 (H). Shaded areas (below) mark Pax2$^+$ cells within BLBP$^+$Olig2$^-$, BLBP$^+$Olig2$^+$, and BLBP$^-$Olig2$^+$ populations. Pax2 expression in BLBP/Olig2 populations (I) and BLBP expression in Pax2/Olig2 populations (J) in the P0.5 distal ON were quantified. Red boxes indicate BLBP$^+$ populations.

(K and L) Co-labeling and quantification of Pax2 or Olig2 in the P0.5 distal ON.

(M and N) Co-labeling and quantification of p-Erk and Olig2 in the P0.5 distal ON. Arrows mark p-Erk$^+$Olig2$^+$ cells.

(O and P) Co-labeling and quantification of td-Tomato and Olig2 in the P0.5 distal ON. Arrows mark td-Tomato$^+$Olig2$^+$ cells. Arrowheads mark td-Tomato$^-$Olig2$^+$ cells.

(Q) Schematic of the impact of different levels of Mek-Erk signaling on migrating GPs.

Quantifications are presented as mean ± SEM. Statistical analysis used unpaired two-tailed Student's t test. Ns, not significant; VB, ventral brain; III, third ventricle; ON, optic nerve; APC, astrocyte precursor cell; GP, glial progenitor; CTR, control group; MUT, *Nf1*^{hGFAP}CKO mutant group; M0, *Mek*1/2 double-knockout group. Scale bar: 50 μm.

See also Figure S1.

suggests that the Mek-Erk/MAPK dependency leads to the vulnerability of the migrating lineage(s) to tumor formation upon *Nf1* loss (Figures 1F and 1G).

Unexpectedly, a major proportion of the increased BLBP$^+$ populations in the *Nf1*^{hGFAP}CKO ON expressed Pax2, which were also present in the control ON (Figures 1H and 1I). Based on the timing (neonatal) and location (distal ON), these observations are most consistent with a model wherein upon arrival to the distal ON, a subset of BLBP$^+$ migrating GPs acquire the local APC marker, Pax2. Three observations supported this model: (1) nearly the entire expansion of the Pax2$^+$ cells was caused by those co-expressing BLBP in the distal ON of P0.5 *Nf1*^{hGFAP}CKO mice (Figure 1J), (2) the similar number of BLBP$^+$ cells was found between P0.5 control and *Nf1*^{Pax2}CKO ON (Figures S1L and S1M), and (3) the increased Pax2$^+$ cells overlapped with the migrating front of Olig2$^+$ cells in the distal ON of P0.5 *Nf1*^{hGFAP}CKO mice (Figures 1K and 1L). In the control distal ON, we calculated that ~15% of the total Pax2$^+$ cells arose from migrating BLBP$^+$/Olig2$^+$ GPs that acquired Pax2 expression (Figure 1H), which was in agreement with an ~11% of

loss of Pax2$^+$ cells in the P0.5 M0 ON (Figures 1K and 1L). Importantly, abnormal activation of Erk signaling was enriched in Olig2$^+$ cell populations of the P0.5 *Nf1*^{hGFAP}CKO ON (Figures 1M and 1N). This increase was almost exclusively observed in the Nf1$^{-/-}$ compartment, evidenced by the td-Tom$^+$ reporter expression (Figures 1O and 1P). Together, the developmental timing (neonatal) and location (distal ON) of initial expansion observed in the ON of the *Nf1*^{hGFAP}CKO model, not the *Nf1*^{Pax2}CKO model, demonstrate that brain-derived migrating GPs, not local APCs, are susceptible to hyperactive Erk/MAPK signaling for tumor formation as a result of the Mek-Erk/MAPK dependency (Figure 1Q).

Disruption of the balance between stem-cell maintenance and gliogenesis of Nf1$^{-/-}$ hVZ-RG

No increase in the proliferative index of the BLBP$^+$ cells in the P0.5 *Nf1*^{hGFAP}CKO ON suggests a possibility that the expansion of Nf1$^{-/-}$ BLBP$^+$ cells occurs prior to their migration from the brain (Figures S1N and S1O). We therefore investigated how *Nf1* loss impacted BLBP$^+$ cells in the embryonic brain (Figure 2A). Consistent with the onset of hGFAP-cre-mediated recombination at E14.5–E15.5, we observed no abnormality in the hypothalamic region of *Nf1*^{hGFAP}CKO mice at E15.5 (Figures S2A–S2C). However, a dramatic increase in BLBP$^+$ cells was observed in the hypothalamic mantle zone (MZ) of *Nf1*^{hGFAP}CKO brains at E17.5 (Figures 2B and S2D). Importantly, BLBP$^+$ cells in the both control and *Nf1*^{hGFAP}CKO hypothalamic MZ exhibited RG-like morphology, expressing the same RG markers, including Sox9 and hGFAP-Cre, as those by BLBP$^+$ hVZ-RG in the III ventricle (Figures 2B, 2C, and S2D). Indeed, these RG-like cells in the MZ were recently characterized as hypothalamic MZ-RG (hMZ-RG) cells in both the mouse and human embryonic hypothalamic region, which were direct descendants of hVZ-RG cells (Zhou et al., 2020). Thus, the dramatic increase of BLBP$^+$ hMZ-RG-like cells in the E17.5 hypothalamic region is the earliest abnormality detected in the brain of *Nf1*^{hGFAP}CKO mice (Kim et al., 2014; Wang et al., 2012; Zhu et al., 2005).

In the dorsal hypothalamic region, the number and proliferation of hVZ-RG cells (BLBP$^+$Olig2$^-$) in the III ventricle between control and *Nf1*^{hGFAP}CKO mice were not significantly different (Figures 2D–2F). However, the number of BLBP$^+$Olig2$^+$ cells, which were often clustered on the border of the VZ and MZ, was significantly increased in the dorsal hypothalamic region of E17.5 *Nf1*^{hGFAP}CKO brains (Figures 2E and 2F). Importantly, BLBP- and/or Olig2-expressing cells, which were abnormally expanded in the P0.5 distal ON, had already increased in the E17.5 *Nf1*^{hGFAP}CKO hypothalamic MZ (Figures 2E and 2F). BLBP$^+$ cells, regardless of Olig2 expression, exhibited a proliferative rate comparable with control in the both E17.5 hypothalamic MZ and P0.5 distal ON of *Nf1*^{hGFAP}CKO mice (Figures 2E and 2F). Instead, more differentiated BLBP$^-$Olig2$^+$ cells were the only progenitor population showing increased proliferation in the *Nf1*^{hGFAP}CKO hypothalamic MZ at E17.5 (Figure 2F). Given that apoptosis was rare in both control and *Nf1*^{hGFAP}CKO brains, the increased cell numbers, but lack of proliferative advantage, of BLBP$^+$ cells in the hypothalamic MZ, suggests an alternative mechanism. While the normal VZ structure were relatively maintained in the dorsal hypothalamic region (Figures 2E, S2E, and S2F), focal disruption of the VZ structure was consistently found in the ventral hypothalamic region of *Nf1*^{hGFAP}CKO brains at E17.5 (Figures 2B, 2C, and S2D). This abnormal ventricular phenotype was more readily revealed by two markers (Cre and Sox9) that label the nuclei of hVZ-RG and hMZ-RG cells inside and immediately outside the ventral III ventricle, respectively (Figures 2G and 2H). Loss of Cre$^+$Sox9$^+$BLBP$^+$ hVZ-RG stem cells in the focally disrupted III-VZ was accompanied by the increase of Cre$^+$Sox9$^+$BLBP$^+$ hMZ-RG cells in the surrounding MZ (Figures 2G and 2H). These results are most consistent with a model wherein Nf1 loss disrupts the balance of stem-cell maintenance and gliogenesis in the embryonic hypothalamic region, overproducing BLBP$^+$ hMZ-RG cells in the MZ at the expense of hVZ-RG inside the III ventricle. By E17.5, BLBP$^+$ cells in the optic chiasm had not been targeted by hGFAP-cre-mediated recombination but at P0.5 exhibited similar expansion to what was observed in the distal ON of *Nf1*^{hGFAP}CKO mice (Figures S2G–S2J). The 2-day delay in the expansion of BLBP$^+$ cells between the E17.5 hypothalamic MZ and P0.5 optic chiasm/distal ON further support the model that initial expansion of the BLBP$^+$ progenitors must occur in the embryonic brain, but subsequently migrate into the optic chiasm and distal ON at birth.

The MADM-Nf1 model validates altered balance between hVZ-RG and hMZ-RG-like cells

In order to further investigate how *Nf1* loss disrupts the balance between stem-cell maintenance in the VZ and gliogenesis in the MZ of the embryonic hypothalamic region, we developed a model for NF1-OPG by crossing the *Nf1*^{hGFAP}CKO mice with the mosaic analysis with double markers (MADMs) strain (referred to as MADM-Nf1) (Liu et al., 2011). The MADM system provides two unique features. First, due to random and insufficient Cre-mediated recombination between chromosomes during mitotic divisions (Liu et al., 2011), the MADM model generates much fewer (1%–5%) recombined cells than the conventional *Nf1*^{hGFAP}CKO model, which allows for quantification in regions with high cellular density such as the III-VZ. Second, the MADM system generates one Nf1$^{-/-}$ cell and one sibling *Nf1* wild-type (Nf1$^{+/+}$) cell from a common parental *Nf1* heterozygous (Nf1$^{+/-}$) cell at a 1:1 ratio during mitotic divisions, marked by red (R) and green (G) fluorescent protein, respectively (Figure 3A). These features allow for direct comparison of proliferation, differentiation, and morphology between sibling control and mutant cells within the same tissues.

We first used a MADM-wild-type (MADM-WT) model in which both red and green sibling cells were WT for *Nf1* (Liu et al., 2011). In the MADM-WT model, due to the random assortment of symmetric and asymmetric divisions of stem cells, we observed some variations in the R/G ratio between individual brain sections at E17.5 (Figures 3B, 3C, and S3A). However, this individual variation balanced to a net 1:1-R/G ratio (0.988) when we combined multiple sections from each of the 6 MADM-WT brains (Figure 3D). Having validated the MADM-WT system, we next investigated their littermates, the MADM-Nf1 mice. In the hypothalamic region as a whole, Nf1$^{-/-}$ cells only exhibited a minor growth advantage over sibling Nf1$^{+/+}$ cells with a R/G ratio of 1.159. Strikingly, when we compared the R/G ratio inside the III-VZ with that in the surrounding MZ, we consistently observed a reverse patten of the R/G ratio inside the III-VZ with more green Nf1$^{+/+}$ cells versus in the surrounding MZ with more red Nf1$^{-/-}$

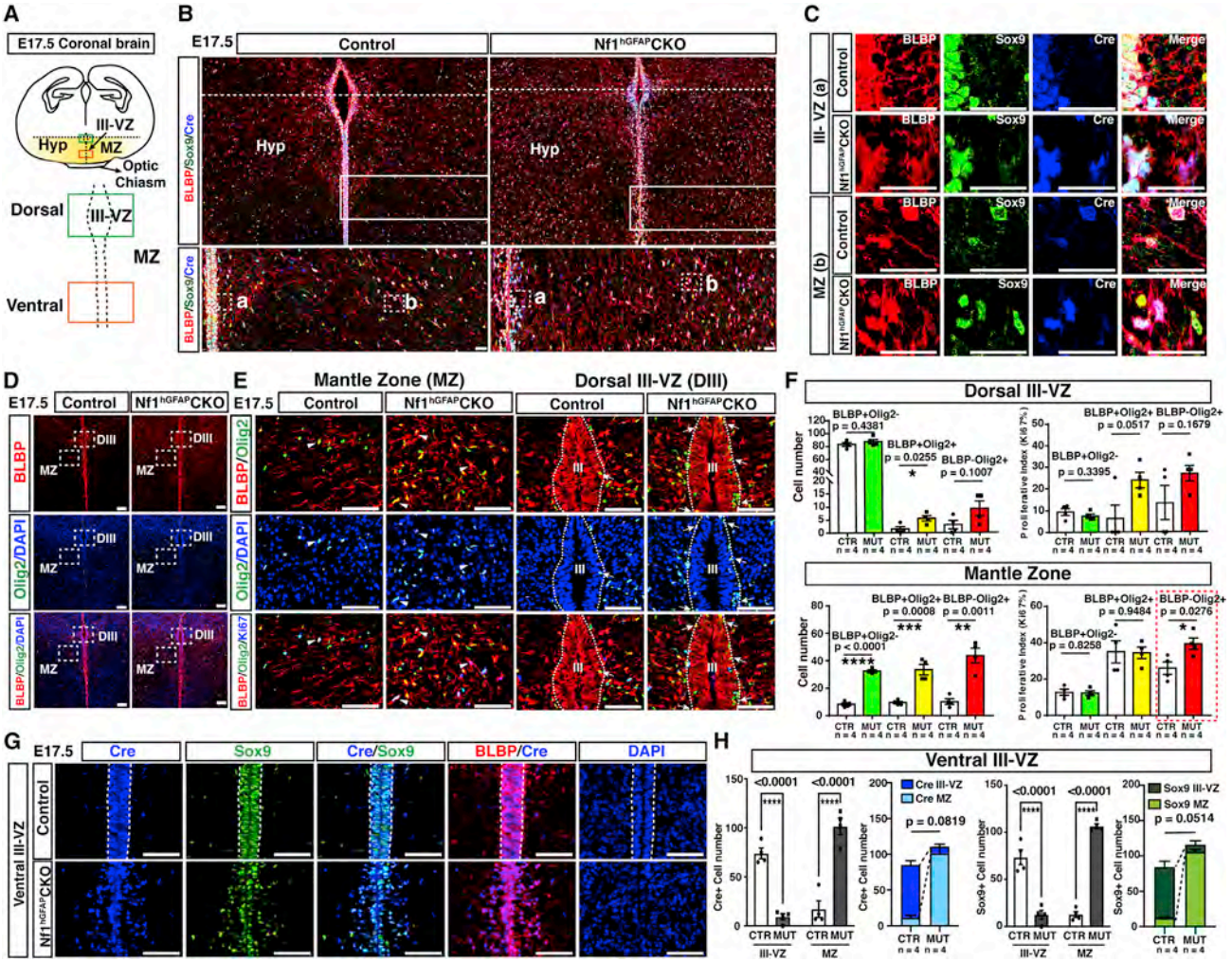

Figure 2. *Nf1* loss disrupts the balance between stem-cell maintenance and gliogenesis of the embryonic hVZ-RG

(A) Schematic of E17.5 mouse coronal brain section with the hypothalamic (h) region highlighting the dorsal III-VZ, ventral III-VZ and the mantle zone (MZ) analyzed.

(B and C) Confocal images of coronal sections from E17.5 control and Nf1^{hGFAP}CKO brains co-labeled with BLBP, Sox9, and Cre. Solid-line boxes indicate enlarged areas (below). Dashed-line boxes (B) are shown (C), showing a RG-like morphology of hVZ-RG in the III-VZ and adjacent MZ (A) and hMZ-RG cells in the MZ (B) of the embryonic hypothalamus.

(D–F) Co-labeling and quantification of BLBP, Olig2, and Ki67 in E17.5 control and Nf1^{hGFAP}CKO hypothalamic regions. Boxes (D) show the dorsal III-VZ and MZ of the hypothalamus (E). Dashed lines (E) denote the border between the III-VZ and surrounding MZ. Arrowheads indicate BLBP^{+}Olig2^{+}Ki67^{+} cells in the MZ. Arrows indicate BLBP^{+}Olig2^{+} cells on the border of the III-VZ.

(G and H) Co-labeling and quantification of BLBP, Sox9, and Cre in the ventral III-VZ and MZ at E17.5.

Quantifications are presented as mean ± SEM. Statistical analysis used unpaired two-tailed Student's t test. III-VZ, third ventricular zone; MZ; mantle zone; hVZ-RG, hypothalamic ventricular zone radial glia; hMZ-RG, hypothalamic mantle zone radial glia; MP, migrating progenitor. Scale bars: 50 μm.

See also Figure S2.

cells, 0.4 versus 1.8, respectively (Figures 3D and 3E). These results provide more direct evidence that *Nf1* loss disrupts the balance between stem-cell maintenance and differentiation, driving hVZ-RG cells out of the III ventricle to become hMZ-RG cells in the MZ (Figure 3F).

While the R/G ratio inside the III-VZ was maintained between 0.4 and 0.45 from E17.5 to P0.5, red Nf1$^{-/-}$ cells continued to expand with a R/G ratio increasing to 3.12 in the MZ of the MADM-Nf1 brain at P0.5 (Figures 3G and 3H). This continuous expansion could at least partially be caused by the higher proliferative rate of Nf1$^{-/-}$ BLBP^{-}Olig2^{+} cells in the MZ (the red box, Figure 2F). Importantly, the sibling green Nf1$^{+/+}$ cells and red Nf1$^{-/-}$ cells were also distinct in the differentiation status. The percentage of the green Nf1$^{+/+}$ cells expressing BLBP was dramatically reduced from 70% inside the III-VZ to 16% in the MZ, while the percentage of green Nf1$^{+/+}$ cells expressing Olig2 was inversely increased from only 9% in the III-VZ to 69% in the MZ (Figures 3I and 3J). This pattern is consistent with normal glial differentiation from hVZ-RG stem cells to more differentiated oligodendrocyte precursor cells (OPCs) (BLBP^{+}Olig2^{-} → BLBP^{+}Olig2^{+} → BLBP^{-}Olig2^{+}). In contrast, the majority of the abnormally expanded red Nf1$^{-/-}$ cells in the MZ expressed both BLBP and

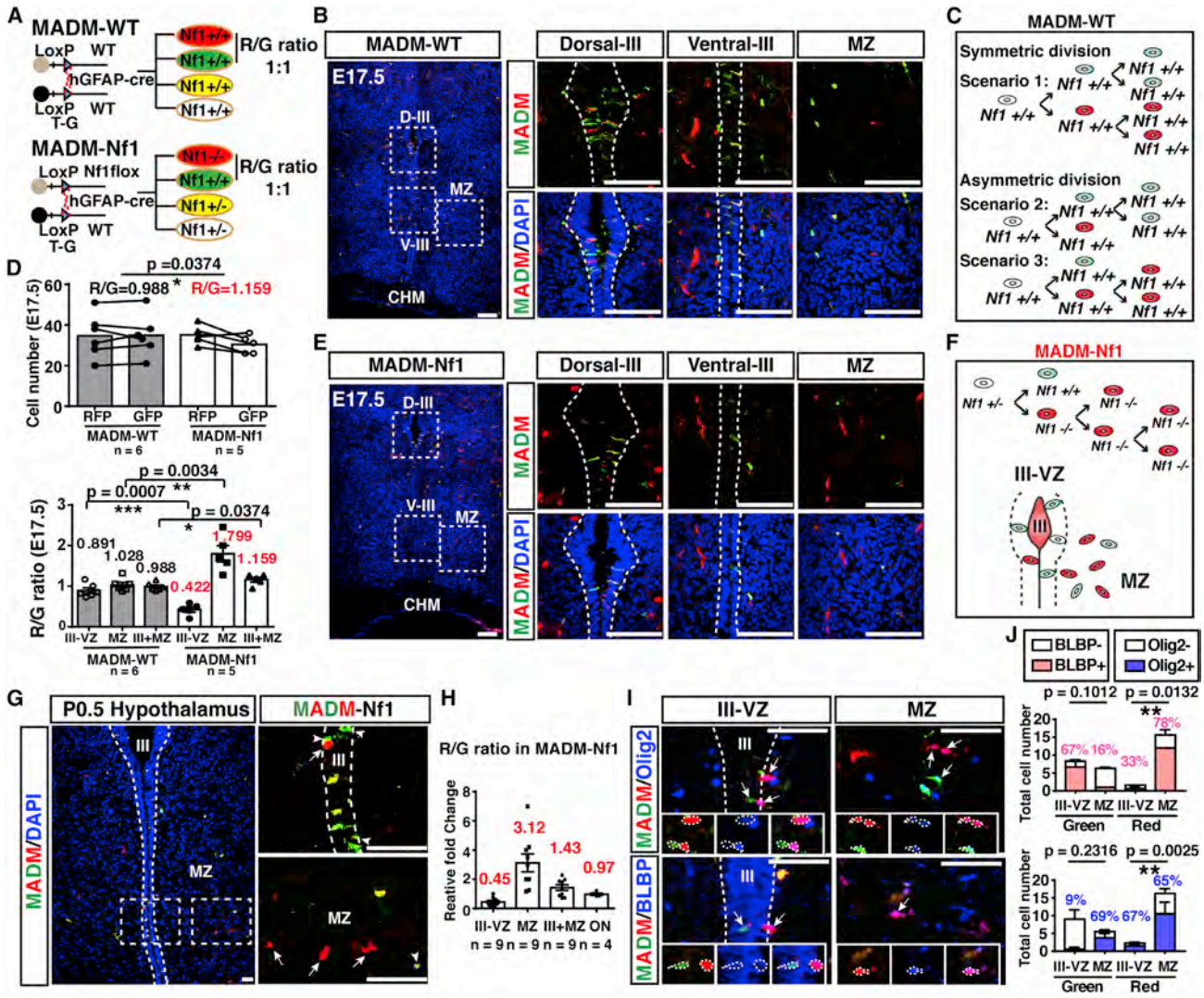

Figure 3. MADM-based model validates the role of *Nf1* in maintaining the balance between hVZ-RG and hMZ-RG cells

(A) Schematic of the MADM-WT and MADM-Nf1 models under the hGFAP-cre driver.

(B–F) Confocal images of coronal sections from MADM-WT (B) and E17.5 MADM-Nf1 (E) hypothalamic regions co-labeled with GFP and RFP. Boxes (left) show the dorsal III-VZ, ventral III-VZ and the MZ (right). Dashed lines delineate the III-VZ. Models summarizes expected outcomes from symmetric and asymmetric division in MADM-WT (C) and MADM-Nf1 (F) models. Total green and red cells and the red/green (R/G) ratio in the III-VZ, the MZ, the ventral brain (III-VZ and MZ combined) and the ON were quantified (D).

(G) Horizontal sections of P0.5 MADM-Nf1 mice were co-labeled with GFP and RFP. Boxes show III-VZ (right, upper) and MZ (right, lower). Arrowheads indicate $Nf1^{+/+}$ cells (green). Arrows label $Nf1^{-/-}$ cells (red).

(H) The R/G ratio was quantified in the III-VZ, the MZ, the ventral brain (III-VZ and MZ combined) and the ON of P0.5 MADM-Nf1 mice.

(I and J) Co-labeling and quantification of GFP/RFP and either Olig2 (top) or BLBP (bottom) on horizontal sections of P0.5 MADM-Nf1 brains (I). Insets show single channel staining of cells (arrows), including a pair of dividing cells on the border of the III-VZ with an $Olig2^{-}$ green cell inside and an $Olig2^{+}$ red cell outside the III-VZ.

Quantifications are presented as mean ± SEM. Statistical analysis used unpaired two-tailed Student's t test. GFP, green fluorescent protein; RFP, red fluorescent protein; hVZ-RG, hypothalamic ventricular zone radial glia; hMZ-RG, hypothalamic mantle zone radial glia; VB, ventral brain; III-VZ, third ventricular zone; D-III, dorsal third ventricular zone; V-III, ventral third ventricular zone; MZ, mantle zone. Scale bars, 50 μm.

See also Figure S3.

Olig2 with each at 78% and 65%, respectively (Figure 3J). When a pair of sibling green and red cells was captured during mitotic division on the border of the III-VZ niche, the red $Nf1^{-/-}$ cell with Olig2 expression was always observed on the border of the niche, while the sibling green $Nf1^{+/+}$ cells lacking Olig2 expression remained inside the niche (Figure 3I). These results suggest premature, but impaired, glial differentiation as a mechanism for the disruption of the balance between stem-cell maintenance and gliogenesis of hVZ-RG cells in the III-VZ. Despite not directly causing increased proliferation, *Nf1* loss increases $BLBP^{+}$ hMZ-RG cells in the hypothalamic region via two mechanisms: (1) overproducing $BLBP^{+}Olig2^{-}$ and $BLBP^{+}Olig2^{+}$ cells in the MZ by

dislocating hVZ-RG stem cells out of the III ventricle and (2) impairing differentiation of BLBP$^+$ cells in the MZ, which serve as the source of migrating GPs for the ON (Figure S3B).

Nf1$^{-/-}$ cells undergo transient expansion in the neonatal ON and initiate OPG formation

We used the MADM-Nf1 system to further validate the model wherein BLBP$^+$ migrating GPs, but not Pax2$^+$ local APCs, contribute to initial expansion in the *Nf1*-deficient ON. At birth, almost the entire population of red and green cells (>99%) were observed within local Pax2$^+$ populations, but not migrating BLBP$^+$ populations in the distal ON of the MADM-Nf1 model, which was due to infrequent Cre-mediated interchromosomal recombination (Figures S3C and S3D). No difference in the R/G ratio was observed in the P0.5 MADM-Nf1 ON, further validating the model that *Nf1* loss has no effect on local APCs (Figures S3C and S3D). We next used the fluorescence-activated cell sorting (FACS) method to investigate red and green fluorescent cells from the same ON of both MADM-WT and MADM-Nf1 mice at different post-natal stages (P15, P21, and P30) (Figures 4A and 4B). Both green and red Nf1$^{+/+}$ cells in the MADM-WT ON, or green Nf1$^{+/+}$ cells in the MADM-Nf1 ON, were similarly low and comprised 2% to 4% of the total cells (Figures 4A and 4B). While a 1:1-R/G ratio was constantly observed in the MADM-WT ON, a dramatic increase in the R/G ratio was observed in the MADM-Nf1 ON (Figures 4A and 4B). Importantly, the increase of Nf1$^{-/-}$ cells over their sibling Nf1$^{+/+}$ cells reached a plateau with about a 9-fold increase (~20% of the total cells) in the MADM-Nf1 ON during the first three post-natal weeks (Figure 4B). Despite only a small number of cells being targeted with *Nf1* deletion, some MADM-Nf1 mice did develop OPGs with robust GFAP expression similar to those observed in the conventional *Nf1*^{hGFAP}CKO model (Figure S3E). The R/G ratio in the OPGs remains consistent at 7–8 from P30 to P60, indicating this cell population no longer significantly undergoes expansion in the mature ON (Figures 4B and S3F). More importantly, red Nf1$^{-/-}$ cells with expression of BLBP and Olig2 greatly contributed to the tumor masses in the MADM-Nf1 model (Figures S3E and S3F). The MADM-Nf1 system not only validates the model wherein *Nf1* loss in brain-derived migrating progenitors leads to NF1-OPG formation, but also shows that abnormal expansion of migrating GPs mainly occurs during a specific developmental time window in the ON.

Similar to the MADM-Nf1 ON, the *Nf1*^{hGFAP}CKO ON also exhibited abnormal expansion during the first two post-natal weeks and then reached a plateau (Figures 4C, S4A, and S4B). At P0.5 when increased numbers of BLBP$^+$ GPs migrated into the *Nf1*^{hGFAP}CKO ON, relatively normal numbers of microglia expressing Iba1 and P2Y12 (a marker for homeostatic or resting microglia) were observed, but no CD68 (a marker for activated microglia) was detected (Figures 4D–4F). Importantly, CD68 was highly and specifically expressed in the ON with OPG, but not control ON (Figures 4G and 4H). Increased infiltration and accumulation of microglia, evidenced by Iba1 expression, became detectable at P15—after the major expansion of Nf1$^{-/-}$ cells had already occurred (Figures 4I, S4C, and S4D). Abnormal immune response dramatically increased with an activated morphology of Iba1$^+$ microglia at later stages when degeneration of axons, myelin, and RGCs became evident at P60 or later (Figures 4I, 4J, and S4C–S4F). Loss of RGCs in the *Nf1*^{hGFAP}CKO mice was accompanied by apoptosis, which was completely eliminated in the absence of a proapoptotic regulator, Bax (Figures 4K, 4L, and S5A–S5D). As previously published (Péquignot et al., 2003), *Bax* deficiency eliminated naturally occurring apoptosis in RGCs during normal development, leading to increased numbers of RGCs even in the *Nf1*^{hGFAP}CKO model (comparable with that in the *Bax* single-mutant retina) (Figures 4K and 4L). Despite no apoptosis in RGCs, *Bax*/*Nf1*-double mutant mice exhibited a greater ON enlargement with larger tumors accompanied by more severe tumor-associated events, including degeneration of axons and myelin as well as accumulation of activated microglia than those observed in the *Nf1*^{hGFAP}CKO ON (Figures 4K, 4L, and S5A–S5E). Together, these results suggest that developmental defects in Nf1$^{-/-}$ BLBP$^+$-migrating GPs precede an abnormal immune response and axonal degeneration, triggering Bax-mediated apoptosis in RGCs (Figure 4M).

Mouse and human NF1-pLGGs express BLBP with mixed glial precursor characteristics

As a transient developmental precursor population(s), BLBP$^+$ cells were rare in the normal mature ON but were increased by 10-fold and contributed to 25% of *Nf1*^{hGFAP}CKO OPG cells (Figures 5A–5C). The major increase of *Nf1*^{hGFAP}CKO OPG cells expressing GFAP, Olig2 or both was mainly contributed by those co-expressing BLBP (Figures 5D, 5E, and S6A–S6C). The expression pattern of p-Erk in these three glial populations of *Nf1*^{hGFAP}CKO OPGs was remarkably similar to that of BLBP (Figures 5F–5J). Using a BLBP-driven GFP reporter, nearly 40% of p-Erk+ cells co-expressed BLBP-GFP in *Nf1*^{hGFAP}CKO OPGs, which were also rare cells in the control ON (Figures 5K and 5L). Moreover, high levels of BLBP$^+$ and p-Erk$^+$ cells were observed at every stage analyzed during tumor progression (Figures S6D and S6E). These results suggest that abnormal activation of Erk/MAPK signaling not only drives initial expansion of BLBP$^+$ cells during the neonatal stages but also may be responsible for maintaining this transient developmental RG-like population(s) throughout tumorigenesis. Similar to BLBP, Pax2 expression is transient during normal development, becoming a rare marker entirely restricted to GFAP$^+$Olig2$^-$ astrocytes in the control ON (Figures S6F and S6G). Approximately a 3-fold increase of Pax2$^+$ cells was observed in *Nf1*^{hGFAP}CKO OPGs, and, notably, 13% of them expressed both GFAP and Olig2, reminiscent of triple-positive BLBP$^+$Olig2$^+$Pax2$^+$ cells observed in the neonatal *Nf1*-deficient ON (Figures S6F and S6G). Expression of PDGFRα, an OPC marker, was exclusively observed in the Olig2$^+$ oligodendrocyte lineage in the control ON, while in *Nf1*^{hGFAP}CKO OPGs, exhibiting nearly a 4-fold increase with abnormal GFAP expression (Figures 5M and 5N). Together, these results provide further support for the model wherein *Nf1*^{hGFAP}CKO OPGs arise from developmentally transient RG-like GPs with impaired differentiation and exhibit mixed OPC and APC characteristics.

In order to further determine the clinical relevance of our findings, tumor samples were collected from four NF1 patients in three locations: the optic chiasm, the brainstem, and the cerebellum. One NF1-pLGG could not be analyzed due to high blood contamination. The remaining three NF1-pLGG samples were

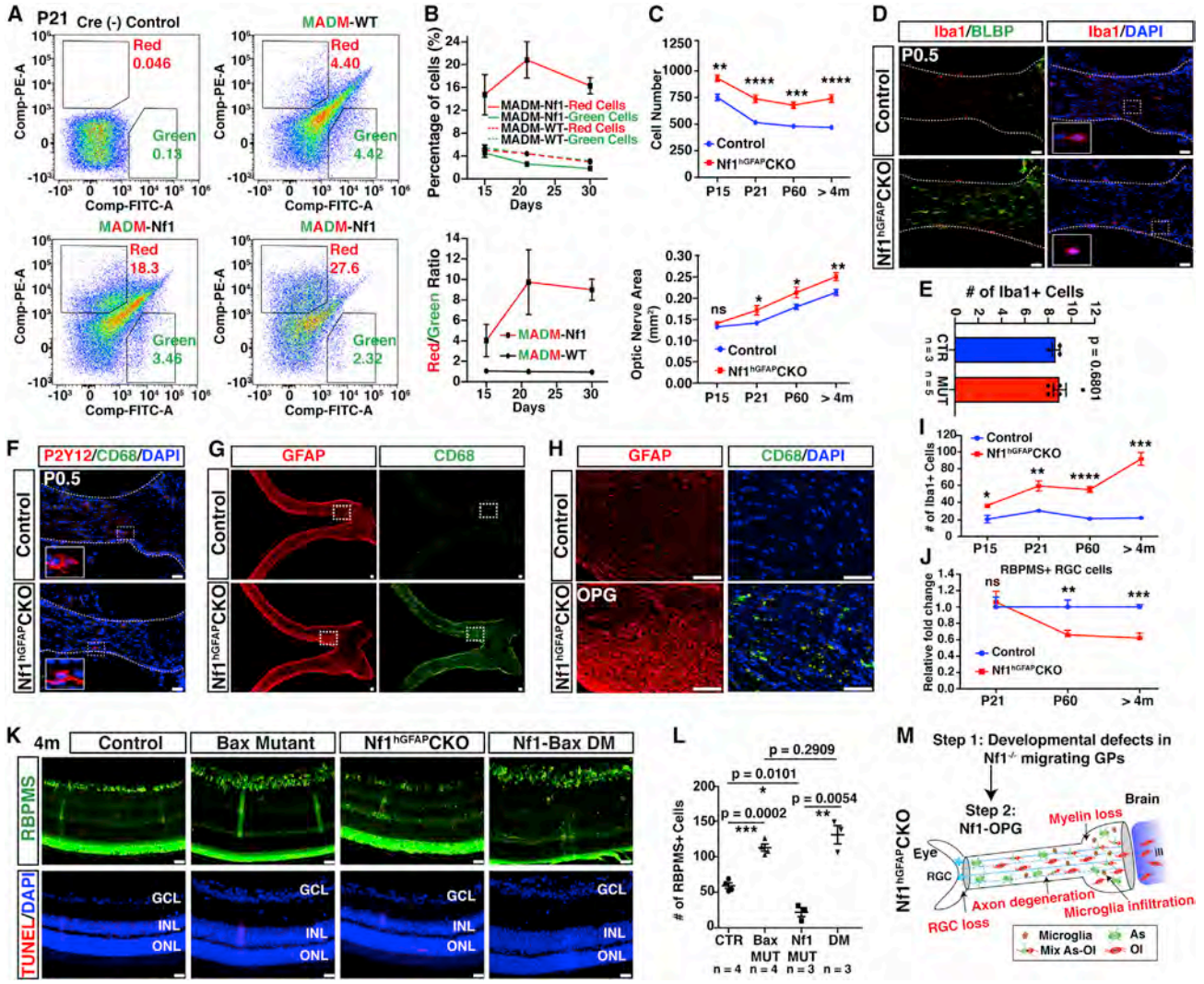

Figure 4. Transient expansion of migrating Nf1$^{-/-}$ cells in the neonatal ON is followed by microglia infiltration, axon/myelin degeneration, and neuronal death

(A and B) FACS analysis of GFP$^+$ and RFP$^+$ cells in the P15, P21, and P30 ON. Representative FACS images show the distribution of red and green cells at P21 in one control, one MADM-WT, and two MADM-Nf1 ONs (A). The percentage of red or green cells and the R/G ratio were quantified (B).

(C) The total cell number and the surface area of the distal ON in control and *Nf1*^{hGFAP}CKO mice at P15, P21, P60, and >4 months were quantified.

(D and E) Co-labeling and quantification of Iba1 and BLBP in P0.5 distal ON (D). Boxed areas are shown in insets.

(F) CD68 and P2Y12 in P0.5 distal ON. Boxed areas are shown in insets.

(G and H) GFAP and CD68 in control and *Nf1*^{hGFAP}CKO ON with an OPG (G). Boxed areas (G) show prechiasmatic regions of the control ON and OPG (H).

(I) The number of Iba1$^+$ microglia were quantified in the ON at different ages.

(J) Relative RBPMS$^+$ RGCs in control and *Nf1*^{hGFAP}CKO retinas at P21, P60, and >4 months were quantified.

(K and L) Co-labeling and quantification of RBPMS and TUNEL in 4-month-old retinas of control, Bax, *Nf1*^{hGFAP}CKO, and *Nf1*^{hGFAP}CKO/Bax mice (K).

(M) A model summarizes the pathogenic sequence of NF1-OPG formation: (1) developmental defects in migrating progenitors and (2) subsequent immune responses of increased microglial infiltration and activation, axonal/myelin degeneration, and RGC loss.

Quantifications are presented as mean ± SEM. Statistical analysis used unpaired two-tailed Student's t test. WT, wild type; RGC, retinal ganglion cell; APC, astrocyte precursor cell; GP, glial progenitor; GP/OL, glial progenitor/oligodendrocyte; AS/OL, astrocyte/oligodendrocyte; GCL, ganglion cell layer; INL, inner nuclear layer; ONL, outer nuclear layer; ns, not significant. Scale bar: 50 μm.

See also Figures S4 and S5.

analyzed and exhibited hyperactive ERK signaling (Figure 5O), as well as robust GFAP and OLIG2 expression (Figure 5P), as previously reported (Ligon et al., 2004; Reitman et al., 2019). Consistent with the literature (Kim et al., 2014; Zhang et al., 2016), GFAP$^+$OLIG2$^+$ astrocytes (Figures S6H and S6I) and BLBP$^+$ cells were rare populations in the normal brain, with the exception of the BLBP$^+$ Bergmann glia in the both human and mouse cerebellum (Figure 5Q). Importantly, two of the three tumors, including one from the optic chiasm, expressed high levels of BLBP with BLBP$^+$OLIG2$^+$ cells (Figure 5R). Thus, similar to the

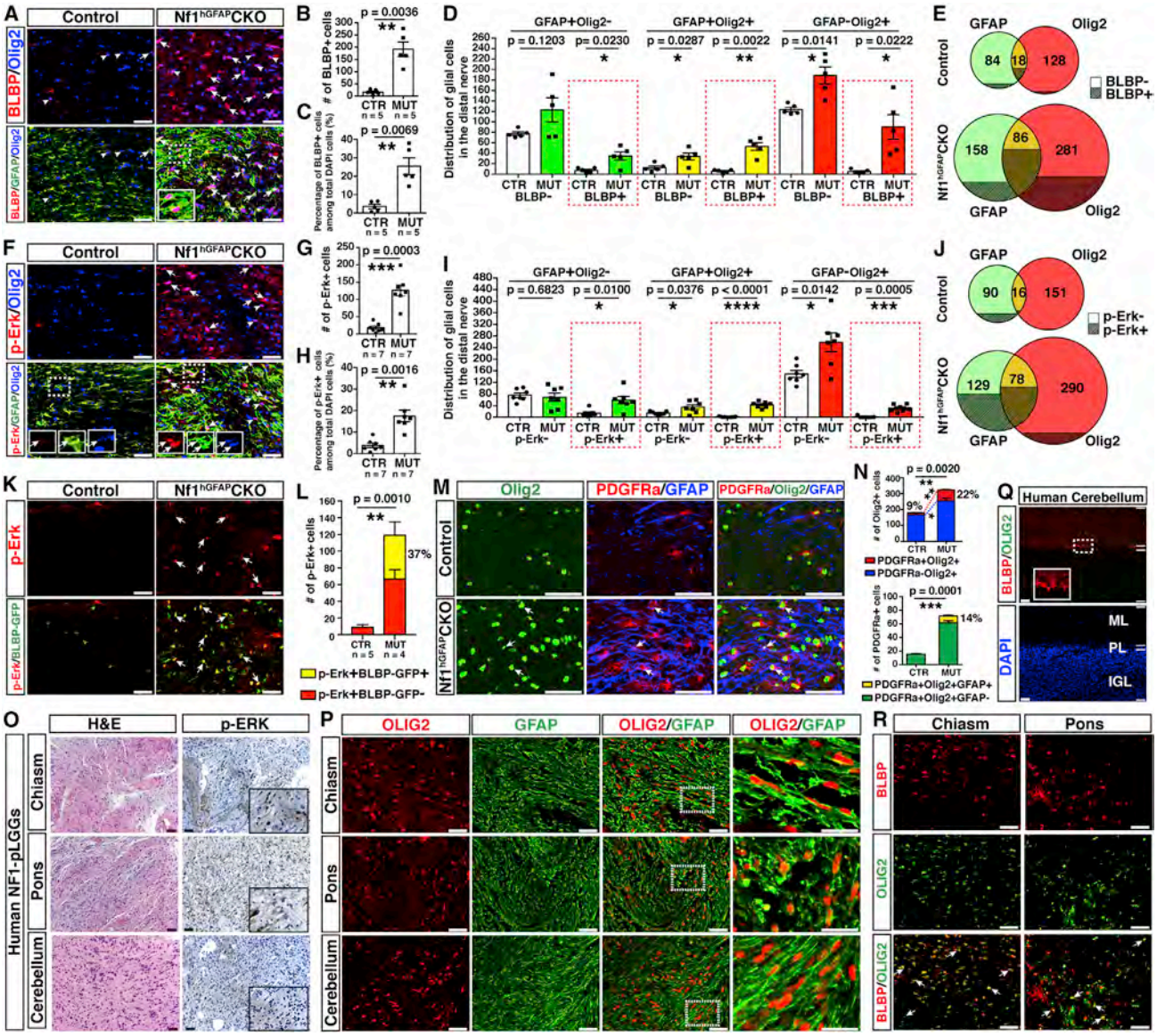

Figure 5. ***Nf1***^{hGFAP}**CKO OPGs exhibit mixed OPC-APC characteristics with hyperactive Erk**

(A–J) Co-labeling and quantification of GFAP, Olig2, and BLBP (A), or GFAP, Olig2, and p-Erk (F) was performed on the ON of control and *Nf1*^{hGFAP}CKO mice (>4 months). Arrowheads and arrows (A) indicate GFAP^{-}Olig2^{+}BLBP^{+} and GFAP^{+}Olig2^{+}BLBP^{+} cells, respectively. Arrowheads and arrows (F) indicate GFAP^{-}Olig2^{+}p-Erk^{+} and GFAP^{+}Olig2^{+}p-Erk^{+} cells, respectively. Boxed areas (A and F) are shown in insets. The number and percentage of BLBP^{+} (B and C) or p-Erk^{+} (G and H) cells were quantified. Quantitative analysis of BLBP^{-} and BLBP^{+} (D and E) or p-Erk^{-} and p-Erk^{+} (I and J) cells in the three GFAP^{+}Olig2^{-}, GFAP^{+}Olig2^{+} and GFAP^{-}Olig2^{+} glial populations was performed on the age-matched control ON and *Nf1*^{hGFAP}CKO OPG. Red boxes show expansion of BLBP-expressing cells (D) or p-Erk-expressing cells (I) from all glial populations of *Nf1*^{hGFAP}CKO OPGs. Venn diagrams summarize expansion of BLBP^{+} (E) or p-Erk^{+} (J) cells (shaded areas) in *Nf1*^{hGFAP}CKO OPGs.

(K and L) Co-labeling and quantification of p-Erk and GFP in the control ON and *Nf1*^{hGFAP}CKO OPG with the BLBP-GFP reporter. Arrows indicate double-positive p-Erk^{+}BLBP-GFP^{+} cells.

(M and N) Co-labeling and quantification of PDGFRα, GFAP and Olig2 in the control ON and *Nf1*^{hGFAP}CKO OPG. Arrows indicate PDGFRα^{+}Olig2^{+}GFAP^{+} cells only found in *Nf1*^{hGFAP}CKO OPGs.

(O) H&E staining and immunohistochemical labeling of p-Erk in human pLGGs from the chiasm, pons, and cerebellum.

(P) GFAP and OLIG2 expression in human pLGGs. Boxed areas are shown (right).

(Q and R) BLBP and OLIG2 in juvenile human cerebellum (Q) and human pLGGs (R). Boxed area (Q) shown in inset. Arrows indicate BLBP^{+}OLIG2^{+} cells (R).

Quantifications are presented as mean ± SEM. Statistical analysis used unpaired two-tailed Student's t test. pLGG, pediatric low-grade glioma; ML, molecular layer; PL, Purkinje cell layer; IGL, internal granule layer. Scale bar, 50 μm.

See also Figure S6.

Nf1^{hGFAP}CKO mouse model, NF1-associated human pLGGs exhibit the characteristics of migrating RG-like GPs, including BLBP^{+}OLIG2^{+} cells.

Reduction of Erk/MAPK signaling can eliminate tumorigenic potential of Nf1$^{-/-}$ GPs

The sequential events during NF1-OPG formation described above suggest that hyperactivation of Erk/MAPK signaling leads to abnormal expansion, impaired differentiation, and persistence of developmentally transient BLBP^{+} RG-like cells, driving tumor formation. Therefore, we generated *Nf1*^{hGFAP}CKO models with different levels of Erk inhibition to test whether prevention of these developmental defects—the emergence and persistence of BLBP^{+} progenitors—is sufficient to prevent OPG formation. First, we investigated complete elimination of Erk signaling in the M0 model with deletion of all four *Mek1/2* alleles (Li et al., 2012). Regardless of the presence (M0) or absence of *Nf1* (N-M0), the near-complete elimination of BLBP^{+} cells in the hypothalamic MZ validated the essential role of Erk signaling in gliogenesis of hVZ-RG stem cells in the III-VZ (Figures 6A and 6B). However, a lack of Erk signaling also caused early post-natal lethality (median survival of 8 days, Figure 6C), precluding the analysis to prevent OPG formation. To improve survival while maintaining high levels of Erk inhibition, we generated a model with one *Mek* allele, either *Mek1* or *Mek2* (M1), on the *Nf1*^{hGFAP}CKO background (N-M1), as one *Mek* allele was sufficient to rescue the early post-natal lethality of the M0 mouse (Li et al., 2012). We found that N-M1 mice rescued many neurological deficits observed in the *Nf1*^{hGFAP}CKO mice (for comparison referred to as N-M4), including the hindlimb crossing and paralysis associated with infertility in these mice (Kim et al., 2014; Wang et al., 2012). Thus, these results demonstrate that the neurological deficits observed in the *Nf1*^{hGFAP}CKO model are caused by abnormal activation of Erk signaling. All the M1 and N-M1 mice tested survived normally until they developed dermatitis at old age, requiring euthanasia (Figure 6C). More importantly, we found that loss of three *Mek* alleles almost entirely eliminated tumor formation (Figures 6D–6F), and consequently, almost no loss or apoptosis of RGCs was detected in the N-M1 mice (Figures 6G and 6H). Importantly, normalization of the number of BLBP^{+} and/or Olig2^{+} cells in the neonatal ON (Figures 6I and 6J) and the hypothalamic MZ (Figure S7C) provides the mechanistic basis for the prevention of NF1-OPG formation in N-M1 mice.

The *Nf1*^{hGFAP}CKO mice with two or three *Mek* alleles (N-M2 and N-M3) exhibited an intermediate survival rescue. As littermate positive controls, age-matched N-M4 *Nf1*^{hGFAP}CKO mice exhibited robust apoptosis and RGC loss, similar to the *Nf1*^{hGFAP}CKO model before mutant *Mek* alleles were introduced (Figures 6G and 6H). Similar to N-M1 mice, a subset of the N-M2 and N-M3 mice also did not develop tumors or show loss of RGCs (Figures 6D–6H, S7A, and S7B). Of note, the mice that had reduced *Mek* alleles, but did not develop OPGs, all exhibited robust Erk inhibition, while those that still developed tumors all maintained high levels of Erk activation, similar to the N-M4 mice (Figures 6D–6H, and S7A). These results collectively demonstrate that dose-dependent inhibition of Mek-Erk/MAPK signaling rescues the emergence of increased Nf1$^{-/-}$ BLBP^{+} migrating GPs and prevents NF1-OPG formation. Equally importantly, the degree of Erk inhibition required for NF1-OPG formation not only support the viability of the mice but also greatly improve the health and survival of *Nf1*^{hGFAP}CKO mice.

A transient low-dose MEKi treatment of neonatal mice prevents NF1-OPG formation

In order to translate the genetic findings into a potential clinical application, we used a ''MEKi-in-Milk'' protocol, which we previously developed to treat developmental defects of the *Nf1*^{hGFAP}CKO brain (Kim et al., 2014; Wang et al., 2012) (Figures 7A and 7B). Under the ''MEKi-in-milk'' protocol, pups indirectly received MEKi via milk of a lactating mother. Approximately 1%–2% of the mother's MEKi/PD901 dose was delivered to pups, a number estimated based on the observation that a 10-mg/kg PD901 dose given to lactating female mice (Figures S8A and S8B) or direct IP injection at a 0.125 mg/kg dose (Figures S8E and S8F) achieved similar Erk inhibition (50%) in brain tissues. Of note, PD901 was specific for inhibiting Erk/MAPK, but not PI3K/Akt or mTORC1 signaling pathway (marked by p-Akt or p-S6) (Figures S8A–S8D). Similar to the dose-dependent inhibitory effects by the genetic approaches, a dose-dependent effect of MEKi was also observed: 5 mg/kg PD901 (PD5) caused inconsistent Erk/MAPK inhibition, while the 20 mg/kg dose (PD20) exerted the most consistent inhibition of both Erk/MAPK signaling and rescue of tumor phenotypes (Figures S9A–S9D). Unfortunately, most of the PD20-treated mice did not achieve long-term survival into P60.

We therefore selected an intermediate dose of 10 mg/kg PD901 (PD10) to be administered from P0.5–P21. At P21, the PD10 protocol almost completely inhibited Erk activation and rescued the increased cellularity and enlarged ON that were consistently observed in the untreated or vehicle-treated *Nf1*^{hGFAP}CKO mice (Figures S9E–S9G). At P60, nearly 40 days after termination of MEKi treatment, we observed the rescue of enlarged ON size and cellularity (Figures 7C and 7D), as well as sustained inhibition of Erk signaling, the elimination of abnormally expanded GFAP^{+}Olig2^{+} and BLBP^{+} cells in 8 of the 9 MEKi-treated *Nf1*^{hGFAP}CKO mice (Figures 7E–7I). The only exception was correlated with insufficient inhibition of Erk signaling within the ON, which might be due to a lack of MEKi uptake in this treated litter (Figure 7F). The numbers and differentiation of RG-like GPs within the treated ON were normalized (Figures 7E–7I), and as a result, abnormal accumulation of activated microglia, axonal degeneration, and loss of RGCs were all prevented by this protocol with the same one exception (Figures 7J–7M). These results demonstrate that transient neonatal treatment with a low-dose MEKi is sufficient to rescue the developmental defects, which appear to cause NF1-OPG formation and tumor-associated neuronal degeneration.

DISCUSSION

In this study, we employed multiple GEM models, including the MADM-Nf1 model, to identify the brain-derived migrating glial lineage(s) as the lineage-of-origin for NF1-OPG. Based on the Erk dependency and transient developmental window identified for these cells, we designed a transient, low-dose, chemopreventative strategy, which prevented these tumors entirely.

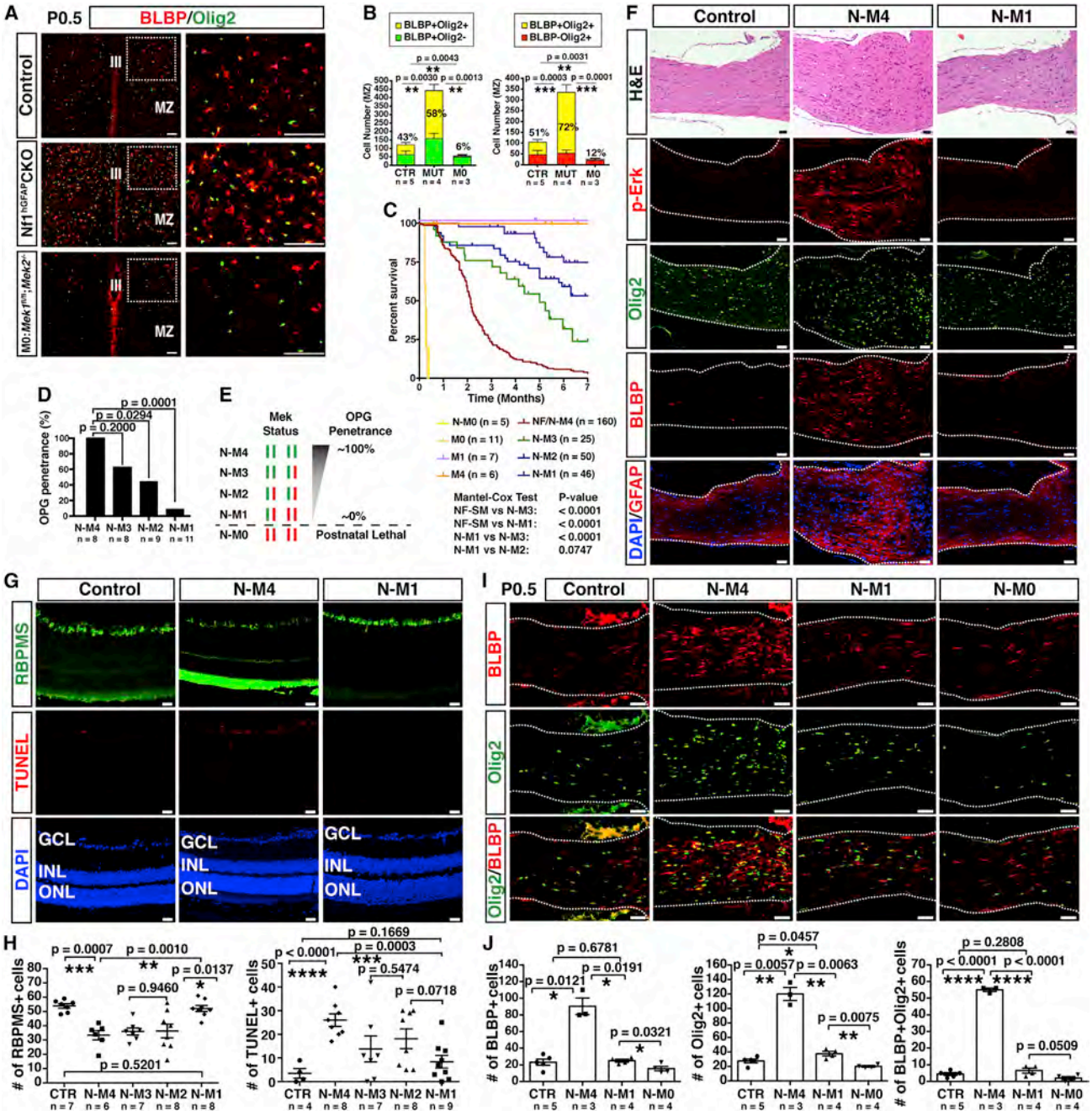

Figure 6. Reduction of Erk/MAPK signaling is sufficient to prevent OPG formation

(A and B) Co-labeling and quantification of BLBP and Olig2 in the hypothalamic regions of P0.5 control, *Nf1*^{hGFAP}CKO, and *Mek*1/2-deficient (M0) mutant mice.

(C) Kaplan-Meir survival curves and Mantel-Cox (log-rank) test for *Mek*1/2 and *Nf1*^{hGFAP}CKO; *Mek*1/2 mutant mice. M0-M4 represents the number of wild-type *Mek*1/2 alleles in each genotype.

(D) Penetrance of OPG in *Nf1*^{hGFAP}CKO mice in N-M4 to N-M1. Statistical analysis used Fisher's exact test.

(E) Schematic of the relationship between *Mek*1/2 alleles in the N-M4 to N-M0 mice and OPG penetrance.

(F) H&E staining and immunolabeling of p-Erk, Olig2, BLBP, and GFAP in the distal ON of age-matched (>4 month) control, N-M4, and N-M1 mice.

(G and H) Co-labeling and quantification of RBPMS and TUNEL from the retinas of control, N-M4, and N-M1 mice.

(I and J) Co-labeling and quantification of BLBP and Olig2 from the distal ON of P0.5 control and N-M4, N-M1, and N-M0 mice.

Quantifications are presented as mean ± SEM. Statistical analysis used unpaired two-tailed Student's t test. III, third ventricle; MZ, mantle zone; GCL, ganglion cell layer; INL, inner nuclear layer; ONL, outer nuclear layer. Scale bar, 50 μm.

See also Figure S7.

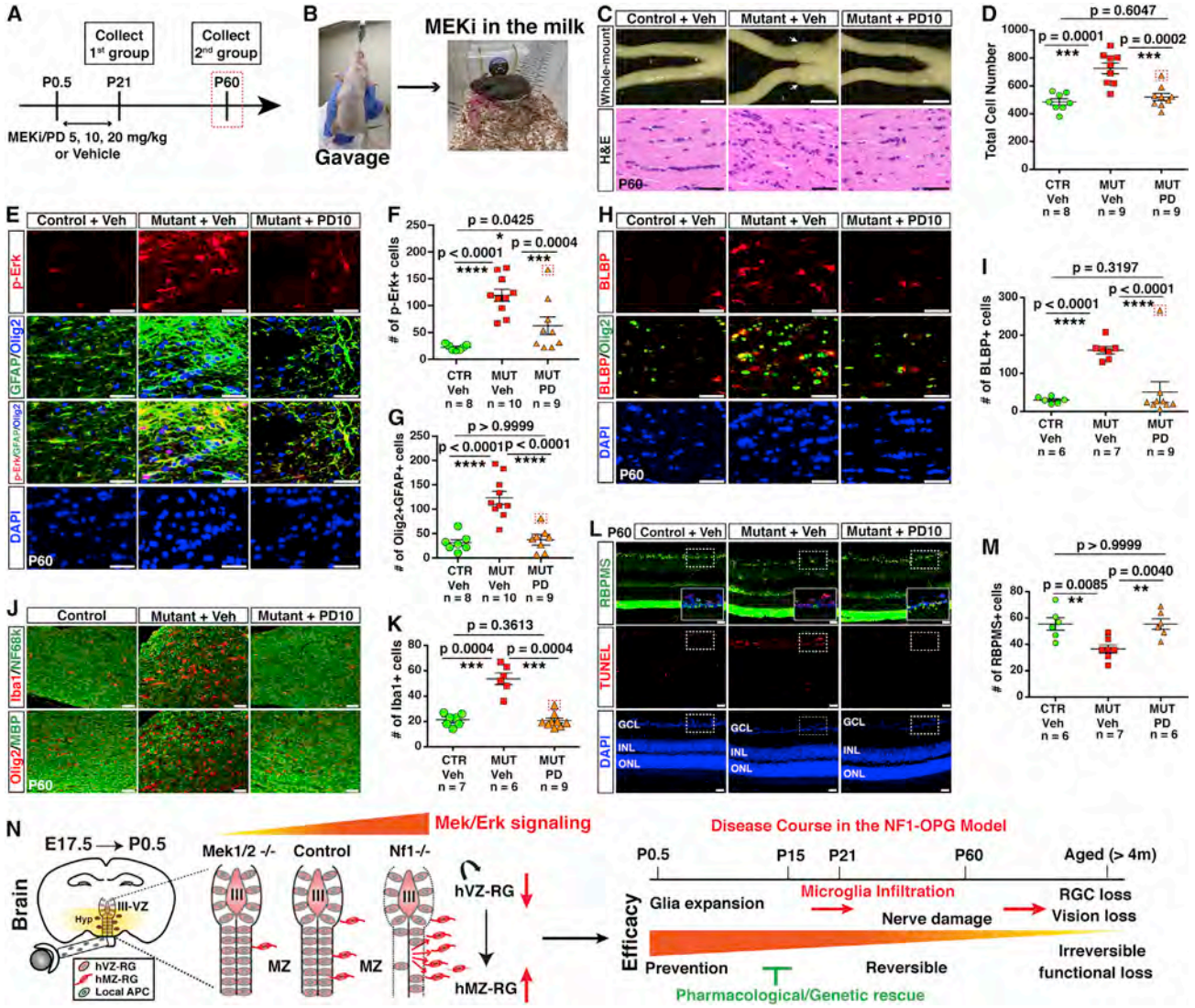

Figure 7. The transient MEKi treatment prevents OPG formation

(A) Experimental design of the P0.5–P21 "MEKi-in-milk" treatment protocol with different doses. Cohorts of vehicle or MEKi-treated mice were collected at either P21 (4 h after last treatment) or P60 (around 40 days after last treatment) for short- and long-term analysis, respectively.

(B) The "MEKi-in-milk" strategy delivers MEKi into newborn pups via lactating females.

(C and D) Whole-mount images and H&E-stained sections of the distal ON from P60 vehicle (VEH) and MEKi (10 mg/kg PD0325901, PD10) treated control and *Nf1*^{hGFAP}CKO mice (C). The total cell number in the distal ON was quantified (D). Red box (D, F, G, I, K, and M) indicates a single non-rescued MEKi-treated *Nf1*^{hGFAP}CKO mouse.

(E–K) Co-labeling and quantification of p-Erk/Olig2/GFAP (E-G), BLBP/Olig2 (H and I), Iba1/NF68k (J, above, and K), and Olig2/MBP (J, below) in the distal ON of P60 vehicle- and MEKi-treated control and *Nf1*^{hGFAP}CKO mice.

(L and M) Co-labeling and quantification of RBPMS and TUNEL in the retinas of P60 vehicle- and MEKi-treated control and *Nf1*^{hGFAP}CKO mice. Boxed areas are shown in insets.

(N) A model for the pathogenic sequence of NF1-OPG formation and the potential efficacy of therapeutic strategies delivered at different disease stages.

Quantifications are presented as mean ± SEM. Statistical analysis used unpaired two-tailed Student's t test. MEKi, MEK inhibitor; GCL, ganglion cell layer; INL, inner nuclear layer; ONL, outer nuclear layer; hVZ-RG, hypothalamic ventricular zone radial glia; GP, glial progenitor; APC, astrocyte precursor cell; OPC, oligodendrocyte precursor cell; III-VZ, third ventricular zone; MZ, mantle zone. Scale bar, 50 μm.

See also Figures S8 and S9.

Erk-dependent migrating GPs causes vulnerability to pLGG formation during development

We used two molecular mechanisms to determine which of the two transient precursor cell populations in the developing ON was vulnerable to NF1-OPG formation: (1) susceptibility to *Nf1* loss and (2) Erk signaling dependency. First, we show that loss of *Nf1* in local Pax2^{+} APCs caused no abnormality in the ON of the *Nf1*^{Pax2}CKO model, whereas the expanded cell population in the ON of the *Nf1*^{hGFAP}CKO model was not observed until P0.5, the time when migrating GPs arrive from the brain

during normal development. Second, in a completely *Mek*-deficient model (the M0 model), the local APCs were largely unaffected, whereas the migrating BLBP$^+$ progenitors were almost entirely absent, affirming that the migrating GPs are the transient progenitor cell-lineage-of-origin vulnerable to NF1-OPG formation as a result of Mek/Erk dependency. Given that NF1 is a negative regulator of RAS-mediated Erk/MAPK signaling, Erk signaling dependency is of particular interest in identifying the cell lineage of origin for NF1-OPG. A recent comprehensive analysis of the molecular mechanisms and clinical correlates of 1,000 pLGGs demonstrated that upregulation of the RAS-ERK/MAPK pathway is nearly universal in these childhood tumors (Ryall et al., 2020), suggesting that Erk signaling dependency can be used as a tool to identify the lineage(s)-of-origin for sporadic pLGGs arising from different regions of the developing brain.

Consistent with the model wherein NF1-OPG arise from migrating GPs, we observed the earliest defect from *Nf1* loss in the hypothalamic region during embryonic stages. Using the conventional the *Nf1*^{hGFAP}CKO model and the MADM-Nf1 model, we observed that the earliest phenotype caused by *Nf1* loss is a disruption in the balance between stem-cell maintenance and gliogenesis in the III-VZ. Upon *Nf1* loss, the hVZ-RG cells generate an initial expanded pool of BLBP$^+$ progenitors by disproportionally dislocating out of the III ventricle to become hMZ-RG cells in the hypothalamic MZ at the expense of depleting III-VZ population. These BLBP$^+$ progenitors, despite exhibiting no significant increase in proliferation, maintain RG-like characteristics, migrate from the MZ into the optic chiasm and finally enter the ON at P0.5, where they initiate OPG formation. Importantly, our model demonstrates that it is the persistence of BLBP$^+$ RG-like progenitors that drives NF1-OPG formation, a finding consistent with a recent study showing that pLGGs from the hypothalamic and chiasmic region exhibited a RG-like signature, while those from the other common pLGG site, the cerebellum, did not (Tchoghandjian et al., 2009).

Clinical implication

NF1-OPG or pLGG in general, despite their non-malignant (benign) status, pose a great clinical challenge, as they cause substantial morbidity in many children (Fisher et al., 2012; Jones et al., 2018; Packer et al., 2020). To date, an ideal therapy to prevent or alleviate tumor/therapy-induced neurological deficits, preserving the quality of life for these affected children, has yet to be discovered. Here, we show that the persistence of Nf1$^{-/-}$ BLBP$^+$ RG-like cells appeared to drive OPG initiation, preceding the downstream tumor-associated events: (1) increased infiltration and activation of microglia accompanied by myelin and axonal degeneration and (2) Bax-mediated apoptosis in RGCs (Figure 7N). This finding opens up the exciting possibility for a more effective therapeutic strategy, one that prevents NF1-OPG formation by targeting the earliest developmental defect in the immature ON long before tumor-associated neurological damages enter an irreversible phase. The essential role of Erk/MAPK signaling in the lineage genesis of BLBP$^+$ hVZ-RG stem cells in the III ventricle provided a challenge in balancing tumor prevention with viability. In this study, however, we identified a rough threshold level of Mek-Erk/MAPK signaling at which abnormal differentiation and expansion of Nf1$^{-/-}$ BLBP$^+$ progenitors were almost completely normalized and OPGs were prevented, while maintaining the viability and rescuing fertiblity of the *Nf1*^{hGFAP}CKO mice, by removing three *Mek* alleles. Of note, the rescue effect was also observed when only one or two *Mek* alleles were removed, albeit with greater variability among mice, thereby demonstrating a dose-dependent effect. By using a very low dose of MEKi during the neonatal stages via the "MEKi-in-Milk" protocol, we show that this treatment protocol, despite its temporary nature, achieved long-term prevention of NF1-OPG formation and tumor-associated RGC loss. Thus, we provide the proof-of-principle necessary to inform chemoprevention therapeutic trials for children with NF1-OPG. The ongoing clinical trials using MEKi at 10–20 times higher doses than the one used in this study on infants with NF1 (as young as 1 month of age) will provide the necessary safety information for the feasibility of this chemopreventative strategy (Fangusaro et al., 2021). The low-dose and transient nature of the "MEKi-in-Milk" protocol also avoids long-lasting MEKi treatment and its potential adverse effects on the developing CNS. This principle may be applicable to children with the developmental disorders with high risks of developing pediatric tumors, such as other RASopathies (i.e., Costello syndrome) that exhibits much more severe neurodevelopmental defects (Castel et al., 2020; Gripp et al., 2019; Gross et al., 2020; Kim et al., 2014; Wang et al., 2012).

Limitations of the study

It will be important to validate these mouse studies in the developing human brain.

STAR★METHODS

Detailed methods are provided in the online version of this paper and include the following:

- KEY RESOURCES TABLE
- RESOURCE AVAILABILITY
  - Lead contact
  - Material availability
  - Data and Code Availability
- EXPERIMENTAL MODELS AND SUBJECT DETAILS
  - Nf1^{hGFAP}CKO
  - Nf1^{Pax2}CKO
  - Nf1^{hGFAP}CKO-*Mek1/2*
  - MADM-*Nf1*
  - Human pLGG Samples
- METHOD DETAILS
  - Genotyping and PCR
  - MEK inhibitor treatment
  - Tissue preparation and processing from adult, embryonic and neonatal tissues
  - Whole-mount imaging, histopathological analysis, and immunofluorescence
  - Mosaic analysis with double markers (MADM) staining
  - TUNEL assay
  - Western blotting
  - Flow cytometry
- QUANTIFICATION AND STATISTICAL ANALYSIS

SUPPLEMENTAL INFORMATION

Supplemental information can be found online at https://doi.org/10.1016/j.devcel.2021.08.004.

ACKNOWLEDGMENTS

We thank J. Lau and Dr. Y. Huang for technical assistance, Dr. A. Groves for providing the Pax2-cre mice, Dr. W.D. Snider for the *Mek1*$^{flox/flox}$/*Mek2*$^{-/-}$ mice, Dr. B. Novitch for the Olig2 antibody, and members of the Zhu lab for support. This work is supported by grants from the DOD NFRP (W81XWH1810685), the NIH Neuroscience training grant (T32-NS076401), Francis S. Collins Neurofibromatosis Therapeutic Association Program, Hyundai Hope On Wheels Young Investigator Award, and the National Science Foundation Graduate Research Fellowship Program.

AUTHOR CONTRIBUTIONS

E.S.J., W.Z., M.B., and Y.Z. conceived and designed the study. E.S.J., W.Z., M.B., and Y.L. performed the experiments. E.J., W.Z., M.B., Y.L., D.M.T., and Y.Z. analyzed the results. S.F.A., Y.W., J.J., D.M.T, S.F.S., W.L., H.Z., and R.J.P. assisted with supervision and resources. D.M., A.F., M.K., F.N., and S.H. provided technical assistance. Y.Z. acquired the funding and wrote the manuscript with contributions from all of the authors.

DECLARATION OF INTERESTS

The authors declare no competing interests.

Received: February 19, 2021
Revised: July 11, 2021
Accepted: August 3, 2021
Published: August 23, 2021

REFERENCES

Akgül, S., Li, Y., Zheng, S., Kool, M., Treisman, D.M., Li, C., Wang, Y., Gröbner, S., Ikenoue, T., Shen, Y., et al. (2018). Opposing tumor-promoting and -Suppressive functions of Rictor/mTORC2 signaling in adult glioma and pediatric SHH medulloblastoma. Cell Rep *24*, 463–478.e5.

Castel, P., Rauen, K.A., and McCormick, F. (2020). The duality of human oncoproteins: drivers of cancer and congenital disorders. Nat. Rev. Cancer *20*, 383–397.

D'Angelo, F., Ceccarelli, M., Tala, Garofano, L., Zhang, J., Frattini, V., Caruso, F.P., Lewis, G., Alfaro, K.D., Bauchet, L., et al. (2019). The molecular landscape of glioma in patients with Neurofibromatosis 1. Nat Med *25*, 176–187.

Fangusaro, J., Onar-Thomas, A., Poussaint, T.Y., Wu, S., Ligon, A.H., Lindeman, N., Campagne, O., Banerjee, A., Gururangan, S., Kilburn, L., et al. (2021). A phase 2 trial of selumetinib in children with recurrent optic pathway and hypothalamic low-grade glioma without NF1: a pediatric brain tumor consortium study. Neuro-Oncology. https://doi.org/10.1093/neuonc/noab047.

Fisher, M.J., Loguidice, M., Gutmann, D.H., Listernick, R., Ferner, R.E., Ullrich, N.J., Packer, R.J., Tabori, U., Hoffman, R.O., Ardern-Holmes, S.L., et al. (2012). Visual outcomes in children with neurofibromatosis type 1-associated optic pathway glioma following chemotherapy: a multicenter retrospective analysis. Neuro-Oncology *14*, 790–797.

Gripp, K.W., Morse, L.A., Axelrad, M., Chatfield, K.C., Chidekel, A., Dobyns, W., Doyle, D., Kerr, B., Lin, A.E., Schwartz, D.D., et al. (2019). Costello syndrome: clinical phenotype, genotype, and management guidelines. Am. J. Med. Genet. A *179*, 1725–1744.

Gross, A.M., Frone, M., Gripp, K.W., Gelb, B.D., Schoyer, L., Schill, L., Stronach, B., Biesecker, L.G., Esposito, D., Hernandez, E.R., et al. (2020). Advancing RAS/RASopathy therapies: an NCI-sponsored intramural and extramural collaboration for the study of RASopathies. Am. J. Med. Genet. A *182*, 866–876.

Gutmann, D.H., Ferner, R.E., Listernick, R.H., Korf, B.R., Wolters, P.L., and Johnson, K.J. (2017). Neurofibromatosis type 1. Nat. Rev. Dis. Primers *3*, 17004.

Jones, D.T.W., Kieran, M.W., Bouffet, E., Alexandrescu, S., Bandopadhayay, P., Bornhorst, M., Ellison, D., Fangusaro, J., Fisher, M.J., Foreman, N., et al. (2018). Pediatric low-grade gliomas: next biologically driven steps. Neuro-Oncology *20*, 160–173.

Kim, E., Wang, Y., Kim, S.J., Bornhorst, M., Jecrois, E.S., Anthony, T.E., Wang, C., Li, Y.E., Guan, J.L., Murphy, G.G., and Zhu, Y. (2014). Transient inhibition of the ERK pathway prevents cerebellar developmental defects and improves long-term motor functions in murine models of neurofibromatosis type 1. eLife *3*, e05151.

Lee, D.Y., Gianino, S.M., and Gutmann, D.H. (2012). Innate neural stem cell heterogeneity determines the patterning of glioma formation in children. Cancer Cell *22*, 131–138.

Li, X., Newbern, J.M., Wu, Y., Morgan-Smith, M., Zhong, J., Charron, J., and Snider, W.D. (2012). MEK is a key regulator of gliogenesis in the developing brain. Neuron *75*, 1035–1050.

Li, Y., Li, B., Li, W., Wang, Y., Akgül, S., Treisman, D.M., Heist, K.A., Pierce, B.R., Hoff, B., Ho, C.-Y., et al. (2020). Murine models of IDH-wild-type glioblastoma exhibit spatial segregation of tumor initiation and manifestation during evolution. Nat. Commun. *11*, 3669.

Ligon, K.L., Alberta, J.A., Kho, A.T., Weiss, J., Kwaan, M.R., Nutt, C.L., Louis, D.N., Stiles, C.D., and Rowitch, D.H. (2004). The oligodendroglial lineage marker OLIG2 is universally expressed in diffuse gliomas. J. Neuropathol. Exp. Neurol. *63*, 499–509.

Liu, C., Sage, J.C., Miller, M.R., Verhaak, R.G., Hippenmeyer, S., Vogel, H., Foreman, O., Bronson, R.T., Nishiyama, A., Luo, L., and Zhong, H. (2011). Mosaic analysis with double markers reveals tumor cell of origin in glioma. Cell *146*, 209–221.

Ma, T., Wong, S.Z.H., Lee, B., Ming, G.L., and Song, H. (2021). Decoding neuronal composition and ontogeny of individual hypothalamic nuclei. Neuron *109*, 1150–1167.e6.

Marsters, C.M., Rosin, J.M., Thornton, H.F., Aslanpour, S., Klenin, N., Wilkinson, G., Schuurmans, C., Pittman, Q.J., and Kurrasch, D.M. (2016). Oligodendrocyte development in the embryonic tuberal hypothalamus and the influence of Ascl1. Neural Dev *11*, 20.

Micallef, L., and Rodgers, P. (2014). eulerAPE: drawing area-proportional 3-Venn diagrams using ellipses. PLoS One *9*, e101717.

Miller, R.H., Ffrench-Constant, C., and Raff, M.C. (1989). The macroglial cells of the rat optic nerve. Annu. Rev. Neurosci. *12*, 517–534.

Ohyama, T., and Groves, A.K. (2004). Generation of Pax2-Cre mice by modification of a Pax2 bacterial artificial chromosome. Genesis *38*, 195–199.

Ono, K., Hirahara, Y., Gotoh, H., Nomura, T., Takebayashi, H., Yamada, H., and Ikenaka, K. (2018). Origin of oligodendrocytes in the vertebrate optic nerve: a review. Neurochem. Res. *43*, 3–11.

Packer, R.J., Iavarone, A., Jones, D.T.W., Blakeley, J.O., Bouffet, E., Fisher, M.J., Hwang, E., Hawkins, C., Kilburn, L., MacDonald, T., et al. (2020). Implications of new understandings of gliomas in children and adults with NF1: report of a consensus conference. Neuro-Oncology *22*, 773–784.

Péquignot, M.O., Provost, A.C., Sallé, S., Taupin, P., Sainton, K.M., Marchant, D., Martinou, J.C., Ameisen, J.C., Jais, J.P., and Abitbol, M. (2003). Major role of BAX in apoptosis during retinal development and in establishment of a functional postnatal retina. Dev. Dyn. *228*, 231–238.

Reitman, Z.J., Paolella, B.R., Bergthold, G., Pelton, K., Becker, S., Jones, R., Sinai, C.E., Malkin, H., Huang, Y., Grimmet, L., et al. (2019). Mitogenic and progenitor gene programmes in single pilocytic astrocytoma cells. Nat. Commun. *10*, 3731.

Ryall, S., Zapotocky, M., Fukuoka, K., Nobre, L., Guerreiro Stucklin, A., Bennett, J., Siddaway, R., Li, C., Pajovic, S., Arnoldo, A., et al. (2020). Integrated molecular and clinical analysis of 1,000 pediatric low-grade gliomas. Cancer Cell *37*, 569–583.e5.

Sellmer, L., Farschtschi, S., Marangoni, M., Heran, M.K.S., Birch, P., Wenzel, R., Mautner, V.F., and Friedman, J.M. (2018). Serial MRIs provide novel insight

into natural history of optic pathway gliomas in patients with neurofibromatosis 1. Orphanet J. Rare Dis. *13*, 62.

Song, M., Vogelstein, B., Giovannucci, E.L., Willett, W.C., and Tomasetti, C. (2018). Cancer prevention: molecular and epidemiologic consensus. Science *361*, 1317–1318.

Tao, C., and Zhang, X. (2014). Development of astrocytes in the vertebrate eye. Dev. Dyn. *243*, 1501–1510.

Tchoghandjian, A., Fernandez, C., Colin, C., El Ayachi, I., Voutsinos-Porche, B., Fina, F., Scavarda, D., Piercecchi-Marti, M.D., Intagliata, D., Ouafik, L., et al. (2009). Pilocytic astrocytoma of the optic pathway: a tumour deriving from radial glia cells with a specific gene signature. Brain *132*, 1523–1535.

Tomasetti, C., Li, L., and Vogelstein, B. (2017). Stem cell divisions, somatic mutations, cancer etiology, and cancer prevention. Science *355*, 1330–1334.

Wang, Y., Kim, E., Wang, X., Novitch, B.G., Yoshikawa, K., Chang, L.S., and Zhu, Y. (2012). ERK inhibition rescues defects in fate specification of Nf1-deficient neural progenitors and brain abnormalities. Cell *150*, 816–830.

Wang, Y., Yang, J., Zheng, H., Tomasek, G.J., Zhang, P., McKeever, P.E., Lee, E.Y., and Zhu, Y. (2009). Expression of mutant p53 proteins implicates a lineage relationship between neural stem cells and malignant astrocytic glioma in a murine model. Cancer Cell *15*, 514–526.

Zhang, Y., Sloan, S.A., Clarke, L.E., Caneda, C., Plaza, C.A., Blumenthal, P.D., Vogel, H., Steinberg, G.K., Edwards, M.S., Li, G., et al. (2016). Purification and characterization of progenitor and mature human astrocytes reveals transcriptional and functional differences with mouse. Neuron *89*, 37–53.

Zhou, X., Zhong, S., Peng, H., Liu, J., Ding, W., Sun, L., Ma, Q., Liu, Z., Chen, R., Wu, Q., and Wang, X. (2020). Cellular and molecular properties of neural progenitors in the developing mammalian hypothalamus. Nat. Commun. *11*, 4063.

Zhu, Y., Harada, T., Liu, L., Lush, M.E., Guignard, F., Harada, C., Burns, D.K., Bajenaru, M.L., Gutmann, D.H., and Parada, L.F. (2005). Inactivation of NF1 in CNS causes increased glial progenitor proliferation and optic glioma formation. Development *132*, 5577–5588.

Zhu, Y., Romero, M.I., Ghosh, P., Ye, Z., Charnay, P., Rushing, E.J., Marth, J.D., and Parada, L.F. (2001). Ablation of NF1 function in neurons induces abnormal development of cerebral cortex and reactive gliosis in the brain. Genes Dev *15*, 859–876.

STAR★METHODS

KEY RESOURCES TABLE

Reagent or resource	Source	Identifier
Antibodies		
Rabbit anti-PTEN	Cell Signaling	9559; RRID: AB_390810
Mouse anti-Olig2	Millipore	MABN50; RRID: AB_10807410
Goat anti-Olig2	R&D systems	AF2418; RRID: AB_2157554
Rabbit anti-Olig2	Millipore	AB9610; RRID: AB_570666
Guinea pig anti-Olig2	Dr. B. Novitch	Homemade
Goat anti- PDGFRα	R&D systems	AF1062; RRID: AB_2236897
Mouse anti-GFAP	BD PharMingen	556330; RRID: AB_396368
Mouse anti-Ki67	BD PharMingen	550609; RRID: AB_393778
Rabbit anti-Ki67	Abcam	16667; RRID: AB_302459
Rabbit anti-Iba1	Wako	013-27691
Goat anti-Pax2	R&D systems	AF3364; RRID: AB_10889828
Rabbit anti-Pax2	BioLegend	PRB-276P; RRID: AB_291611
Guinea pig anti-RBPMS	Cedarlane	1832
Chicken anti-GFP	Abcam	AB13970; RRID: AB_300798
Rabbit anti-GFP	Millipore	MAB3580; RRID: AB_94936
Mouse anti-RFP	Abcam	AB125244; RRID: AB_10973556
Rabbit anti-RFP	Abcam	AB62341; RRID: AB_945213
Rat anti-MBP	Millipore	MAB386; RRID: AB_94975
Chicken anti-Neurofilament 68kDa (NF68k)	Abcam	AB72997; RRID: AB_1267598
Rat anti-CD68	Bio-Rad	MCA1957; RRID: AB_322219
Rabbit anti-Cre	BioLegend	908001; RRID: AB_2565079
Rabbit anti-P2Y12	AnaSpec	AS-55043A
Goat anti-Sox9	R&D systems	AF3075; RRID: AB_2194160
Rabbit anti-pErk1/2$^{T202/Ty204}$	Cell Signaling	9101S; RRID: AB_331646
Rabbit anti-Erk1/2	Cell Signaling	9102L; RRID: AB_330744
Mouse anti-BLBP	LifeSpan Biosciences	LS-B6684-50; RRID: AB_11143615
Rabbit anti-BLBP	Millipore	ABN14; RRID: AB_10000325
Rabbit anti-pAkt^{S473}	Cell Signaling	4060L; RRID: AB_2315049
Rabbit anti-Akt	Cell Signaling	9272S; RRID: AB_329827
Rabbit anti-S6	Cell Signaling	2217S; RRID: AB_331355
Rabbit anti-pS6$^{S240/244}$	Cell Signaling	5364S; RRID: AB_10694233
Mouse anti-β-Actin	Sigma-Aldrich	A5316; RRID: AB_476743
Alexa Fluor 488	Invitrogen, Life Technologies	A11001; RRID: AB_2535850; A11034; RRID: AB_2576217
Alexa Fluor 555	Invitrogen, Life Technologies	A21429; RRID: AB_2535850; A21424; RRID: AB_141780
Alexa Fluor 647	Invitrogen, Life Technologies	A31571; RRID: AB_162542; A21236; RRID: AB_2535805; A21247; RRID: AB_141778; A21245; RRID: AB_2535813
HRP-conjugated secondary antibodies	BioRad	1706515; RRID: AB_2617112; 1706516; RRID: AB_11125547
Fc receptor blocking	BioLegend	101320; RRID: AB_1574975
Rat PE-anti-CD3	BioLegend	100206; RRID: AB_1574975
Hamster FITC-anti-CD3	Invitrogen	11-0031-85; RRID: AB_464883

(*Continued on next page*)

Continued		
Reagent or resource	Source	Identifier
Chemicals, Peptides, and Recombinant Proteins		
PD0325901	Sigma	PZ0162
Critical commercial assays		
Click-it® TUNEL Alexa Fluor®	Invitrogen, Life Technologies	C10247
Experimental models: Organisms/strains		
Mouse; Nf1	Zhu et al., 2001	N/A
Mouse; hGFAP-cre	Wang et al., 2009	N/A
Mouse; Pax2-cre	Ohyama and Groves, 2004	N/A
Mouse; Mek1/Mek2	Li et al., 2012	N/A
Mouse; MADM	Liu et al., 2011	
Oligonucleotides		
Primers for genotyping PCR see method details	This paper	N/A
Software and algorithms		
ImageJ (Version 1.52c)	N/A	https://imagej.nih.gov/ij/
Graphpad Prism 8.0	GraphPad Software Inc.	https://www.graphpad.com/scientific-software/prism/
EulerAPE	N/A	http://www.eulerdiagrams.org/eulerAPE/

RESOURCE AVAILABILITY

Lead contact

Further information and requests for resources and reagents should be directed to the Lead Contact, Yuan Zhu, Ph.D. (yzhu@childrensnational.org).

Material availability

All the reagents and mice generated in this study are available upon request.

Data and Code Availability

The original data generated in this study are available upon request.

EXPERIMENTAL MODELS AND SUBJECT DETAILS

$Nf1^{hGFAP}$CKO

The $Nf1^{hGFAP}$CKO mice were previously described (Kim et al., 2014; Wang et al., 2012; Zhu et al., 2005). The control mice used in this study are a pool of phenotypically indistinguishable mice with genotypes $Nf1^{flox/flox}$; $Nf1^{flox/+}$; and hGFAP-cre^{+}; $Nf1^{flox/+}$. The $Nf1^{hGFAP}$CKO mice used was of the genotype hGFAP-cre^{+}; $Nf1^{flox/flox}$ and was maintained in the mixed backgrounds of C57Bl6, 129Svj, and FVB.

$Nf1^{Pax2}$CKO

$Nf1^{Pax2}$CKO mice were generated by crossing Pax2-cre (Ohyama and Groves, 2004) and $Nf1^{flox/flox}$ mice. The control mice used in this study are a pool of phenotypically indistinguishable mice with genotypes $Nf1^{flox/flox}$; $Nf1^{flox/+}$; and Pax2-cre^{+}; $Nf1^{flox/+}$. The mutant $Nf1^{Pax2}$CKO used was of the genotype Pax2-cre^{+}; $Nf1^{flox/flox}$ and was maintained in the mixed backgrounds of C57Bl6, 129Svj, CD1 and FVB.

$Nf1^{hGFAP}$CKO-*Mek1/2*

The $Mek1^{flox/flox}$ and Mek2$^{-/-}$ mice were described previously (Li et al., 2012). They were later crossed into the hGFAP-cre or $Nf1^{hGFAP}$CKO background described above to generate four groups of mutant mice with different numbers of *Mek1/2* alleles:

M0 (hGFAP-cre^{+};$Mek1^{flox/flox}$;Mek2$^{-/-}$)
N-M0 (hGFAP-cre^{+};$Nf1^{flox/flox}$;$Mek1^{flox/flox}$;Mek2$^{-/-}$)
N-M1 (hGFAP-cre^{+};$Nf1^{flox/flox}$;$Mek1^{flox/flox}$;Mek2$^{-/+}$ or hGFAP-cre^{+};$Nf1^{flox/flox}$;$Mek1^{flox/+}$;Mek2$^{-/-}$)
N-M2 (hGFAP-cre^{+};$Nf1^{flox/flox}$;$Mek1^{flox/+}$;Mek2$^{-/+}$, or hGFAP-cre^{+};$Nf1^{flox/flox}$;$Mek1^{flox/flox}$;Mek2$^{+/+}$, or hGFAP-cre^{+};$Nf1^{flox/flox}$;Mek1$^{+/+}$;Mek2$^{-/-}$)
N-M3 (hGFAP-cre^{+};$Nf1^{flox/flox}$;$Mek1^{flox/+}$;Mek2$^{+/+}$, or hGFAP-cre^{+};$Nf1^{flox/flox}$;Mek1$^{+/+}$;Mek2$^{-/+}$)
N-M4 (hGFAP-cre^{+};$Nf1^{flox/flox}$;Mek1$^{+/+}$;Mek2$^{+/+}$)

MADM-*Nf1*

The MADM mice used in this study were previously described (Liu et al., 2011). TG mice were crossed with hGFAP-cre^{+};*Nf1*$^{flox/+}$ mice. They were subsequently crossed with GT mice to generate TG/GT hGFAP-cre^{+};*Nf1*$^{flox/+}$ mice for MADM analysis. Cre negative mice and Cre positive Nf1$^{+/+}$ MADM mice were used for controls.

All mice in this study were cared for according to the guidelines that were approved by the Animal Care and Use Committees of the University of Michigan at Ann Arbor as well as the Institutional Animal Care and Use Committee of Children's National Medical Center in Washington, DC. Age and littermate-matched control and mutant mice were used for the developmental analyses to minimize the impact of modifier genes. Similar numbers of mice with both genders were used for the experiments.

Human pLGG Samples

FFPE (Formalin-fixed paraffin-embedded) tissue specimens from NF1 patients diagnosed with low-grade gliomas (LGGs) were obtained from the Department of Pathology at the Children's National Hospital at Washington DC. The case list included a pLGG from the pons of a 5-year-old female, a pLGG from the cerebellum of 10-year-old, and two pLGGs from the chiasms of a 14-year-old female and an 18-year-old male. The de-identified specimens were collected under the exempt Children's National Hospital Institutional Review Board Protocol "Cellular Analysis of Low-Grade Gliomas," Pro 00008541; PI: Miriam Bornhorst, MD. Normal tissue samples for comparison (pons, cerebellum, optic nerve) were collected from pediatric patients who consented for post-mortem tissue collection through Pro 00001339; PI: Javad Nazarian, PhD. Hematoxylin and Eosin staining was performed in each tissue location to ensure that the tissues were not infiltrated with tumor.

METHOD DETAILS

Genotyping and PCR

Genetic analysis of mice in the colony used genomic DNA extracted from tail snips incubated overnight at 50°C in SDS-EDTA TAE Buffer with Proteinase K (Roche Diagnostics). The resulting solution was mixed with isopropanol (1:1) to allow DNA to precipitate. The precipitate was then transferred and diluted into ultrapure water before PCR analysis was performed for each individual target listed below using the Taq 2X MeanGreen Master Mix (Empyrical BioScience) or 2X PCR Super Master Mix (Bimake) in conjuncture with the following primers:

Cre primers	
Icres	5′-CCG TTT GCC GGT CGT GGG-3′
IcreAs	5′-CG TAT ATC CTG GCA GCG ATC- 3′
Pax2-Cre primers	
IRES forward	5′-CCGAAGCCGCTTGGAATAA-3′
IRES reverse	5′-CCCAGATCAGATCCCATACAATG-3′
Nf1 Primers	
Yuan 11	5′-CTT CAG ACT GAT TGT TGT ACC TGA- 3′
Yuan 6.1	5′-AAA TCA GCA GAG GTT GTC AGA ATC- 3′
Yuan 6.2	5′-AGT TCC ATC ACA CGT AAA ATT GAG- 3′
tdTomato Primers	
RT 1	5′-AAG GGA GCT GCA GFG GAG TA- 3′
RT 2	5′-CCG AAA ATC TGT GGG AAG TC- 3′
RT 3	5′-GGC ATT AAA GCA GCG TAT CC- 3′
RT 4	5′-CTG TTC CTG TAC GGC ATG G- 3′
GFP Primers	
eGFP-F	5′-GAG CTG GAC GGC GAC GTA AAC- 3′
eGFP-R	5′-CGT TGT GGC TGT TGT TAG TGT TAC- 3′
Mek1/2 Primers	
Mek1-Olig9	5′-CAG AAG TTC CCA CGA CAC TA- 3′
Mek1-2772Flox	5′-GTC TGT CAC TTG TCT TCT GG- 3′
Mek2WT-13131	5′-CTG ACC TTC CTG TAG GTG- 3′
Mek2WT-13424	5′-ACT CAC GGA CAT GTA GGA- 3′
Mek2KO-Neo25	5′-CGT GCA ATC CAT CTT GTT C- 3′

(*Continued on next page*)

Continued	
MADM primers	
Chr11_CS1	5′-TGGAGGAGGACAAACTGGTCAC-3′
Rosa4	5′-TCAATGGGCGGGG GTCGTT-3′
Chr11_CS2	5′-TTCCCTTTCTGCTTCATCTTGC-3′

MEK inhibitor treatment

MEK inhibitor (MEKi) PD0325901 (Sigma, PZ0162-25MG) was dissolved in 0.5% hydroxypropyl methyl-cellulose plus 0.2% Tween 80 (Sigma) at a concentration of 1mg/ml. The solution was administered by oral gavage at the dosage of 5, 10 or 20 mg/kg (body weight) every day from P0.5-P21 to lactating females (termed the "MEKi-in-milk" protocol) (Kim et al., 2014; Wang et al., 2012). Mice that received vehicle (0.5% hydroxypropyl methyl-cellulose plus 0.2% Tween 80) treatment were used as controls. Entire litter received either vehicle or MEKi treatment. For the MEKi pharmacodynamic studies, PD0325901 (10mg/kg) or vehicle was given to the lactating females via gavage or directly administered to the pups via intraperitoneal injection (IP) using various doses at 0.125mg/kg, 0.25mg/kg, 0.5mg/kg and 1mg/kg as indicated in the figure.

Tissue preparation and processing from adult, embryonic and neonatal tissues

Adult mice (>P15) were perfused with 4% paraformaldehyde (PFA), then optic nerves and brains were dissected, followed by overnight post-fixation in 4% PFA at 4°C. Optic nerves, retinas, and brains were processed through a sequence of dehydration steps prior to paraffin embedding. Optic nerves were separated into two portions and embedded separately: the distal nerves, including the pre-chiasmatic nerve and the chiasm, and the proximal portion, which included the retina and the optic nerve head (ONH). Paraffin embedded optic nerves were sectioned horizontally and brains were sectioned sagittally or coronally at 5 μm thickness by using a rotary microtome (Leica RM2235). For cross-sectional analysis, eyes from pigmented mice were embedded whole in paraffin and sectioned horizontal to the ONH. Tissues were sectioned at 5 μm thickness. Two criteria were used to select slides for histological analysis: (1) presence of the ONH, and (2) a single layer of RGC in the GCL. For cryostat sections, tissues were fixed overnight in 4% PFA at 4°C, cryoprotected in 30% sucrose and embedded in Tissue-Tek OCT compound (Sakura). Tissues were sectioned at 10 μm thickness using a cryostat (Leica CM 1950). All sections were collected on Superfrost Plus microscope slides (Fisher Scientific).

To prepare for cryostat sections from embryonic and neonatal optic nerves, entire heads, excluding the lower mandible, were embedded. Tissue embedding molds (Polysciences) were coated with OCT and the head was positioned ventral side-down on top of the OCT. The remaining OCT was carefully poured over the head to avoid bubbles until none of the tissue remained exposed. The molds were placed in a dry ice-methanol bath for rapid freezing, then transferred to -80°C for storage. To analyze embryonic or neonatal brains, the brain was carefully dissected out of the skull, placed ventral side up in a brain slicer matrix (Zivic), and the forebrain was divided into two portions. Each brain portion was individually cryopreserved for sectioning. Cryopreserved samples were sectioned at 8 μm thickness.

For protein analysis, P8 pups treated with single dose of MEKi or vehicle through gavage or IP injection were sacrificed between 2–6 h after treatment. Mice were perfused with PBS and the cerebellum and spleen were frozen immediately in liquid nitrogen. Samples were stored in -80°C freezer for western blotting analysis.

Whole-mount imaging, histopathological analysis, and immunofluorescence

Chiasms and optic nerves were micro-dissected, cleaned, and imaged using an Olympus BX-51 fluorescence microscope for whole-mount imaging. The paraffin sections of brain and optic nerve were subjected to histopathological analysis with hematoxylin and eosin (H&E) staining. For immunofluorescence, paraffin sections were deparaffinized through Xylene, 100% ethanol, 95% ethanol, 50% ethanol and 30% ethanol and rehydrated in distilled water. Antigen retrieval was performed with Retrieve-all antigen retrieval solution (BioLegend) in heated coplin jars. Cryosections do not require deparaffinization or antigen retrieval steps and were therefore directly fixed in 4% PFA for 15 min. Sections were then permeabilized by 0.3% Triton-X (Sigma) solution for 20 min and blocked for 1 h with 3% normal goat/horse/donkey serum (Sigma) depending on the secondary antibody selection. Slides were put in a humidified chamber and incubated in primary antibodies, dissolved in the blocking solution, at 4°C overnight. The visualization of primary antibodies for colorimetric labeling was performed with biotinylated secondary antibody (Vector, 1:400), treated with an avidin-biotin complex (Vector), and then subjected to DAB staining (VWR). Hematoxylin was used as a counterstain. The visualization of primary antibodies for immunofluorescence was performed by using Alexa 488, Alexa 555 and Alexa 647-conjugated secondary antibodies (Invitrogen, Life-Technologies) at 1:400 dilution and incubated for 1-hour at room temperature. Slides were washed three times in between the steps with 1X PBS. DAPI (1:2000) was used as a counterstain to label individual cell nuclei. Sections were examined under a light and fluorescent microscope (Olympus BX-63).

The embryonic (E17.5) hypothalamic regions (Figures 2 and 3) were imaged with a 20X objective using a LSM 780 Zeiss confocal microscope equipped with computer-driven motorized stage controlled by Zen Lite software (Black edition, Zeiss). Magnifications images (Figure 2) were taken from ventral part of the third ventricular zone and mantle zone areas using a 40X objective for Sox9/BLBP/Cre markers co-expression analysis.

The primary antibodies used in this study were:
BLBP (ABN14, 1:400, rabbit, EMD Millipore),
BLBP (LS-B6684-50, 1:400, mouse, LifeSpan Biosciences),
CD68 (MCA1957, 1:600, rat, Bio-Rad),
Cre (908001, 1:400, rabbit, BioLegend),
GFAP (556330, 1:2000, mouse, BD Pharmingen),
GFP (MAB3580, 1:500, rabbit, EMD Millipore),
GFP (AB13970, 1:500, chicken, Abcam),
Iba1 (013-27691, 1:2000, rabbit, Wako),
Ki67 (550609, 1:500, mouse, BD Pharmingen),
Ki67 (75019, 1:500, rabbit, Abcam),
MBP (MAB386, 1:500, rat, EMD Millipore),
Neurofilament 68kDa (NF68k) (ab72997, 1: 500, Abcam),
Olig2 (AB9610, 1:2000, rabbit, EMD Millipore),
Olig2 (MABN50, 1:300, mouse, EMD Millipore),
Olig2 (1:10000, guinea pig, a kind home-made gift from Dr. B. Novitch),
Olig2 (AF2418, 1:400, goat, R&D systems),
Pax2 (PRB-276P, 1:400, rabbit, BioLegend),
Pax2 (AF3364, 1:400, goat, R&D systems),
PDGFRα (AF1062, 1:1000, goat, RD),
PTEN (9559, 1:400, rabbit, Cell Signaling), p-Erk (9101S, 1:200, rabbit, Cell Signaling),
P2Y12 (AS-55043A, 1:1000, rabbit, AnaSpec), RBPMS (1832, 1:250, guinea pig, Cedarlane),
RFP (AB62341, 1:400, rabbit, Abcam),
RFP (AB125244, 1:400, mouse, Abcam),
Sox9 (AF3075, 1:400, goat, R&D systems).

Mosaic analysis with double markers (MADM) staining

Cryosections were used for immunofluorescence analysis involving the MADM model (for GFP and RFP). GFP and RFP signals were detected by anti-GFP and anti-RFP primary antibodies, which occupied the commonly used green (488 nm laser) and red (555 nm laser) channels under a fluorescent microscope. Staining with additional markers was visualized in the Far-red channel (635 nm laser) using the appropriate secondary antibody.

TUNEL assay

Terminal deoxynucleotidyl transferase (TdT) dUTP Nick-End Labeling (TUNEL) assay was performed on paraffin sections of retinas using the Click-iT® TUNEL Alexa Fluor® Imaging kit from Invitrogen (C10247), according to manufacturer's recommendations.

Western blotting

Snap-frozen samples from vehicle or MEKi treated control and mutant cerebella were homogenized in Pierce RIPA Buffer (Thermo Scientific) (10 μl buffer/1 mg tissue) for 20 min on ice, then subjected to centrifugation at 14,000 rpm for 10 min at 4°C. The supernatant was mixed 1:1 with Laemmli Sample Buffer (BioRad, Hercules, CA) and boiled at 100°C for 10 min. Samples were then subjected to SDS-PAGE using the Criterion TGX Precast gels (BioRad) and transferred onto PVDF membranes (EMD Millipore). Membranes were blocked in 5% non-fat milk prepared in 1X TBST and incubated with primary antibodies at 4°C overnight. The following day, the membranes were washed with TBST and incubated in horseradish peroxidase (HRP)-conjugated secondary antibodies at room temperature for 1 h. The membranes were then exposed to Pierce ECL western blotting substrate (Thermo Scientific) for 3–5 min to detect signal by film development in dark room. The primary antibodies used in this study were:
p-Erk1/2$^{T202/Ty204}$ (9101S, 1:1,000, rabbit, Cell Signaling),
Erk1/2 (9102L, 1:1,000, rabbit, Cell Signaling),
pAkt^{S473} (4060L, 1: 1,000, rabbit, Cell Signaling),
Akt (9272S, 1: 1,000, rabbit, Cell Signaling),
p-S6 (5364S, 1: 2,000, rabbit, Cell Signaling),
S6 (2217S, 1: 2,000, rabbit, Cell Signaling),
β-Actin (A5316, 1: 20,000, mouse, Sigma-Aldrich).

Flow cytometry

Optic nerves/chiasm, and blood from MADM mice were collected at postnatal day 15, 21, and 30. Tissues were transferred to Cold Activated Protease buffer (500μg/ml *Bacillus Licheniformis*, 5mM $CaCL_2$, 12.5U/ml DNase I, 1X PBS) and incubated on ice for 15 min with intermittent trituration. Cell suspension was filtered through a 70μm cell strainer and washed twice with 1X PBS. All subsequent procedures were performed on ice protected from light. Samples were resuspended in Live/Dead Aqua [1:500 in 1X PBS], incubated for 30 min, and washed with 1X PBS. Samples were resuspended in FACS staining buffer (1X PBS, 0.1% FBS, 0.01% Sodium Azide)

and Fc-block (BioLedend, San Diego, CA) for 15 min. Samples were washed twice in FACS staining buffer and acquired using a CytoFLEX S analyzer with CytExpert software (Beckman Coulter, Indianapolis, IN). Blood samples were incubated in ACK lysis buffer, followed by Live/Dead Aqua and PE- or FITC-conjugated anti-CD3 staining for gates setup. At least 10,000 - 50,000 live events were analyzed for red (tdTomato), green (GFP) fluorescence using FlowJo software (BD Biosciences, San Jose, CA).

ACK Lysis buffer (A10492-01, 2mL/test, Gibco)
Compensation beads (01-2222-42, 1 drop/test, Invitrogen)
Arc Amine Reactive Compensation Bead Kit (A10628, 1 drop for each/test, Invitrogen)
Live/dead Aqua fluorescent reactive dye (L34966A, 1:500, Invitrogen)
Fc receptor blocking (101320, 3ul/test, rat, BioLegend)
PE-anti-mouse CD3 (100206, 3ul/test, rat, BioLegend)
FITC-anti-mouse CD3 (11-0031-85, 3ul/test, hamster, Invitrogen)
PE-isotype control (12-4321-42, 3ul/test, rat, eBioscience)
FITC-isotype control (400906, 3ul/test, hamster, BioLegend)

QUANTIFICATION AND STATISTICAL ANALYSIS

Kaplan-Meir survival curves used to compare the survival of mice with different genetic manipulations of *Mek1/2*, with or without *Nf1* deletion were generated using GraphPad Prism. The Mantel-Cox (log-rank) and the Gehan-Breslow-Wilcoxon tests were used to statistically compare the overall survival.

When quantifying the optic nerve diameter, we used H&E-stained sections and imaged the thickest portion of the nerve starting from the chiasm for 100 uM at 20X magnification (adult nerves) or 40X magnification (embryonic or early postnatal). The area was measured using ImageJ (1.52c) image processing software, and cell number and density were quantified using the cell counter plugin in (https://imagej.nih.gov/ij/download.html).

For immunostaining quantification, multiple images from different mice were captured. For the quantification of embryonic (E17.5) MADM slides, three slides of the hypothalamic regions (covered 0.32 mm from the rostral to caudal positions) were analyzed. When possible, single-blind imaging and analysis was conducted. At least three animals from each group were used for quantification.

Statistical analysis was carried out using two-tailed parametric Student's t test in Graphpad Prism based on the Gaussian distribution observed in the data quantification. Data were presented as mean ± Standard Error Mean (SEM). $p < 0.05$ was considered to be statistically significant.

Venn diagrams were generated using EulerAPE (Micallef and Rodgers, 2014).

Developmental Cell, Volume *56*

Supplemental information

Treatment during a developmental window prevents NF1-associated optic pathway gliomas by targeting Erk-dependent migrating glial progenitors

Emmanuelle S. Jecrois, Wang Zheng, Miriam Bornhorst, Yinghua Li, Daniel M. Treisman, Daphine Muguyo, Sharon Huynh, Shayne F. Andrew, Yuan Wang, Jingwen Jiang, Brianna R. Pierce, Hongmei Mao, Matthew K. Krause, Austin Friend, Francisco Nadal-Nicolas, Steven F. Stasheff, Wei Li, Hui Zong, Roger J. Packer, and Yuan Zhu

Figure S1

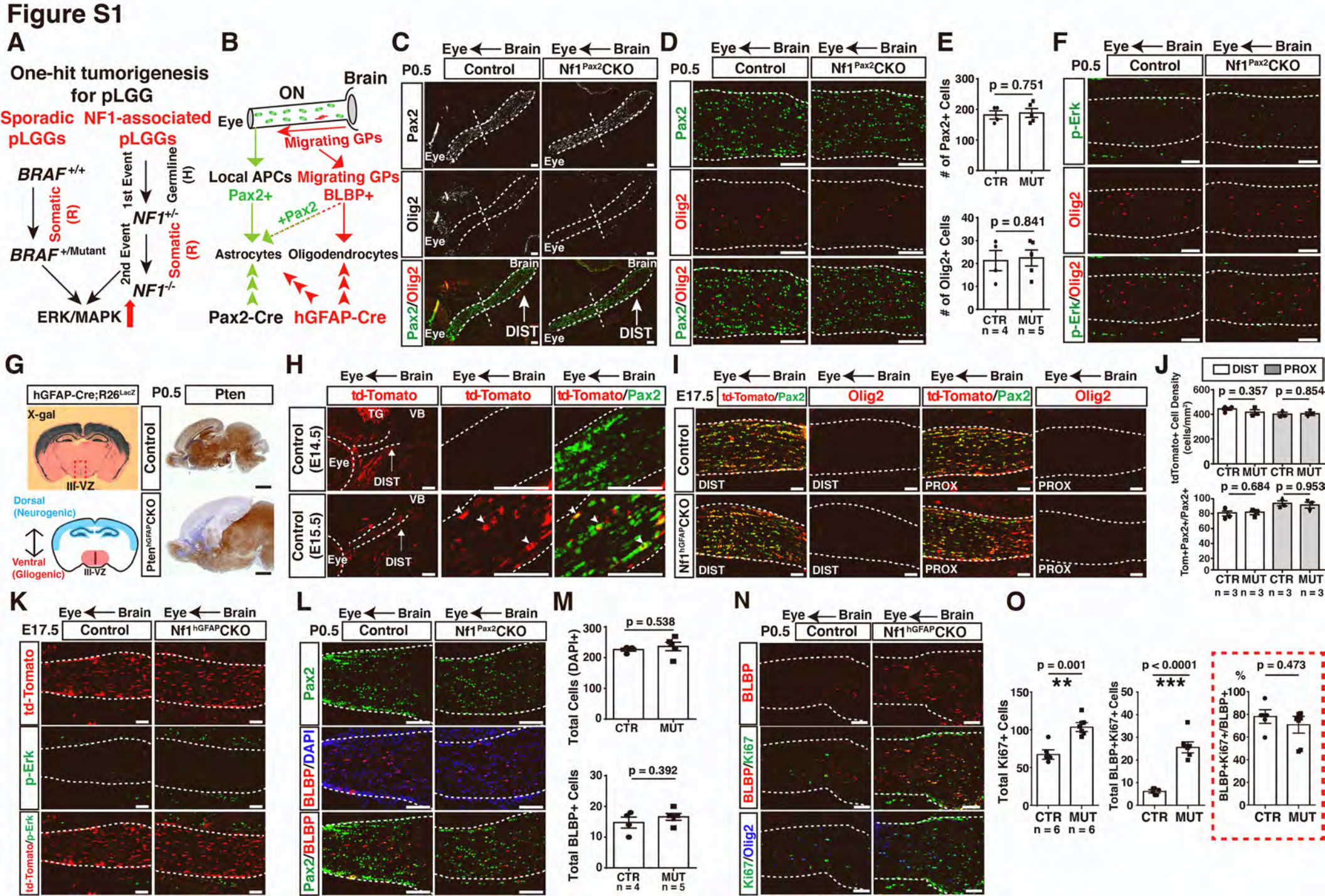
A
One-hit tumorigenesis for pLGG
Sporadic pLGGs
NF1-associated pLGGs
BRAF+/+
Somatic (R)
BRAF+/Mutant
1st Event
Germline (H)
NF1+/-
2nd Event
Somatic (R)
NF1-/-
ERK/MAPK
B
ON
Brain
Eye
Migrating GPs
Local APCs
Migrating GPs
Pax2+
BLBP+
+Pax2
Astrocytes
Oligodendrocytes
Pax2-Cre
hGFAP-Cre
C
P0.5
Eye ← Brain
Control
Nf1Pax2CKO
Pax2
Olig2
Pax2/Olig2
Eye
Brain
DIST
D
P0.5
Control
Nf1Pax2CKO
Pax2
Olig2
Pax2/Olig2
E
# of Pax2+ Cells
p = 0.751
CTR
MUT
# of Olig2+ Cells
p = 0.841
CTR n = 4
MUT n = 5
F
P0.5
Control
Nf1Pax2CKO
p-Erk
Olig2
p-Erk/Olig2
G
hGFAP-Cre;R26LacZ
X-gal
III-VZ
Dorsal (Neurogenic)
Ventral (Gliogenic)
P0.5
Pten
Control
PtenhGFAPCKO
H
Eye ← Brain
td-Tomato
td-Tomato
td-Tomato/Pax2
Control (E14.5)
Control (E15.5)
TG
VB
Eye
DIST
I
E17.5
td-Tomato/Pax2
Olig2
td-Tomato/Pax2
Olig2
Control
Nf1hGFAPCKO
DIST
PROX
J
DIST
PROX
tdTomato+ Cell Density (cells/mm2)
p = 0.357
p = 0.854
CTR MUT CTR MUT
Tom+Pax2+/Pax2+
p = 0.684
p = 0.953
n = 3 n = 3 n = 3 n = 3
K
E17.5
Control
Nf1hGFAPCKO
td-Tomato
p-Erk
td-Tomato/p-Erk
L
P0.5
Control
Nf1Pax2CKO
Pax2
BLBP/DAPI
Pax2/BLBP
M
Total Cells (DAPI+)
p = 0.538
CTR
MUT
Total BLBP+ Cells
p = 0.392
CTR n = 4
MUT n = 5
N
P0.5
Control
Nf1hGFAPCKO
BLBP
BLBP/Ki67
Ki67/Olig2
O
Total Ki67+ Cells
p = 0.001
**
CTR n = 6
MUT n = 6
Total BLBP+Ki67+ Cells
p < 0.0001
***
CTR
MUT
BLBP+Ki67+/BLBP+
%
p = 0.473
CTR
MUT

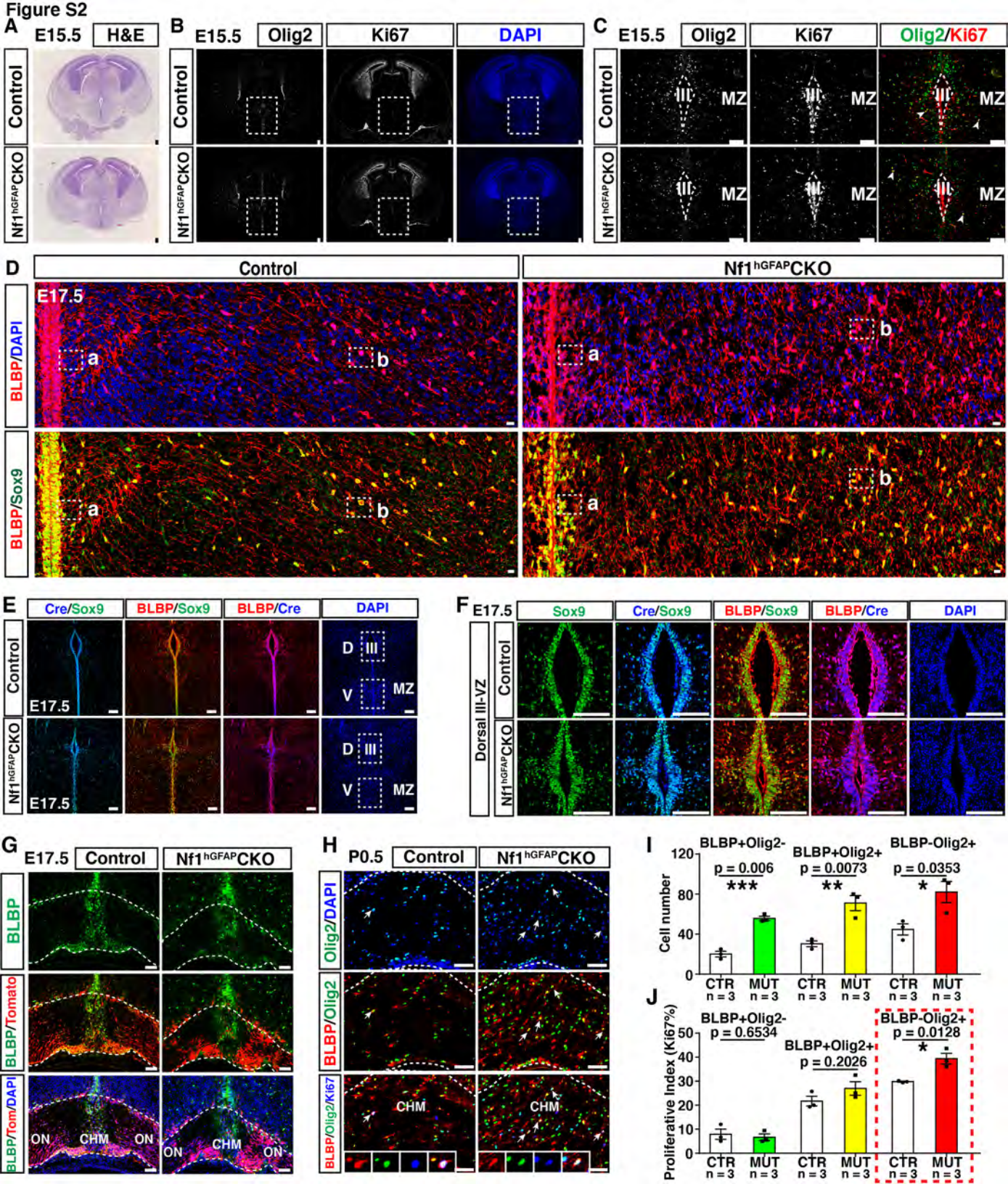
Figure S2
A
E15.5
H&E
Control
Nf1hGFAPCKO
B
E15.5
Olig2
Ki67
DAPI
C
E15.5
Olig2
Ki67
Olig2/Ki67
MZ
D
Control
Nf1hGFAPCKO
E17.5
BLBP/DAPI
BLBP/Sox9
a
b
E
Cre/Sox9
BLBP/Sox9
BLBP/Cre
DAPI
D
V
III
MZ
E17.5
F
E17.5
Sox9
Cre/Sox9
BLBP/Sox9
BLBP/Cre
DAPI
Dorsal III-VZ
G
E17.5
Control
Nf1hGFAPCKO
BLBP
BLBP/Tomato
BLBP/Tom/DAPI
ON
CHM
H
P0.5
Olig2/DAPI
BLBP/Olig2
BLBP/Olig2/Ki67
I
BLBP+Olig2-
p = 0.006
***
BLBP+Olig2+
p = 0.0073
**
BLBP-Olig2+
p = 0.0353
*
Cell number
CTR
MUT
n = 3
J
BLBP+Olig2-
p = 0.6534
BLBP+Olig2+
p = 0.2026
BLBP-Olig2+
p = 0.0128
Proliferative Index (Ki67%)

Figure S3

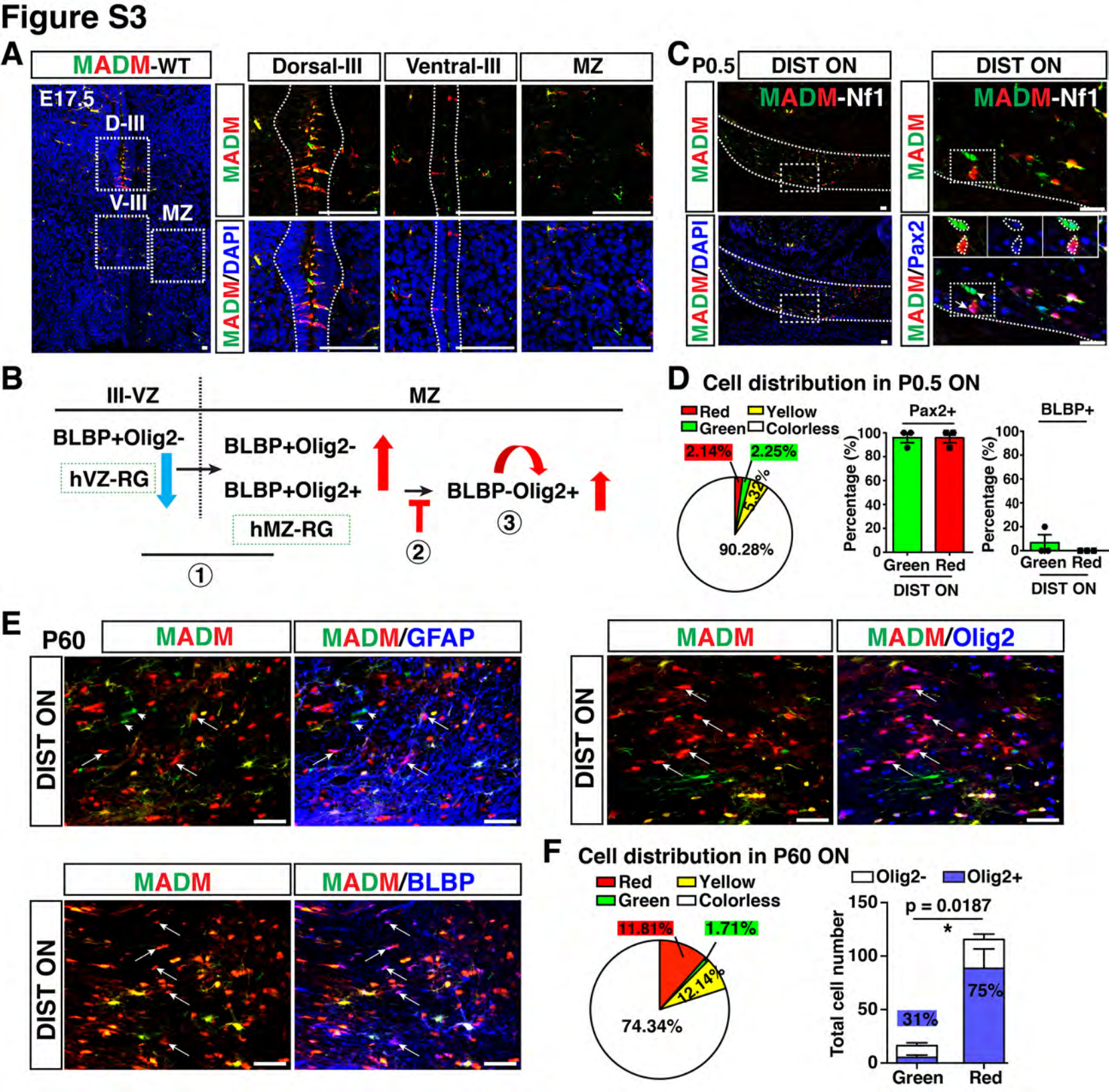
A
MADM-WT
E17.5
D-III
V-III
MZ
Dorsal-III
Ventral-III
MZ
MADM
MADM/DAPI
C
P0.5
DIST ON
MADM-Nf1
MADM/Pax2
B
III-VZ
MZ
BLBP+Olig2-
hVZ-RG
BLBP+Olig2-
BLBP+Olig2+
hMZ-RG
BLBP-Olig2+
①
②
③
D
Cell distribution in P0.5 ON
Red
Yellow
Green
Colorless
2.14%
2.25%
5.32%
90.28%
Pax2+
BLBP+
Percentage (%)
Green
Red
DIST ON
E
P60
MADM
MADM/GFAP
MADM/Olig2
MADM/BLBP
DIST ON
F
Cell distribution in P60 ON
11.81%
1.71%
12.14%
74.34%
Olig2-
Olig2+
p = 0.0187
Total cell number
31%
75%

Figure S4

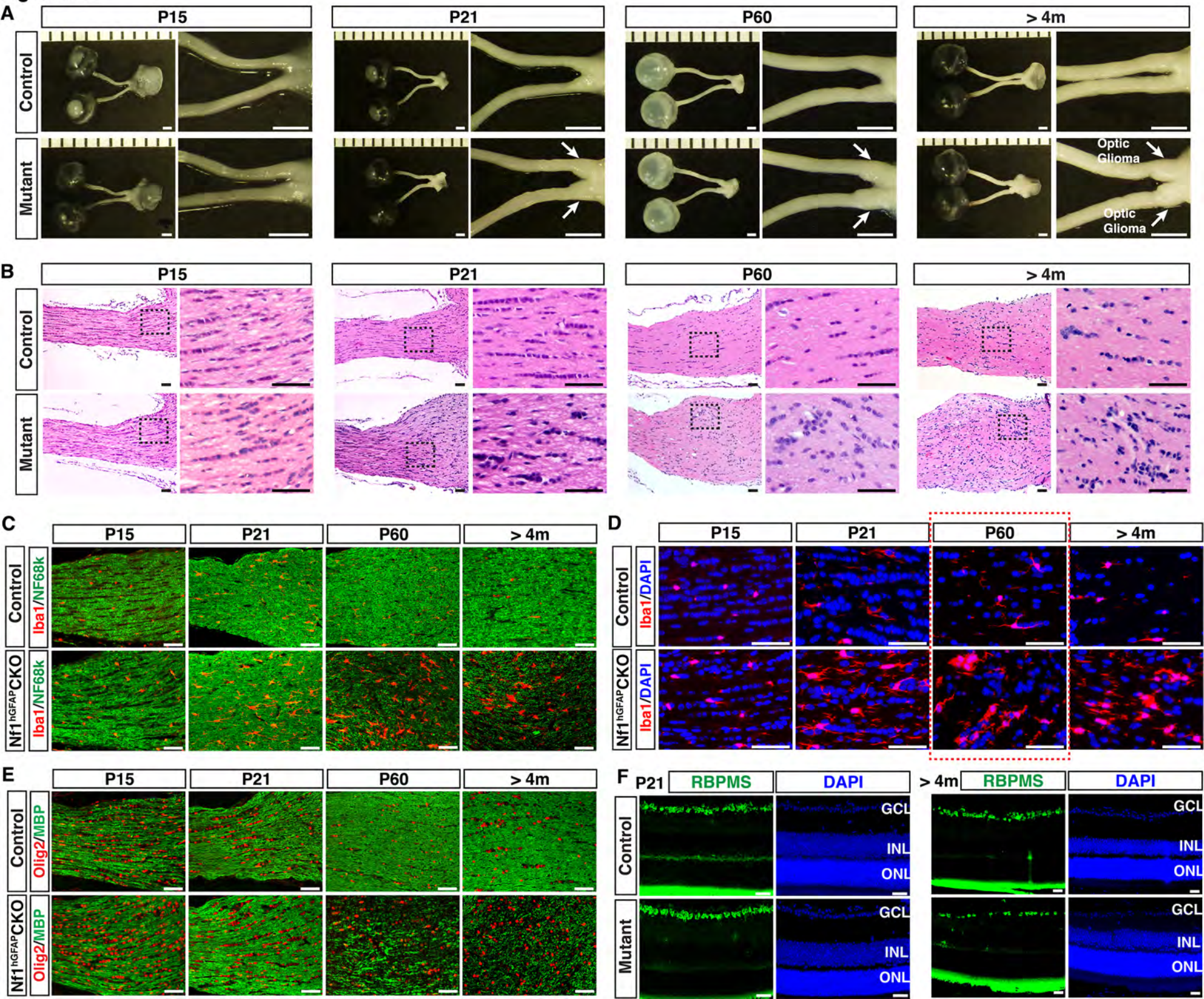
A
P15
P21
P60
> 4m
Control
Mutant
Optic Glioma
Optic Glioma
B
P15
P21
P60
> 4m
Control
Mutant
C
P15
P21
P60
> 4m
Control
Iba1/NF68k
Nf1hGFAPCKO
Iba1/NF68k
D
P15
P21
P60
> 4m
Control
Iba1/DAPI
Nf1hGFAPCKO
Iba1/DAPI
E
P15
P21
P60
> 4m
Control
Olig2/MBP
Nf1hGFAPCKO
Olig2/MBP
F
P21
RBPMS
DAPI
> 4m
RBPMS
DAPI
Control
Mutant
GCL
INL
ONL
GCL
INL
ONL
GCL
INL
ONL
GCL
INL
ONL

Figure S5

A

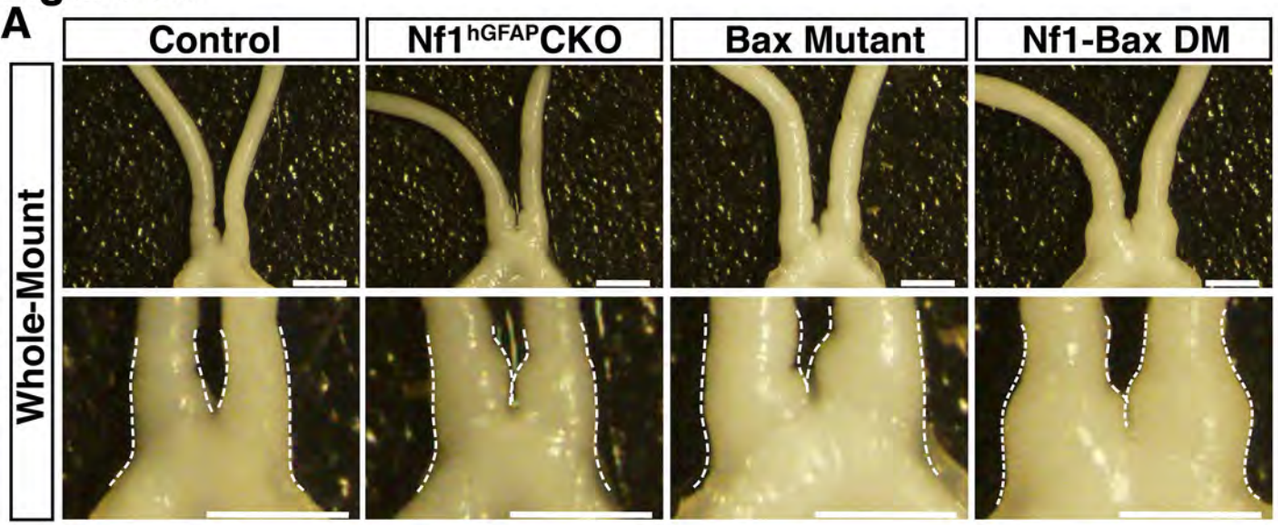

B

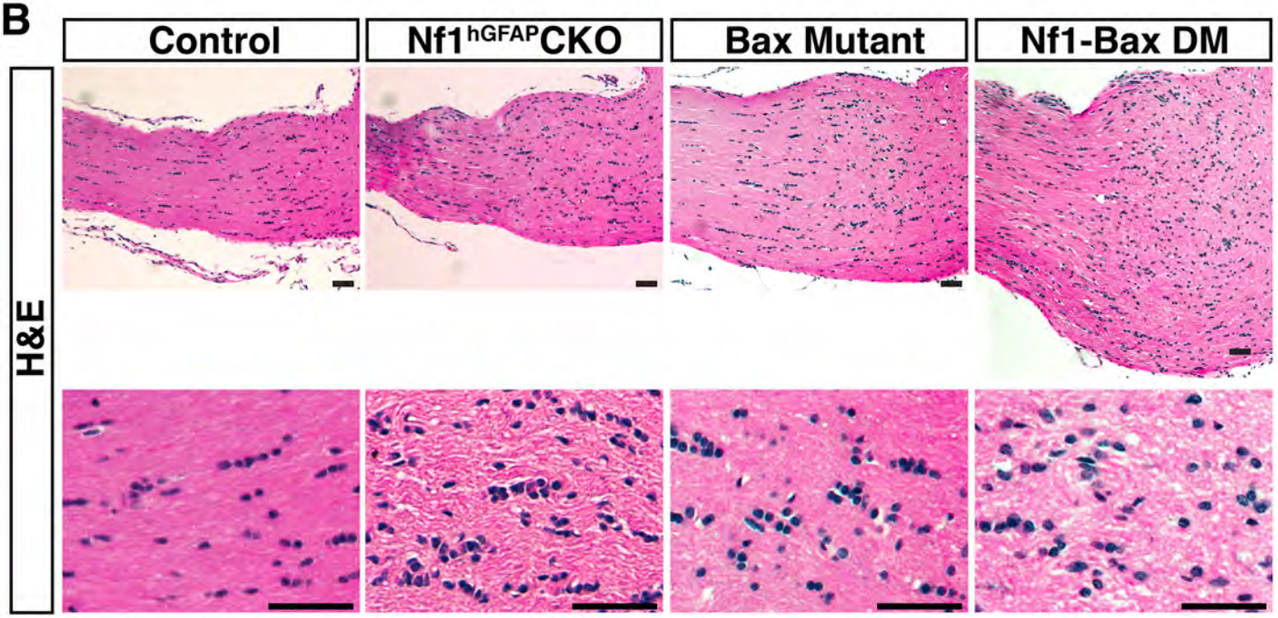

C

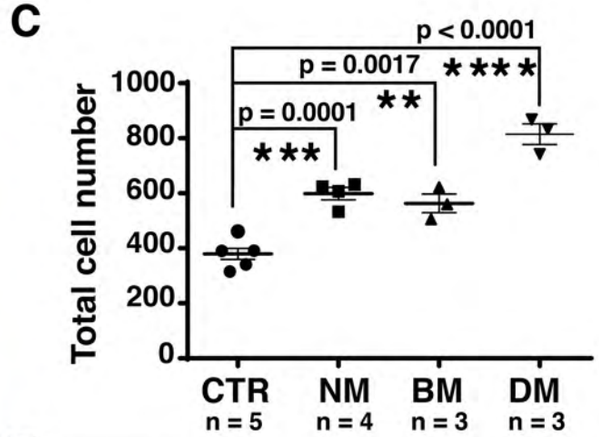

D

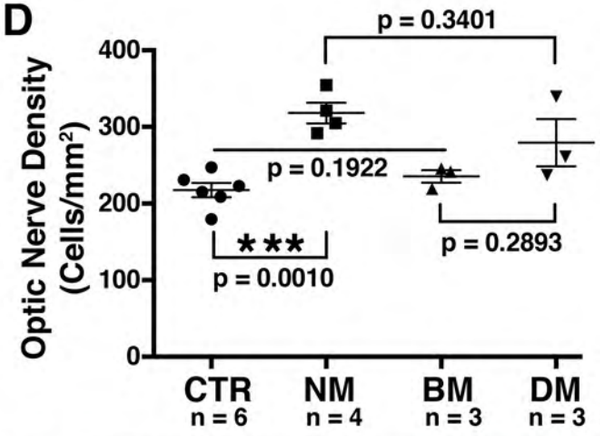

E

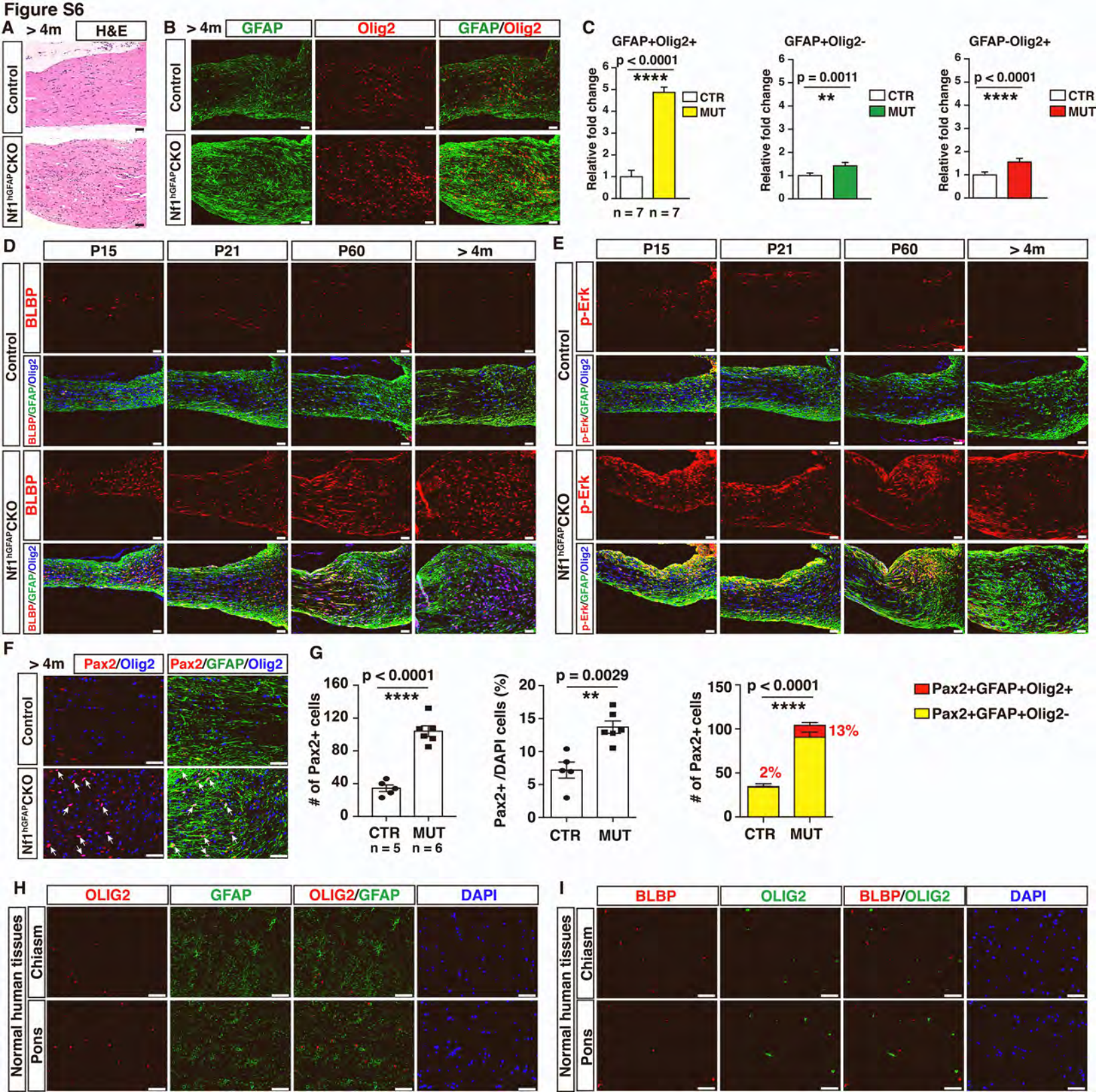
Figure S6
A
> 4m
H&E
Control
Nf1hGFAPCKO
B
> 4m
GFAP
Olig2
GFAP/Olig2
Control
Nf1hGFAPCKO
C
GFAP+Olig2+
p < 0.0001
****
Relative fold change
CTR
MUT
n = 7 n = 7
GFAP+Olig2-
p = 0.0011
**
GFAP-Olig2+
p < 0.0001
****
D
P15
P21
P60
> 4m
Control
Nf1hGFAPCKO
BLBP
BLBP/GFAP/Olig2
E
p-Erk
p-Erk/GFAP/Olig2
F
> 4m
Pax2/Olig2
Pax2/GFAP/Olig2
G
p < 0.0001
****
# of Pax2+ cells
CTR
MUT
n = 5 n = 6
p = 0.0029
**
Pax2+ /DAPI cells (%)
Pax2+GFAP+Olig2+
Pax2+GFAP+Olig2-
2%
13%
H
OLIG2
GFAP
OLIG2/GFAP
DAPI
Normal human tissues
Chiasm
Pons
I
BLBP
OLIG2
BLBP/OLIG2
DAPI

Figure S7

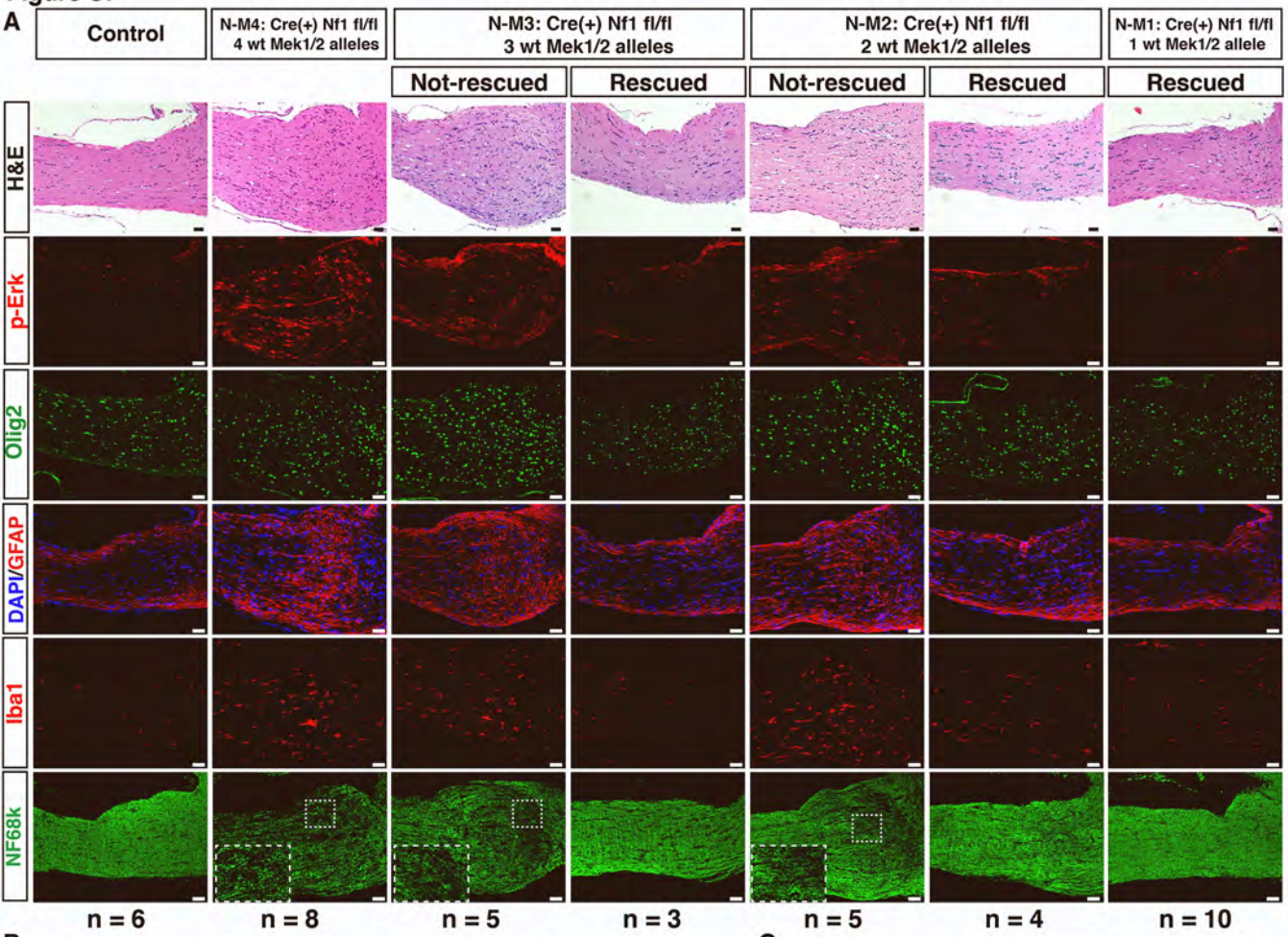
A
Control
N-M4: Cre(+) Nf1 fl/fl
4 wt Mek1/2 alleles
N-M3: Cre(+) Nf1 fl/fl
3 wt Mek1/2 alleles
N-M2: Cre(+) Nf1 fl/fl
2 wt Mek1/2 alleles
N-M1: Cre(+) Nf1 fl/fl
1 wt Mek1/2 allele
Not-rescued
Rescued
Not-rescued
Rescued
Rescued
H&E
p-Erk
Olig2
DAPI/GFAP
Iba1
NF68k
n = 6
n = 8
n = 5
n = 3
n = 5
n = 4
n = 10

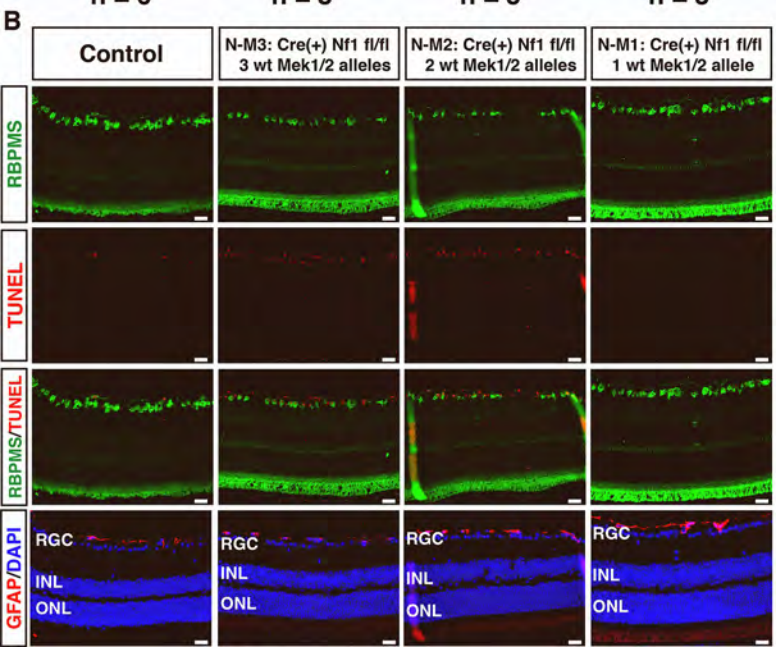
B
Control
N-M3: Cre(+) Nf1 fl/fl
3 wt Mek1/2 alleles
N-M2: Cre(+) Nf1 fl/fl
2 wt Mek1/2 alleles
N-M1: Cre(+) Nf1 fl/fl
1 wt Mek1/2 allele
RBPMS
TUNEL
RBPMS/TUNEL
GFAP/DAPI
RGC
INL
ONL

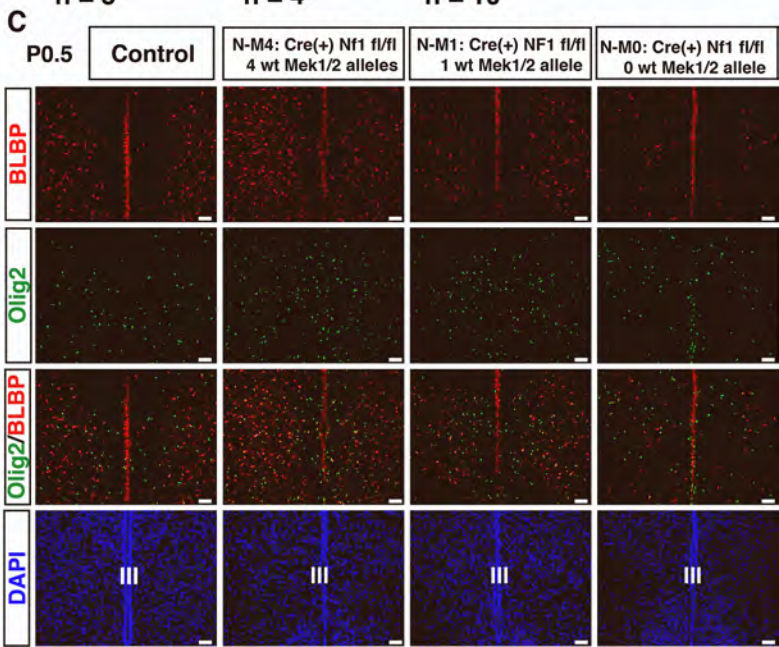
C
P0.5
Control
N-M4: Cre(+) Nf1 fl/fl
4 wt Mek1/2 alleles
N-M1: Cre(+) NF1 fl/fl
1 wt Mek1/2 allele
N-M0: Cre(+) Nf1 fl/fl
0 wt Mek1/2 allele
BLBP
Olig2
Olig2/BLBP
DAPI
III

Figure S8

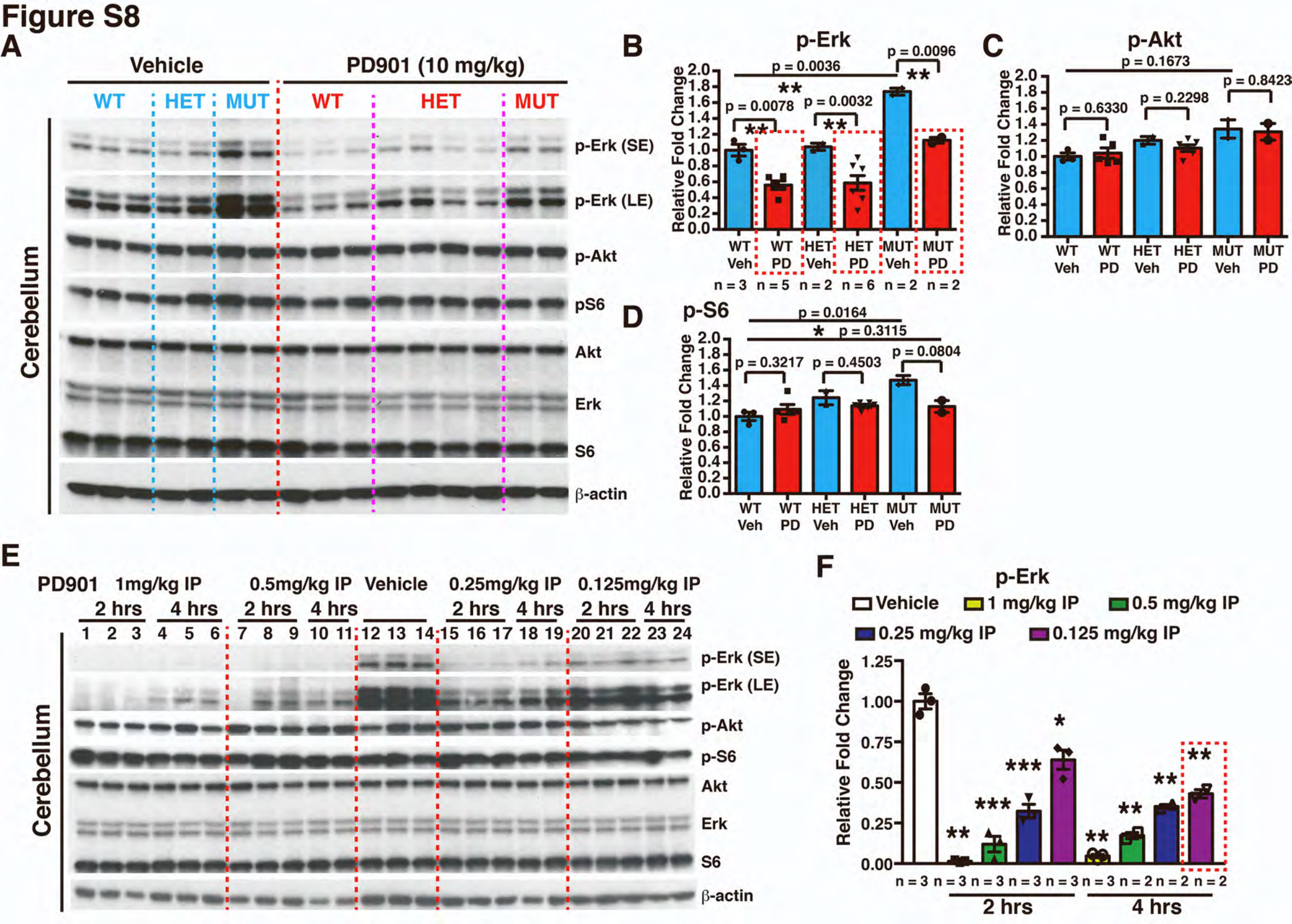
A
Vehicle
PD901 (10 mg/kg)
WT
HET
MUT
WT
HET
MUT
Cerebellum
p-Erk (SE)
p-Erk (LE)
p-Akt
pS6
Akt
Erk
S6
β-actin
B
p-Erk
Relative Fold Change
p = 0.0036
p = 0.0096
p = 0.0078
p = 0.0032
WT Veh
WT PD
HET Veh
HET PD
MUT Veh
MUT PD
n = 3
n = 5
n = 2
n = 6
n = 2
n = 2
C
p-Akt
p = 0.1673
p = 0.6330
p = 0.2298
p = 0.8423
D
p-S6
p = 0.0164
p = 0.3115
p = 0.3217
p = 0.4503
p = 0.0804
E
PD901
1mg/kg IP
0.5mg/kg IP
Vehicle
0.25mg/kg IP
0.125mg/kg IP
2 hrs
4 hrs
1 2 3 4 5 6 7 8 9 10 11 12 13 14 15 16 17 18 19 20 21 22 23 24
F
p-Erk
Vehicle
1 mg/kg IP
0.5 mg/kg IP
0.25 mg/kg IP
0.125 mg/kg IP
n = 3 n = 3 n = 3 n = 3 n = 3 n = 3 n = 2 n = 2 n = 2
2 hrs
4 hrs

Figure S9

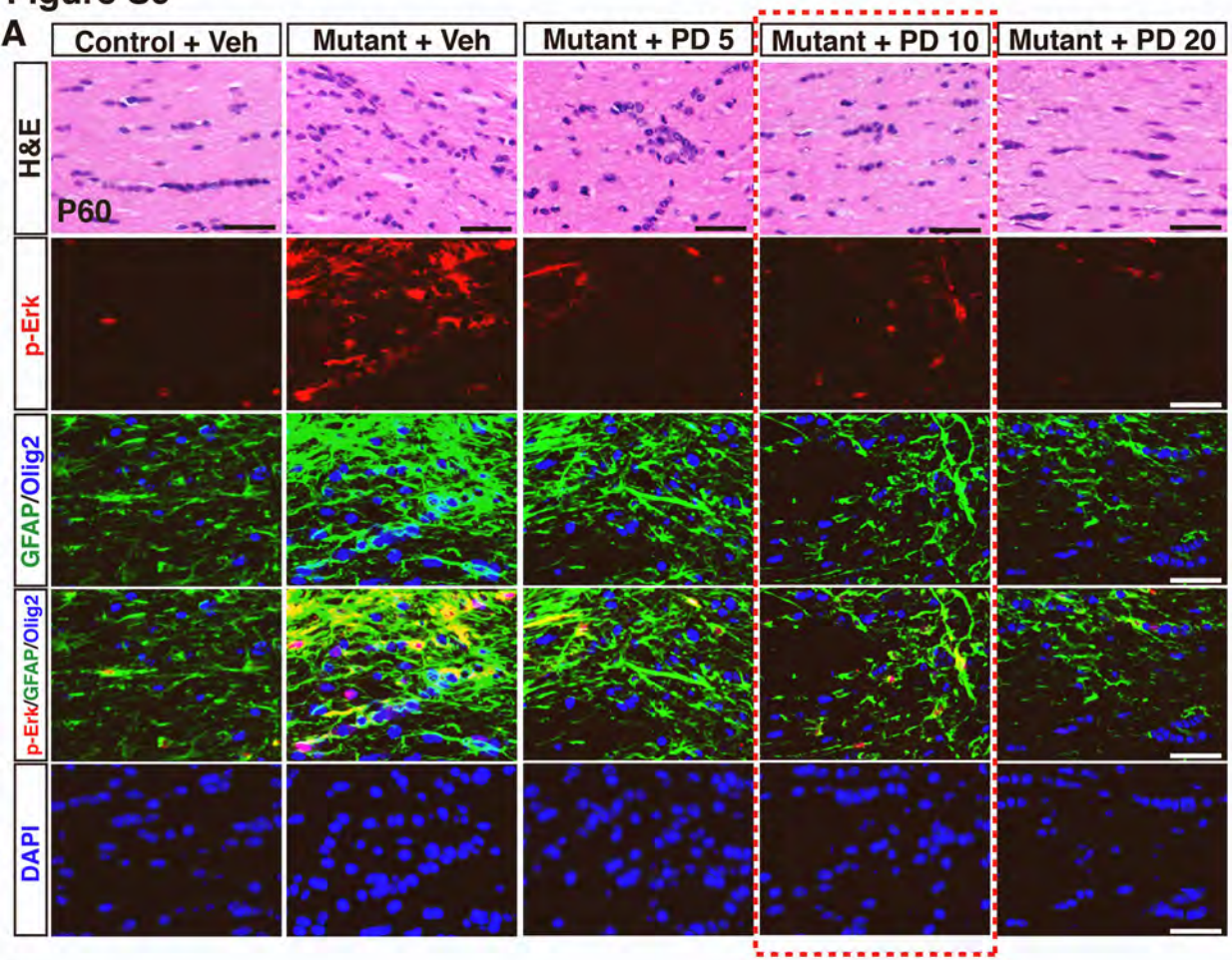
A
Control + Veh
Mutant + Veh
Mutant + PD 5
Mutant + PD 10
Mutant + PD 20
H&E
P60
p-Erk
GFAP/Olig2
p-Erk/GFAP/Olig2
DAPI

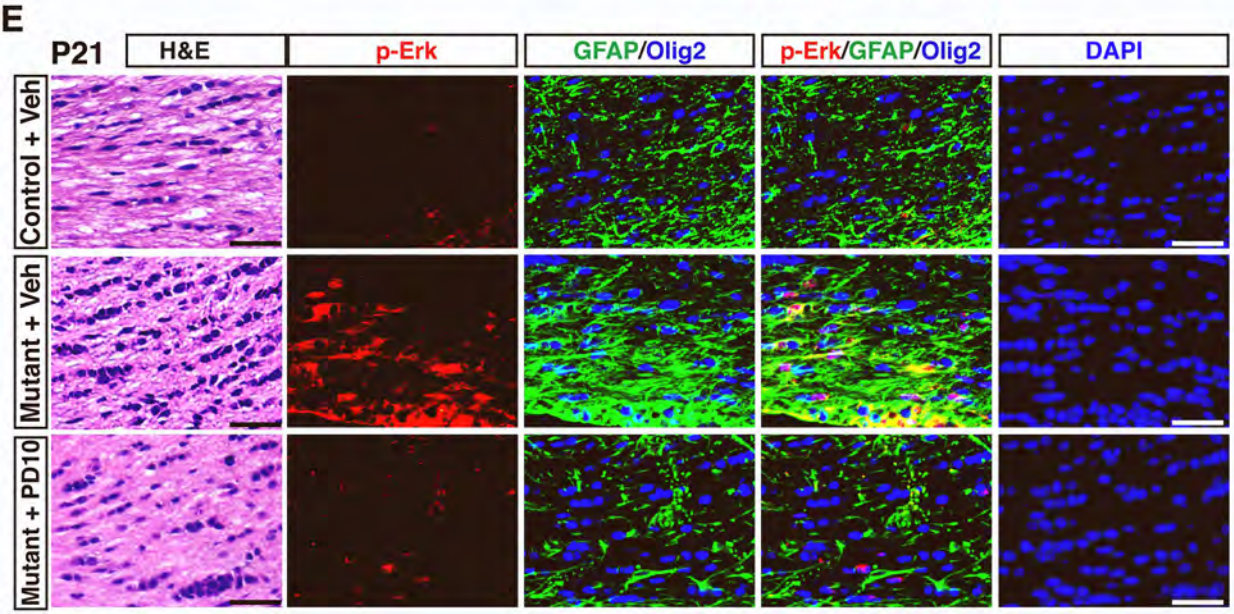
E
P21
H&E
p-Erk
GFAP/Olig2
p-Erk/GFAP/Olig2
DAPI
Control + Veh
Mutant + Veh
Mutant + PD10

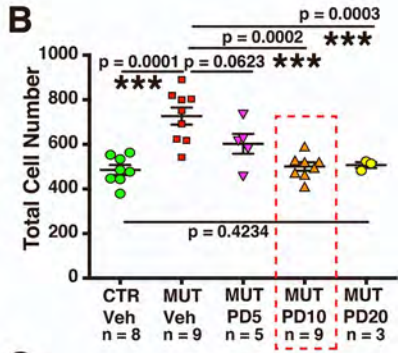
B
Total Cell Number
p = 0.0003
p = 0.0002
p = 0.0001
p = 0.0623
p = 0.4234
CTR Veh n = 8
MUT Veh n = 9
MUT PD5 n = 5
MUT PD10 n = 9
MUT PD20 n = 3

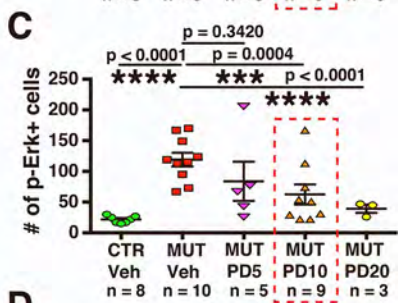
C
# of p-Erk+ cells
p = 0.3420
p < 0.0001
p = 0.0004
p < 0.0001
CTR Veh n = 8
MUT Veh n = 10
MUT PD5 n = 5
MUT PD10 n = 9
MUT PD20 n = 3

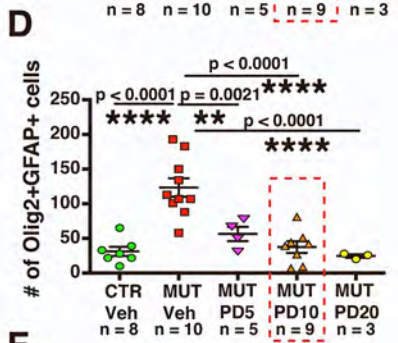
D
# of Olig2+GFAP+ cells
p < 0.0001
p < 0.0001
p = 0.0021
p < 0.0001
CTR Veh n = 8
MUT Veh n = 10
MUT PD5 n = 5
MUT PD10 n = 9
MUT PD20 n = 3

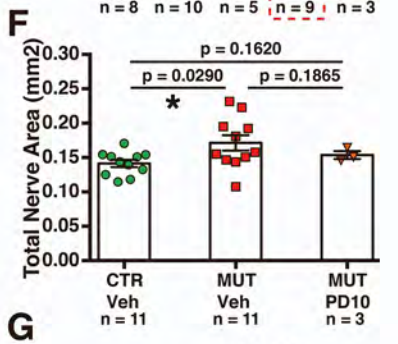
F
Total Nerve Area (mm2)
p = 0.1620
p = 0.0290
p = 0.1865
CTR Veh n = 11
MUT Veh n = 11
MUT PD10 n = 3

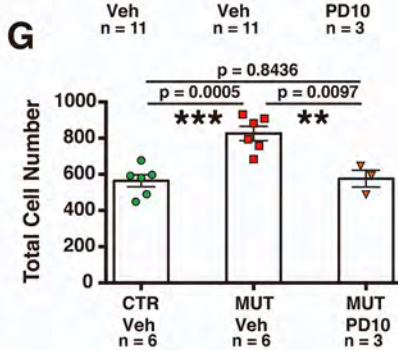
G
Total Cell Number
p = 0.8436
p = 0.0005
p = 0.0097
CTR Veh n = 6
MUT Veh n = 6
MUT PD10 n = 3

Supplemental Figure Legends

Figure S1. *Nf1* deletion leads to no phenotype in the *Nf1*^{Pax2}CKO mice optic nerve or the embryonic optic nerve in *Nf1*^{hGFAP}CKO mice, Related to Figure 1.

(A) Schematic summarizing how the one-hit model of tumorigenesis drives sporadic and NF1-associated pLGGs by converging on abnormal activation of the Erk/MAPK signaling pathway.

(B) Cartoon depicting the glial lineages targeted by the Pax2-cre (local lineage) and hGFAP-cre (both local and migrating lineages). Based on the O-2A (Oligodendrocyte-Type 2 Astrocyte) model, we used a dashed line to highlight the potential of astrocyte differentiation by the migrating lineage(s), in addition to their well-established role to generate oligodendrocytes in the ON.

(C-E) Co-labeling and quantification of Pax2 and Olig2 in the entire (C) and distal (D) ON of control and *Nf1*^{Pax2}CKO mice at P0.5. Dashed lines indicate the migrating forefront of Olig2$^+$ cells and the boundary of the ON. Of note, Pax2$^+$ local APCs were distributed throughout the entire ON. DIST (arrows) indicates the distal portion of the ON populated by migrating Olig2$^+$ cells.

(F) Co-labeling of p-Erk$^+$ and Olig2$^+$ in the distal ON of control and *Nf1*^{Pax2}CKO mice at P0.5.

(G) hGFAP-cre-mediated recombination in the dorsal brain is revealed by Rosa26-driven LacZ reporter expression in coronal sections from the hGFAP-Cre;R26R^{LacZ} mouse (left, top) and a cartoon model (left, bottom). Immunohistochemical labeling of Pten in sagittal sections from the *Pten*^{hGFAP}CKO model (right panels).

(H) Immunolabeling for td-Tomato and Pax2 in the control ON at E14.5 and E15.5 in the ON (left), with high magnification of the distal ON (right). Arrows mark the distal (pre-chiasmatic) portion of the ON. Arrowheads point to the earliest cells detected in the embryonic ON that underwent hGFAP-cre-mediated recombination, which also expressed Pax2.

(I and J) The distal and proximal portion of the control and *Nf1*^{hGFAP}CKO ON were labeled for tdTomato/Pax2, or Olig2 (I). The density of td-Tomato$^+$ cells and the percentage of recombined Pax2$^+$ cells within Pax2$^+$ APCs were quantified (J).

(K) Control and *Nf1*^{hGFAP}CKO distal ON at E17.5 were labeled for tdTomato and p-Erk.

(L and M) The distal ON of P0.5 control and *Nf1*^{Pax2}CKO mice were co-labeled with Pax2 and BLBP (L). The total cell number and BLBP$^+$ number was quantified (M).

(N and O) Representative images with co-labeling of Ki67, BLBP and Olig2 from the distal ON of P0.5 control, *Nf1*^{hGFAP}CKO mice (N). The number of Ki67^{+} cells, BLBP^{+}Ki67^{+} cells and proliferative index of BLBP^{+} cells were quantified (O).

All the quantifications are presented as mean ± SEM. Unpaired, two-tailed Student's t-test was used for statistical analysis. pLGG: pediatric low-grade glioma; ON: optic nerve; CTR: control; MUT: mutant; GP: glial progenitors; APC: astrocyte precursor cells; PROX: proximal; DIST: distal; VB: ventral brain; TG: trigeminal nerve; C/B: chiasm/brain; III-VZ: third ventricular zone. Scale bar: 50 μm.

Figure S2. *Nf1* loss disrupts the balance between the number of RGs inside and outside the embryonic third (III) ventricle, Related to Figure 2.

(A) Coronal sections of control and *Nf1*^{hGFAP}CKO brains were stained with hematoxylin and eosin (H&E) at E15.5.

(B and C) Coronal sections of E15.5 control and *Nf1*^{hGFAP}CKO brains were labeled for Olig2 and Ki67. Dashed boxes (B) mark the hypothalamic region, including the third ventriclular zone (III-VZ) and mantle zone (C). Dashed lines in C delineate the III-VZ.

(D) Confocal images of coronal sections from E17.5 control and *Nf1*^{hGFAP}CKO hypothalamic region with BLBP and Sox9 staining, which were the same triple-labeled images shown in Figure 2B, but exhibited a better view of the radial glia morphology of BLBP^{+} cells in the MZ.

(E and F) Low- (E), and high- magnification (F) images of coronal sections from E17.5 control and *Nf1*^{hGFAP}CKO brains were co-labeled with BLBP, Sox9 and Cre. The dorsal III-VZ is shown in high- magnification in (F).

(G and H) Horizontal sections from the optic chiasm of E17.5 control and *Nf1*^{hGFAP}CKO mice were double-labeled with BLBP and td-Tomato (G). P0.5 samples were triple-labeled with Olig2, BLBP and Ki67 (H). Arrows (H) mark the triple-positive BLBP^{+}Olig2^{+}Ki67^{+} cells.

(I and J) The cell number and proliferative index were quantified for BLBP^{+}Olig2^{-}, BLBP^{+}Olig2^{+} and BLBP^{-}Olig2^{+} cells in the chiasm of P0.5 control and *Nf1*^{hGFAP}CKO mice.

All the quantifications are presented as mean ± SEM. Unpaired, two-tailed Student's t-test was used for statistical analysis. III: third ventricle; III-VZ; third ventricular zone; MZ: mantle zone; D: dorsal; V: ventral; ON: optic nerve; CHM: chiasm; RG: radial glia. Scale bar: 50 μm.

Figure S3. The MADM-Nf1 model validates altered balance between hVZ-RG and hMZ-RG-like cells, Related to Figure 3.

(A) Coronal sections of E17.5 MADM-WT mice were stained with anti-GFP and anti-RFP antibodies. Boxed areas are shown on the right with high-magnification images for the Dorsal III-VZ, ventral III-VZ, and the MZ.

(B) A summary of the three mechanisms by which loss of *Nf1* overproduces RG-like migrating GPs by (1) overproducing hMZ-RG in the MZ while reducing hVZ-RG ($BLBP^+Olig2^-$) in the III-VZ; (2) impairing differentiation of hMZ-RG ($BLBP^+Olig2^-$ and $BLBP^+Olig2^+$) in the MZ; and (3) increasing proliferation of more differentiated GPs ($BLBP^-Olig2^+$).

(C) Representative images of co-labeling of GFP, RFP and Pax2 in the distal ON of P0.5 MADM-Nf1 mice. The boxed areas (left panel) are shown on the right with high-magnification images in which the insets show an example of the $Nf1^{+/+}$ (green, arrowhead) and $Nf1^{-/-}$ (red, arrow) cells in the $Pax2^+$ populations.

(D) The distribution of the red, green, yellow and colorless cells is shown in the distal ON of P0.5 MADM-Nf1 mice (n = 3) (left). The percentage of $Nf1^{+/+}$ (green) and $Nf1^{-/-}$ (red) cells co-expressing Pax2 (middle) or BLBP (right) in their populations was quantified.

(E) Representative images with co-labeling of GFP/RFP (left panels) with additional GFAP, BLBP or Olig2 staining (right panels) from the distal ON of P60 MADM-Nf1 mice. Green cells were marked by arrowheads, which often expressed GFAP, but not Olig2 or BLBP. In contrast, greatly expanded red cells were marked by arrows, which frequently expressed Olig2 and BLBP.

(F) The distribution of the red, green, yellow and colorless (DAPI only) cells in the ON of P60 MADM-Nf1 mice (n = 4) is shown. The percentage of $Olig2^+$ cells within the red and green cell compartments was quantified.

All the quantifications are presented as mean ± SEM. Unpaired, two-tailed Student's t-test was used for statistical analysis. GFP: green fluorescent protein; RFP: red fluorescent protein; III-VZ: third ventricular zone; MZ: mantle zone; hVZ-RG: hypothalamic VZ radial glia; hMZ-RG: hypothalamic MZ radial glia; GP; glial progenitors. Scale bars: 50 μm.

Figure S4. Timeline for $Nf1^{hGFAP}$CKO OPG disease progression characterized by optic nerve dysfunction and neuronal loss, Related to Figure 4.

(A) Representative whole-mount images of the ON from control and *Nf1*^{hGFAP}CKO mice at P15, P21, P60 and >4-months of age. Arrows point to optic pathway gliomas in the prechiasmatic nerve of *Nf1*^{hGFAP}CKO mice.

(B) Sections from distal ON of controls and *Nf1*^{hGFAP}CKOs were stained with H&E P15, P21, P60 and >4-months of age. High magnification images of the boxed areas are shown (right).

(C) Sections from distal ON of control and *Nf1*^{hGFAP}CKO mice were labeled for NF68k and Iba1 at the established time-points.

(D) Sections of distal ON from control and *Nf1*^{hGFAP}CKO mice labeled for Iba1 at different ages show the morphological changes in microglia in mutant ONs from "resting state" to an "activated state" starting around P21, which became more consistently observed at P60 (red boxes) or older when axon/myelin degeneration (E) and RGC loss (F) became readily detected.

(E) Adjacent sections were colabeled for myelin basic protein (MBP) and Olig2 at the established time-points.

(F) Representative sections from control and *Nf1*^{hGFAP}CKO retinas were labeled for RBPMS at P21 and at >4-months of age.

GCL: ganglion cell layer; INL: inner nuclear layer; ONL: outer nuclear layer. Scale bars: 1 mm (A), 50 μm (B-F).

Figure S5. Bax-mediated apoptosis leads to RGC loss in tumor-bearing *Nf1*^{hGFAP}CKO mice Related to Figure 4.

(A and B) Whole-mount ON (A) and H&E stained ON sections (B) from 4-month old controls, *Nf1*^{hGFAP}CKOs, *Bax* mutants and *Bax*/*Nf1*-double mutant mice.

(C and D) Quantification of the total cell number (C) and cell density (D) in the distal ON.

(E) Adjacent slides were labeled for Iba1, NF68k and GFAP. Boxed areas highlight axons at high-magnification in insets.

All the quantifications are presented as mean ± SEM. Unpaired, two-tailed Student's t-test was used for statistical analysis. NM: *Nf1*^{hGFAP}CKOs; BM: *Bax* mutants; DM; *Bax*/*Nf1*-double mutant mice. Scale bar: 1 mm (A), 50 μm (B and E).

Figure S6. *Nf1* loss causes persistence of RG/GP-like cells in both mouse and human pLGG, Related to Figure 5.

(A) H&E staining on ON from control and *Nf1*^{hGFAP}CKO mice at 4 months of age.

(B and C) Sections from distal ON of control and *Nf1*^{hGFAP}CKO mice were labeled with GFAP and Olig2 at >4-months of age (B). The relative fold change of GFAP^{+}Olig2^{+}, GFAP^{+}Olig2^{-}and GFAP^{-}Olig2^{+} cells in controls compared to mutants was quantified (C).

(D and E) Representative sections from control and *Nf1*^{hGFAP}CKO distal ON were triple-labeled with BLBP, GFAP and Olig2 (D), or p-Erk, GFAP and Olig2 (E).

(F and G) Representative sections from >4 month control and *Nf1*^{hGFAP}CKO distal ON were triple-labeled with Pax2, GFAP and Olig2 (F). The number of Pax2^{+} cells, the percentage of Pax2^{+} cells among DAPI cells, and the number/percentage of Pax2^{+} cells among GFAP^{+}Olig2^{+} and GFAP^{+}Olig2^{-} were quantified (G). Arrows (F) indicate triple-positive GFAP^{+}Olig2^{+}Pax2^{+} cells.

(H and I) Representative images from normal human brain tissues of the chiasm and pons were co-labeled with GFAP and Olig2 (H), and BLBP and Olig2 (I).

All the quantifications are presented as mean ± SEM. Unpaired, two-tailed Student's t-test was used for statistical analysis. Scale bar: 50 μm.

Figure S7. Dose-dependent genetic inactivation of *Mek1/2* prevents OPG formation in *Nf1*^{hGFAP}CKO mice, Related to Figure 6.

(A) Sections from optic nerves of control, N-M4, N-M3, N-M2 and N-M1 mutants at 4-8 months of age were stained for H&E, and immunolabeled for p-Erk, Olig2, GFAP, Iba1 and NF68K. Boxed areas highlight areas of axonal loss in insets.

(B) Representative cross-sections of control, N-M3, N-M2 and N-M1 retinas at 4-8 months were labeled with RBPMS, TUNEL and GFAP.

(C) Horizontal sections from the hypothalamic region of P0.5 control, N-M4, N-M1 and N-M0 pups were colabeled for BLBP and Olig2.

RGC: Retinal Ganglion Cells; INL: inner nuclear layer; ONL: outer nuclear layer; III: third ventricule. Scale bar: 50 μm.

Figure S8. MEK inhibitor treatment inactivates Erk signaling in the CNS, Related to Figure 7.

(A-D) Western blot analysis (A) on cerebella of P8 pups from different *Nf1* genotypes (WT, HET, MUT) treated with either vehicle (blue) or MEKi (red, 10 mg/kg PD0325901, PD901) via "MEKi in the milk" protocol. Quantification of the relative fold change in phospho-Erk (p-Erk) (B), p-Akt (C), or p-S6 (D) versus total Erk, Akt, or S6 protein in vehicle and PD-treated cerebella.

(E and F) Western blot analysis (E) was performed on cerebella of P8 wild-type pups treated with PD0325901 at 1/mg/kg, 0.5 mg/kg, 0.25 mg/kg or 0.125 mg/kg via IP injection and collected at 2hrs and 4hrs after treatment. Quantification of the relative fold change in p-Erk level (F) versus total protein in the cerebellum of treated pups compared to untreated littermate controls after treatment.

All the quantifications are presented as mean ± SEM. Unpaired, two-tailed Student's t-test was used for statistical analysis. Asterisks denote statistically significant differences ($* p < 0.05$, $** p < 0.01$, $*** p < 0.001$). Veh: Vehicle; SE: short exposure; LE: long exposure; IP: intraperitoneal; WT: wild-type; HET: *Nf1* heterozygous; MUT: *Nf1*^{hGFAP}CKO.

Figure S9. A three-week MEKi treatment rescues glial defects in the ON of *Nf1*^{hGFAP}CKO mice in a dose-dependent fashion, Related to Figure 7.

(A-D) Control and *Nf1*^{hGFAP}CKO mice were treated from P0.5 to P21 with either vehicle or MEKi (PD0325901) at 5 mg/kg (PD5), 10 mg/kg (PD10) or 20 mg/kg (PD20) and collected at P60. Representative images of H&E and immunofluorescence triple-labeling with p-Erk, Olig2, and GFAP from P60 distal ON (A). The total cell number (B), number of p-Erk$^+$ cells (C) and Olig2$^+$GFAP$^+$ cells (D) were quantified. Red boxes indicate the dosage used in later experiments that showed the greatest recue with minimal side effects.

(E-G) Sections from P21 distal ON from control and *Nf1*^{hGFAP}CKO mice treated with either vehicle or 10mg/kg PD901 and collected 4hrs after their last treatment were stained for H&E and adjacent sections were triple-labeled with p-Erk, Olig2, and GFAP (E). The optic nerve diameter (F) and total cell number (G) were quantified.

All the quantifications are presented as mean ± SEM. Unpaired, two-tailed Student's t-test was used for statistical analysis. MEKi: MEK inhibitor. Scale bar: 50 μm.

Developmental Cell
Previews

Inhibition of ERK/MAPK signaling as potential therapy to prevent optic pathway glioma in infants with neurofibromatosis type 1

Fulvio D'Angelo[1] and Anna Lasorella[1,2,3,4,*]
[1]Institute for Cancer Genetics, Columbia University Medical Center, New York, NY 10032, USA
[2]Department of Pathology and Cell Biology, Columbia University Medical Center, New York, NY 10032, USA
[3]Department of Pediatrics, Columbia University Medical Center, New York, NY 10032, USA
[4]Herbert Irving Comprehensive Cancer Center, Columbia University Medical Center, New York, NY 10032, USA
*Correspondence: al2179@columbia.edu
https://doi.org/10.1016/j.devcel.2021.10.001

Pediatric low-grade gliomas (pLGGs) arise primarily at early stages of development. The molecular mechanisms of pLGG gliomagenesis are unclear, as is the progenitor cell of origin. In this issue of *Developmental Cell*, Jecrois et al. show that NF1-associated optic pathway gliomas originate from migrating glial progenitors that have distinct MEK/ERK dependency.

Pediatric low-grade gliomas (pLGGs) are the most frequently occurring brain tumors in children (Packer et al., 2020). The genetic events that drive pLGG formation converge on the hyperactivation of the RAS/MAPK pathway and consist mostly of *BRAF*-activating mutations or *NF1* loss-of-function alterations (Ryall et al., 2020). Germline mutations of the *NF1* tumor suppressor gene cause neurofibromatosis type 1 (NF1), a common familial cancer predisposition syndrome. NF1-associated pLGGs typically develop along the optic pathway (NF1-OP), and they occur in nearly 20% of affected children. Adhering to the two-hit model, development of NF1-OP glioma (NF1-OPG) requires somatic loss of heterozygosity of the *NF1* gene, which drives hyperactivation of the ERK/MAPK pathway (D'Angelo et al., 2019; Fisher et al., 2021). However, the dynamics of NF1-OPG development are unclear, and the glioma cell of origin remains unidentified (Ryall et al., 2020). NF1-OPGs are commonly diagnosed in children younger than 7 years of age, with a mean of 4.5 years. This clinical characteristic and the molecular consequences of *NF1* loss support the hypothesis that the candidate cell of origin of NF1-OPG is a neural progenitor cell population in the developing central nervous system, which is susceptible (although transiently) to enhanced ERK/MAPK for neoplastic transformation. In this issue of *Developmental Cell*, Jecrois and colleagues use mouse models of NF1-OPG to investigate the identity of the neural stem and/or progenitor cell of origin that is vulnerable to glioma formation in the optic nerve (ON) and to explore the inhibition of the ERK/MAPK signaling as prevention therapy for these tumors (Jecrois et al., 2021).

Early studies have demonstrated separate lineages and origins for astrocytes and oligodendrocytes in the ON (Raff et al., 1993). Although the majority of ON astrocytes (APC) arise from cells of the optic stalk, the majority of oligodendrocytes are derived from progenitor cells (OPC) that migrate into the nerve from regions of the brain that were identified as the floor of the third ventricle or the pre-optic area (Ono et al., 1997; Ono et al., 2017). However, after more than 20 years of research, the origin of the oligodendrocyte lineage in the mammalian ON remains a matter of debate. Moreover, whether the precursor cell that resides in or migrates to the ON is susceptible to neoplastic transformation in *Nf1* mutant cells is a question that awaits clarification. Previous work has shown that neural stem cells in the embryonic third ventricle ventricular zone exhibit abnormal proliferation under *Nf1* inactivation and have implicated these cells in NF1-OPG formation (Lee et al., 2012). In the present work, Jecrois and colleagues examine the two precursor cells that populate the ON, namely resident astrocyte and brain-derived precursors in the absence of *Nf1*, and define the temporal window in which these cells are vulnerable to enhanced ERK/MAPK signaling for neoplastic transformation.

The authors use mouse genetics to study the function of *Nf1* in committed progenitors (PAX2-Cre) and stem cells and/or radial glial cells (GFAP-Cre) and td-Tomato reporter mice to trace the fate of progenitors in the ventral telencephalon that migrate through the optic chiasm and reach the distal ON at birth. Their results reject the notion that local astrocyte precursor cells are the cell of origin for optic glioma in *Nf1*-deficient mice, and they show that migrating precursors, but not resident precursors, are dependent on ERK signaling for proliferation.

Nf1 loss did not affect APC proliferation in the ON of the $Nf1^{Pax2}$-Cre model. In contrast, the number of migrating progenitors expressing brain lipid binding protein (BLBP) markedly increased in the ON of $Nf1^{hGFAP}$-Cre mice at P0.5 stage, the time when these glial progenitors (GPs) migrate from the brain into the ON during normal development. This was also the only progenitor population in the ON that was dependent on ERK signaling as this population was almost completely eliminated in the Mek1/2-deficient M0 model. However, GPs in the ON did not show higher proliferation rate in *Nf1*-null mice as compared with wild-type mice, and this suggests that their expansion had occurred at a different location before migration. The authors thoroughly tested this hypothesis through the use of $Nf1^{hGFAP}$ mice and the mosaic analysis

with double markers (MADM) system. MADM generates genetically mosaic mice in which sibling mutant and wild-type cells are labeled with different fluorescent markers. The phenotype of *Nf1*^{hGFAP} knockout mice was characterized by the increase of radial glia-like, BLBP+ progenitors in the dorsal hypothalamic region at E17.5, in particular at the border of the ventricular and mantle zones. The MADM mouse showed that, compared to the ventricular zone, the hypothalamic mantle zone was enriched in *Nf1* null cells that express precursor cell markers (BLPB+Olig2+ or BLBP-Olig2+). Thus, loss of *Nf1* results in disruption of the balance between stem-cell maintenance and gliogenesis in the hypothalamic region. This causes an initial expansion in the mantle zone of progenitors with impaired differentiation that migrate into the optic chiasm and finally enter the ON at P0.5, where they initiate optic pathway glioma (OPG) formation.

The hyperactivation of ERK/MAPK signaling by loss of *Nf1* was found to be the causal mechanism for the emergence and persistence of *Nf1*$^{-/-}$ BLBP^{+} progenitors that drive the OPG. Therefore, the authors tested whether preventing these developmental alterations by ERK inhibition was sufficient to block OPG formation in the *Nf1*^{hGFAP} model. Genetically removing three Mek1/Mek2 alleles (which are compatible with mice viability) almost completely re-established progenitor differentiation, blocked the expansion of migrating BLBP^{+} progenitors, and prevented NF1-OPG formation. More importantly, transient treatment with a low dose of MEK inhibitor during the neonatal age had a clinically provable effect on OPG.

This study provides new insights toward the understanding of the events that underly tumor initiation in NF1-OPG. In their work, Jecrois and colleagues suggest that brain-derived GPs migrating into the ON are susceptible to OPG formation in *Nf1*$^{-/-}$ mouse models and that MEK/ERK signaling dependency is the key criterion for the identification of the NF1-OPG cell of origin. The study is supported by the use of several mouse models and particularly elegant experiments using the MADM system that show *Nf1* null progenitor cells experience disruption of stem cell maintenance-differentiation balance in the ventricular/mantle zone of the hypothalamic region.

It remains to be determined how the model of NF1-OPG described here recapitulates the human disease. The efficacy of pharmacological MEK inhibition in mitigating the precursor cell embryonic phenotype and consequently OPG formation in the *Nf1* null mouse is exciting. Results from a clinical trial using 10–20 times higher doses of MEK inhibitors in non-NF1 OPGs have indicated tolerable toxicity and some efficacy (Fangusaro et al., 2021). Whether the novel approach of low-dose MEK inhibitors proposed here might be beneficial as a chemo-preventive strategy in children affected by NF1 and possibly RASopathies with high risk of cancer needs to be weighed against the relatively low incidence of OPG and the adverse events of MEK inhibition in very young children.

DECLARATION OF INTERESTS

The authors declare no competing interests.

REFERENCES

D'Angelo, F., Ceccarelli, M., Tala, Garofano, L., Zhang, J., Frattini, V., Caruso, F.P., Lewis, G., Alfaro, K.D., Bauchet, L., et al. (2019). The molecular landscape of glioma in patients with Neurofibromatosis 1. Nat. Med. *25*, 176–187.

Fangusaro, J., Onar-Thomas, A., Poussaint, T.Y., Wu, S., Ligon, A.H., Lindeman, N., Campagne, O., Banerjee, A., Gururangan, S., Kilburn, L., et al. (2021). A Phase 2 Trial of Selumetinib in Children with Recurrent Optic Pathway and Hypothalamic Low-Grade Glioma without NF1: A Pediatric Brain Tumor Consortium Study. Neuro-oncol. *10*, 1777–1788. https://doi.org/10.1093/neuonc/noab047.

Fisher, M.J., Jones, D.T.W., Li, Y., Guo, X., Sonawane, P.S., Waanders, A.J., Phillips, J.J., Weiss, W.A., Resnick, A.C., Gosline, S., et al. (2021). Integrated molecular and clinical analysis of low-grade gliomas in children with neurofibromatosis type 1 (NF1). Acta Neuropathol. *141*, 605–617.

Jecrois, E.S., Zheng, W., Bornhorst, M., Li, Y., Treisman, D.M., Muguyo, D., Huynh, S., Andrew, S.F., Wang, Y., Jiang, J., et al. (2021). Treatment during a developmental window prevents NF1-associated optic pathway gliomas by targeting Erk-dependent migrating glial progenitors. Dev. Cell *56*, S1534-5807(21)00634-1.

Lee, D.Y., Gianino, S.M., and Gutmann, D.H. (2012). Innate neural stem cell heterogeneity determines the patterning of glioma formation in children. Cancer Cell *22*, 131–138.

Ono, K., Yasui, Y., Rutishauser, U., and Miller, R.H. (1997). Focal ventricular origin and migration of oligodendrocyte precursors into the chick optic nerve. Neuron *19*, 283–292.

Ono, K., Yoshii, K., Tominaga, H., Gotoh, H., Nomura, T., Takebayashi, H., and Ikenaka, K. (2017). Oligodendrocyte precursor cells in the mouse optic nerve originate in the preoptic area. Brain Struct. Funct. *222*, 2441–2448.

Packer, R.J., Iavarone, A., Jones, D.T.W., Blakeley, J.O., Bouffet, E., Fisher, M.J., Hwang, E., Hawkins, C., Kilburn, L., MacDonald, T., et al. (2020). Implications of new understandings of gliomas in children and adults with NF1: report of a consensus conference. Neuro-oncol. *22*, 773–784.

Raff, M.C., Barres, B.A., Burne, J.F., Coles, H.S., Ishizaki, Y., and Jacobson, M.D. (1993). Programmed cell death and the control of cell survival: lessons from the nervous system. Science *262*, 695–700.

Ryall, S., Zapotocky, M., Fukuoka, K., Nobre, L., Guerreiro Stucklin, A., Bennett, J., Siddaway, R., Li, C., Pajovic, S., Arnoldo, A., et al. (2020). Integrated Molecular and Clinical Analysis of 1,000 Pediatric Low-Grade Gliomas. Cancer Cell *37*, 569–583.

Title: Develop preventative therapy for NF1-associated optic pathway glioma by targeting developmental vulnerability in a murine model

a) No Financial Disclosure

b) The purpose of the study: This study sought to develop a preventive therapeutic strategy for neurofibromatosis type 1-associated optic pathway glioma (NF1-OPG).

c) Methods: We developed a series of genetically engineered mouse (GEM) models of NF1-OPG by targeting one or both neural stem and progenitor cell populations, which are transiently present in the developing optic nerve (ON). Both genetic and pharmacologic approaches to inhibit Mek/Erk signaling completely prevent NF1-OPG formation by normalizing differentiation of abnormal *Nf1*-deficient (*Nf1*$^{-/-}$) stem-cell-like cells in the developing ON.

d) Results: Nearly 20% of children with NF1 develop low-grade glioma along the optic pathway, also known as NF1-OPG. Most NF1-OPG arise from children younger than 7 years of age with a median of 4 years old. It has been estimated that 30%-50% of children with NF1-OPG suffer from irreversible visual dysfunctions even with effective chemotherapies on tumor inhibition. These clinical observations suggest an urgent need to develop preventive or early interventional treatment for NF1-OPG before tumors cause irreversible death of retinal ganglion cells (RGCs) – the only neuronal population that transmit visual signals to the eye to the brain. The pediatric nature of NF1-OPG suggests developmental vulnerability in the ON. We show that, of the two developmentally restricted precursor populations in the ON, migrating glial progenitors (GPs), but not local astrocyte astrocyte precursors, depend on Erk signaling for lineage development, thus leading to the vulnerability to abnormal activation of Erk signaling by *Nf1* loss. *Nf1*$^{-/-}$ migrating GPs exhibit abnormal stem-cell-like phenotypes, persist through the development and form OPGs, which damage axons, subsequently cause Bax-dependent apoptosis in RGCs and visual dysfunction reminiscent of what occurs in children with NF1-OPG. While the absence of Erk signaling by inactivating both *Mek1* and *Mek2* inhibits gliogenesis and causes neonatal lethality, loss of three *Mek1*/*Mek2* alleles normalizes abnormal differentiation of *Nf1*$^{-/-}$ migrating GPs, prevents OPG formation and tumor-associated RGC death, while not compromising survival. More importantly, a low-dose transient treatment of an MEK inhibitor during neonatal stages provides long-term benefits by completely preventing OPG formation and RGC death.

e) Conclusion: We identify a developmental window during which normalizing Erk signaling in *Nf1*$^{-/-}$ GPs is sufficient to prevent NF1-OPG formation, tumor-associated axonal damage and death of RGCs. These results suggest a potential preventive therapeutic strategy for NF1-OPG by targeting developmental vulnerability.

Submission Details
Emmanuelle S Jecrois1,2,3,4,8, Wang Zheng1,2,3,8, Miriam Bornhorst1,2,3,5,8, Yinghua Li1,2,3, Daniel M. Treisman1,2,3, Matthew K. Krause1,2,3, Francisco Nadal-Nicolas6, Steven F. Stasheff1,6, Wei Li6, Hui Zong7, Roger J. Packer1 and Yuan

Zhu1,2,3,4* 1Gilbert Family Neurofibromatosis Institute, Children’s National Hospital, Washington, DC 20010, USA; 2Center for Cancer and Immunology Research, Children’s National Hospital, Washington, DC 20010, USA; 3Center for Neuroscience Research, Children’s National Hospital, Washington, DC 20010, USA; 4Neuroscience Graduate Program, University of Michigan Medical School, Ann Arbor, MI 48109, USA; 5Center for Genetic Medicine Research, Children's National Hospital, Washington, DC 20010, USA; 6Retinal Neurophysiology Section, National Eye Institute, National Institutes of Health, Bethesda, MD 20892, USA; 7Department of Microbiology, Immunology, and Cancer Biology, University of Virginia, Charlottesville, VA 22908, USA. 8These authors contributed equally. Supported by DOD NFRP (W81XWH-17-1-0083) and Gilbert Family Foundation to Y.Z.